To the Graduate Council:

I am submitting herewith a thesis written by Winthrop P. Smith entitled "Validation of Torsional - Bending Piezoelectric Actuator Concept." I have examined the final copy of this thesis for form and content and recommend that it be accepted in partial fulfillment of the requirements for the degree of Master of Science, with a major in Aerospace Engineering.

Grzegorz Kawiecki

Grzegorz Kawiecki, Major Professor

We have read this thesis
and recommend its acceptance:

Frank H Speckhart

R. J. Bailey

Accepted for the Council:

C W Minkel

Associate Vice Chancellor
and Dean of the Graduate School

STATEMENT OF PERMISSION TO USE

In presenting this thesis in partial fulfillment of the requirements for a Master's degree at The University of Tennessee, Knoxville, I agree that the Library shall make it available to borrowers under rules of the Library. Brief quotations from this thesis are allowable without special permission, provided that accurate acknowledgment of the source is made.

Permission for extensive quotation from or reproduction of this thesis may be granted by my professor, or in his absence, by the Head of Interlibrary Services when, in the opinion of either, the proposed use of the material is for scholarly purposes. Any copying or use of the material in this thesis for financial gain shall not be allowed without my written permission.

Signature Winthp P. Scott

Date 8/20/93

Validation of Torsional - Bending Piezoelectric Actuator Concept

A Thesis

Presented for the

Master of Science

Degree

The University of Tennessee, Knoxville

Winthrop P. Smith

December 1993

ACKNOWLEDGMENTS

I would like to thank the following people for their assistance during my research at The University of Tennessee:

Winston Holmes for his trouble shooting and introduction to the IDEAS™-VI/VII Finite Element Package.
Dennis Higdon for his time trouble shooting any problems with equipment used for experiments.
The machinists of the Mechanical and Aerospace Engineering machine shop for their cooperation and quick turnover time.
Janine Jennings (CPS), Linda Stooksbury (CPS), and Jackie Hurst for their time and cooperation with departmental details and paperwork.

Grzegorz Kawiecki for his insight, motivation, and enthusiasm for my research.

ABSTRACT

The feasibility of generating torque and twist in thin-walled, closed cross-section structural members using piezoelectric elements is shown by investigating analytically, numerically, and experimentally firstly an aluminum flat plate model and then a composite beam model. The investigated concept is based on the application of piezoelectric elements distributed on the surface or embedded in the walls of a structural element. This study shows that this method is feasible as an alternative method of generating twist and control torque in structural members. The magnitude of twist and torque generated using piezoelectric elements is estimated.

TABLE OF CONTENTS

LIST OF TABLES

LIST OF FIGURES

NOMENCLATURE

Symbol		Units
A	Extensional stiffness matrix	N/m^2
a_1	Effective length of beam	m
a_2	Effective distance between a_1 and optic screen (bending experiments)	m m
a_3	Effective distance between a_1 and optic screen (torsion experiments)	m
B	Coupling stiffness matrix	N/m^2
b	Breadth (width) of piezoelements	m
D	Bending stiffness matrix	N/m^2
d1	Bending deflection of composite beam	m
d2	Laser dot displacement (rotational component for bending experiment)	m
d3	Laser dot displacement (torsional displacement experiment)	m
d_{31}	Piezoelectric charge coefficient	m/V
E	Modulus of elasticity	N/m^2
E_{1a}	Longitudinal effective modulus of elasticity	N/m^2
E_{2a}	Transverse effective modulus of elasticity	N/m^2
G	Shear modulus	N/m^2
h	height	m
J_s	Polar moment of area of the composite beam	m^4

k	Bending curvature	Rad/m
N	Force load	N
M	Moment load	N
P	Force	N
t	Thickness	m
T	Transformation matrix	
u	Displacement in x-axis direction	m
v	Displacement in y-axis direction	m
w	Displacement in z-axis direction	m
Q	Stiffness matrix	N/m^2
$\bar{Q}$	Transformed stiffness matrix	N/m^2
V	Voltage	volts
Z_n	Distance from neutral axis of beam (or plate)	m

Exclusive to composite actuating cylinder (conceptual model):

H	Height of composite actuating cylinder	
r	Radius of composite actuating cylinder	
T	Torque produced by model	
t	Wall thickness of composite actuating cylinder	

Exclusive to LSSVM model:

a	thickness of actuator	
b	half of thickness of substrate	
l	half length of piezoelement	
K_n	Constants based on geometrical parameters of model	
M_{at}	Top actuator induced moment	N/m^2
M_{ab}	Bottom actuator induced moment	N/m^2
M_{eq}	Equivalent moment	N/m^2
Ms	Substrate moment	N/m^2
Fat	Top actuator induced force	N

Fab	Bottom actuator induced force	N
Fs	Substrate force	N

Greek Symbols

α	Piezoelement longitudinal bonding angle	degrees
α_1	Substrate equilibrium parameter	
β	Rotation with respect to x-axis of laminate, laminae	degrees
ε	Laminate strain	m/m
γ	Laminate shear strain	m/m
Λ	Free induced strain from piezo-actuator ($d_{31}V/t_a$)	m/m
ν	Poisson's ratio	
θ	Piezoelement longitudinal bonding angle (CLPT)	degrees
τ	Shear strain	m/m
ω	First mode bending frequency	rad/s
ψ	Effective stiffness ratio, $E_s t_s / E_a t_a$	

Exclusive to composite beam model

α	Mirror mounting angle with respect to horizon	degrees
θ	End of beam deflection angle of rotation	degree, radians

Exclusive to LSSVM model

λ_t	Transverse induced strain from piezo-actuator	m/m
λ_b	Longitudinal induced strain from piezo-actuator	m/m
η_n	Constants based on geometrical parameters of model	

Subscripts:

a, *a*	Piezo-actuator

B, b	Substrate
C, c	Piezoelectric actuator
e	External (resultant)
eq	"Equivalent"
l	Laminate
o	Middle surface of laminate
x, xx	x direction
y, yy	y direction
z	z direction
xy, yz	shearing components
s	Substrate

Superscripts:

o	Middle surface value

CHAPTER 1

INTRODUCTION

Active control systems utilizing piezoelectric elements as actuating and sensing devices have been investigated extensively [1], [2], [3], [4]. The research done has demonstrated that piezoelectric elements have the ability to modify the static and dynamic characteristics of structures. The displacement or stiffness and damping characteristics of a structure can be modified by the strain produced by piezoelectric elements. Piezoelectric actuators have many unique characteristics that distinguish them from other actuators. A piezoelectric element excited with an activation voltage to induce a strain upon a structure is referred to as a piezoelectric actuator. Several of the favorable characteristics of piezoelectric actuators are that they can be formed to specific shapes, and are relatively easy to control and to install. Therefore, piezoelectric actuators have favorable characteristics that make them a good choice for use in composite structures where they can be easily embedded.

The basic types of structural displacements are bending, torsional and axial displacements. The dynamic behavior of a structure is mostly affected by the bending and torsional displacements. The reduction of bending and axial vibrations using piezoelectric actuators is already well understood. Bending vibration attenuation in structures constitutes the majority of research involving the application of piezoelectric elements described in literature [1], [2]. However, the survey of available literature shows that the application of piezoelectric elements used as actuators to modify the torsional behavior of structures is very limited, but increasing. To the best of my knowledge the only studies related to this topic has been presented by Chan, Samak and Chopra [5] and Barrett [6], [7]. However, the approach taken by these authors is different than the approach presented in this Thesis.

Control torque generated by piezoelectric actuators can change the torsional characteristics of a structure. In turn, the induced control torque will generate a torsional displacement in the structure. The torsional displacements which are generated in a structure by piezoelectric elements are relatively small. However, they are sufficient to change the aerodynamic forces on structural elements subjected to airflow. This is the reason that this study will consider both the feasibility of generating torque and the feasibility of generating torsional displacements. The ability to alter the torsional characteristics of structures may be important to the control of aircraft structures, e.g., the flutter of aircraft wings and helicopter rotor blades. Also, another important topic is the reduction of helicopter rotor vibrations by means of changing individual blade pitch (Higher Harmonic Control HHC) [8],[9].

CHAPTER 2

LITERATURE REVIEW

Although the applications of piezoelectric elements as actuating and sensing devices in active control systems has been investigated extensively, very few publications deal with the application of piezoelectric elements to modify the torsional behavior of structures. Therefore, the following literature review will be concentrated on those publications that are most closely related to the proposed research.

2.1 Application of piezoelectric elements as actuating and sensing devices in active control systems

2.1.1 Application of piezoelements for vibration control of beams

The majority of research involving piezoelectric materials has been done in their applications to the controlling of structural vibrations of flexible beams, plates, etc.. One method employed to analyze the suppression of vibrations in a flexible structure by the use of discretely attached actuators is the independent modal-space control (IMSC) method. In an attempt to develop a method to optimize the control of the vibrations of a multi-mode flexible system with piezoelectric actuators, a modification of the IMSC method was developed [3]. A modified independent modal space control (MIMSC) method was developed to determine the optimal placement of the control actuators through the application of an efficient control algorithm that ensures minimal amplitudes of oscillation and a minimization of input control. The results of the application of MIMSC method showed that a small number of actuators have the ability to control the vibrations of flexible beams that have a large number of degrees of freedom. Another method developed to predict how effective piezoelectric elements are for actively damping vibrations in a cantilevered beam (Figure 1) was developed by Cudney, Alberts and Colvin [10]. The goal of their research was to develop a solution to the differential equation of motion in transfer function form. It was shown that transfer function modeling of these systems was advantageous because it allows the systems to be analyzed in the Laplace domain.

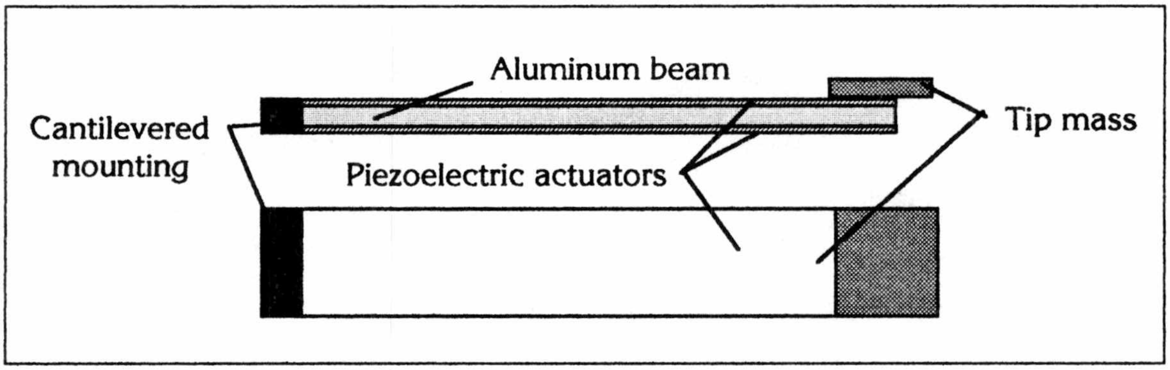

Figure 1 - Composite beam geometry [10]

The characteristics of both surface bonded and embedded piezoelectric elements was investigated by Crawley and de Luis [1]. A model of the dynamic characteristics of an activated piezoelectric element was formulated. The model of the activated piezoelectric element was then integrated into a dynamic model of a cantilevered Bernoulli-Euler beam. The conclusion of their research was that piezoelectric actuators performed well for both vibration control and bending shape control in cantilevered beams.

An active vibration model of a cantilevered beam with distributed piezoelectric elements and a distributed-parameter control theory was developed by Bailey and Hubbard [2]. The distributed-parameter control theory was governed by Lyapunov's second method. The results of the experiment showed that the method did not work well for large amplitudes of vibration, but it might keep resonant vibration from building up.

2.1.2 Application of piezoelements for vibration control of plates

In general, a finite element analysis approach was adopted to study the vibration reduction and control for the more complicated cases of composite plates with surface mounted or embedded piezoelectric elements. A variety of approaches to numerically analyze the static and dynamic characteristics of these composite structures have been developed. The work by Hughes and Allik [11] described a finite element formulation to incorporate the 'piezoelectric effect'. They refer to the piezoelectric effect as being the displacement potential of an activated piezoelectric actuator. Their model reduces to strictly applying the principle of virtual displacements upon a structure from the mechanical forces due to the activated piezoelectric elements. This is an early paper dealing with the subject of piezoelectric elements, and is lacking with respect to the more refined finite element models formulated recently. However, it does serve as an indication of the magnitude of recent research in this field. Subsequently, no data correlation or experimental validation of the method has been given.

More recent results of research into composite plate vibration reduction appear in the work of Lee and Moon [12]. They used a laminate plate theory with embedded piezoelectric elements to develop a class of modal sensors/actuators. The modal equations developed showed that piezoelectric elements could be used to measure/excite specific modes of plates and beams, thus eliminating the need for extensive signal processing.

2.1.3 Application of piezoelements for vibration control of more advanced structures

Tzou and Garde [4] have presented a method to study the active vibration control of a multilayered shell coupled with piezoelectric actuators. The dynamic equations governing the model were based on Love's theory and Hamilton's principle. For experimental validation, a cantilevered beam model was built. The results of these experiments demonstrated that the piezoelectric elements dual role of sensing/actuating enabled the vibration of the beam to be continuously monitored. This enabled undesirable vibrations to be damped out before they became very large.

2.2 Application of piezoelectric elements as shape control actuators

2.2.1 Application of piezoelectric elements as shape control actuators in beams

There exist several publications related to the application of piezo-actuators to induce deformations in bending and extension in cantilevered and simply supported beams. Crawley and de Luis [1] developed analytical models to predict the response of beams due to the induced strain transfer from both surface mounted and embedded piezoelectric actuators. The analytical expressions for the axial forces (pure extension and contraction), and an expression for an induced bending moment transferred to the structure by a single actuator or actuator pair were developed. The resulting force models are known as the 'pin-force' equivalent force models. The pin-force model only gives constant axial force and bending moment values, which results in a discontinuity at the actuator boundary [13]. These analytical models were developed for both surface mounted and embedded aluminum and composite beams. In addition, the non-dimensional parameter known as the *effectiveness* was derived. The effectiveness is the maximum amount of strain that an actuator can transfer to the structure that it is bonded to. Assuming a perfect bond, the expression for the effectiveness is given as follows:

$$\text{Effectiveness} = (\varepsilon_{MAX} d_{31})\left[\frac{\alpha_1}{\alpha_1 + (E_b t_b / E_c t_c)}\right] \quad (1)$$

The conclusions of the experiments on the test specimens showed that the piezoelectric actuators proved to be viable for both vibration and shape control of structures. In addition, it was shown that embedding the actuators into composite structures had a minimal effect on the structural characteristics of the composite structures tested.

Another model developed to analyze the beam problem is the 'strain-energy' equivalent force model presented by Wang and Rogers [14]. Their model was based on the principle of conservation of strain-energy to determine the linear strain distribution induced by attached or embedded actuators. This in turn provided the equivalent axial force and bending moment induced by the actuators. The results of this study agreed well with the pin-force models derived by Crawley and de Luis. As with the pin-force model, the expressions for the equivalent axial force and bending moment were constant.

A more accurate model developed to analyze the beam problem was the Linear Shear Stress Model (LSSVM) by Lin and Rogers [13]. The LSSVM was based on the assumption of an approximated linear shear stress field that previous models had failed to describe. Whereas the previous models have been modeled subject to external loading, the LSSVM describes the more accurate internal actuation due to the highly integrated nature of the system. It was shown that the LSSVM more accurately described the variable nature of the bending moment and forces along the axial direction of the beam. A diagram of the equivalent forces due to the activation of the piezoelectric actuators in pure bending and pure tension for the models discussed are shown in Figure 2

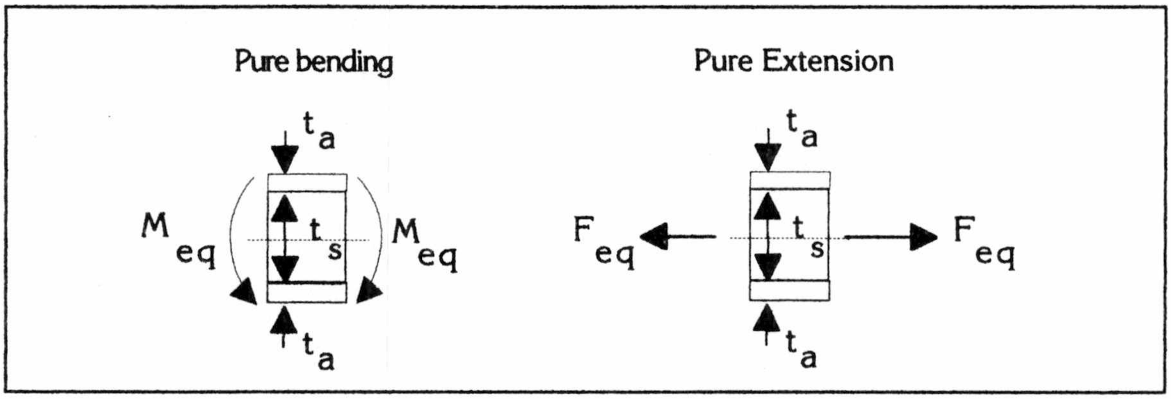

Figure 2 - Equivalent force diagram [13]

In all of the afore mentioned research, the actuators were modeled as either embedded or surface mounted to the structure. In a different approach, an investigation of discretely mounted piezoelectric actuators (Figure 3) was investigated by Chaudry and Rogers [15]. The conclusions of the research were that the offset nature of the actuators enabled a larger induced moment to be generated, and thus greater structural control.

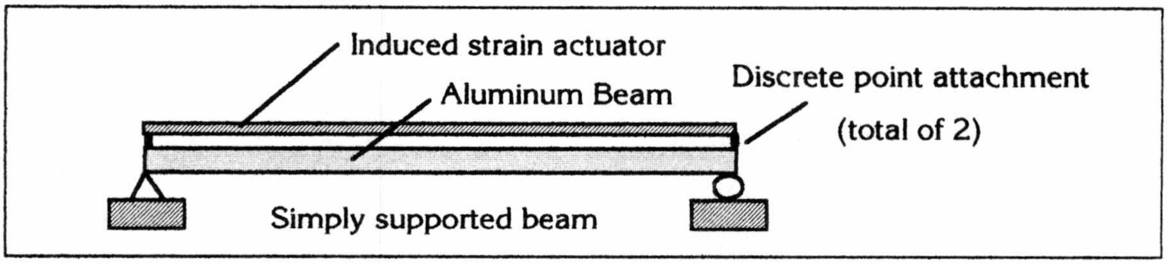

Figure 3 - Discretely attached piezoelectric elements [15]

2.2.2 Application of piezoelectric elements as shape control actuators in plates

Numerical analysis and analytical modeling methods have been adopted to study the shape control for plates incorporating piezoelectric elements. One of the methods of analyzing the structural control of composite plates is classical laminated plate theory (CLPT). Wang and Rogers [16] modeled pure bending and extension, as well as the coupling of bending and extension in an orthotropic angle-ply laminate with embedded piezoelectric elements. Additional research employing CLPT was performed by Lee and Moon [17]. They used a CLPT model to design several types of PVDF sensors and actuators.

Another method to predict the behavior of actuated plates was presented by Crawley and Lazarus [18]. They developed strain equations for the activated piezoelectric actuators mounted on the substructure and solved them using a Rayleigh-Ritz technique. The model derived was called the consistent plate actuation model. The term 'consistent plate model' comes from the assumption that any deformations in the laminate are consistent (equal throughout). The assumptions for their model are the same as those for thin and classical laminated plate theory. The cantilevered plate models were compared with experimental models to validate the method. In the model, the layout of actuators were considered as a layer in a laminated plate. The experimental results showed that the developed model predicted accurate results. In addition it was shown that relatively large deflections could be obtained through the induced strain actuation of piezo-actuators.

Ha, Keilers, and Chang [19] developed a finite element formulation derived from the variational principle. The variational principle took into account the potential energy of the structures and the electrical potential energy of the piezoelectric actuators. A numerical model was designed for the composite plate containing surface-bonded distributed piezoelectric actuators built by Crawley and Lazarus [18]. The numerical data generated agreed with the experimental data by Crawley and Lazarus [18] very well.

Wang and Rogers [14] incorporated their expressions for the strain-energy equivalent axial force and bending moments into a previously developed CLPT model. They concluded that the method developed resulted in an accurate prediction of the equivalent axial force and bending moments induced by multiple spatially- distributed actuators in plates. Another conclusion was that the strain-energy model was accurate for a wide range of actuator to substrate thickness ratios in plates.

2.2.3 Application of piezoelectric elements as shape control actuators in more advanced structures

A related structure to the research conducted in this Thesis is that of a directionally attached piezoelectric (DAP) bearingless blade torque tube developed by Barrett [6]. A correlation between the actuation potential versus the amount of static torsional deflection was experimentally developed. The results of the tests showed that a substantial amount of twist could be induced by the DAP arrangement. It was shown that a sustained deflection could be maintained for a considerable amount of time with the use of piezoelectric actuators as shape control actuators.

More recent research by Barrett [7] include the manufacturing and testing of a proposed missile wing controlled using piezoelectric actuators. The research shows that a subsonic graphite/epoxy wing is capable of twist deflections in excess of 9° . A supersonic graphite/epoxy wing demonstrated active pitch deflections in excess of 2°.

To date, the magnitude of research of strain induced deformations generated by piezoelectric actuators has been done in four main categories. These categories can be summed up as follows: 1) pure extension, 2) pure bending, 3) coupled bending and extension, and 4) coupled twisting and extension of beams and plates. In the literature cited, any twisting or shear displacements induced to the structure are accompanied by an axial displacement as well. These displacements are said to be coupled: that is, one deformation (shear displacement) is always accompanied by the other (axial displacement). Throughout the literature review, no research has been found that is involved in non-coupled twist or shear generated in structures by piezoelectric actuators.

CHAPTER 3

PRESENTATION OF CONCEPT

The method of generating non-coupled twist and torque in thin-walled composite and metal structural members using piezoelectric elements is presented. This method is based on the application of piezoelectric elements distributed in an appropriate manner on the surface or imbedded between the walls of a structural element [20]. This method is described below in detail.

3.1 Method of generating shear elongation and bending in plates

Piezoelectric actuators may have two forms, that of PVDF (polyvinylidene fluoride) thin film and PZT (lead, zirconate, titanate) ceramic. The actuators are embedded or surface mounted in a composite plate or surface mounted to a metal plate. Figure 4 is a graphical representation of this concept. The actuators are surface mounted so that half of the elements are aligned with the positive α direction and the other half of the elements are aligned with the negative α direction. Each depicted actuator designates one pair of elements surface mounted on both sides of the plate. The orientation of the element pairs is shown in Figure 5. In Figure 4, the element pairs in the positive α direction are activated so that an axial strain will be transferred to the plate in the direction of angle $+\alpha$. Likewise, the element pairs in the negative α direction are activated so that an axial strain will be transferred to the plate in the direction of angle $-\alpha$. When all of the element pairs

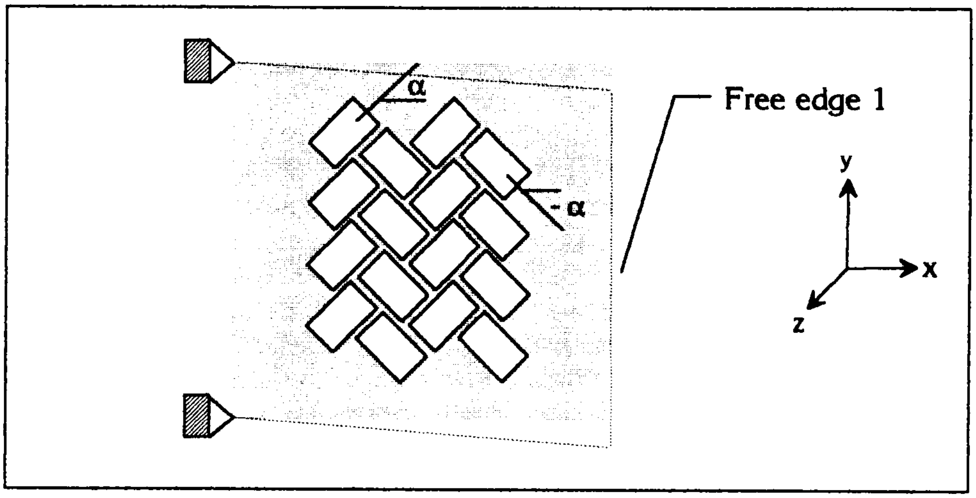

Figure 4 - Generation of shear displacement in aluminum plate using piezoelectric elements [20]

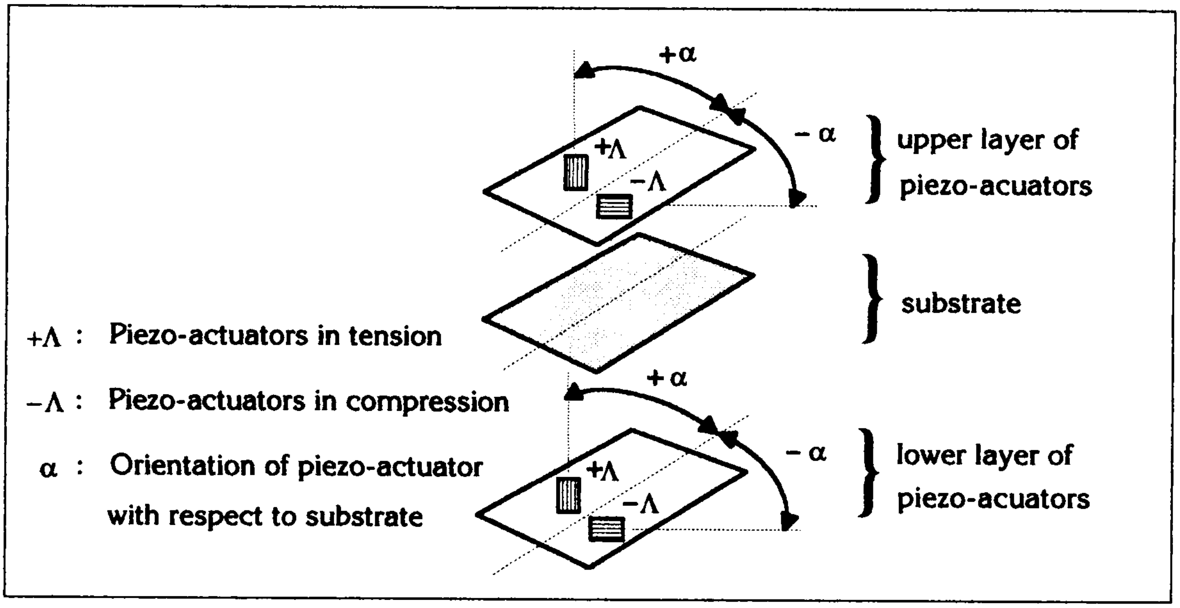

Figure 5 - Orientation of element pairs [20]

transfer strain in the above manner, the plate will shear to the position indicated by the dotted line. Since the strain transferred from each of the elements to the plate is assumed to be equal, the shear elongation is developed without extension of the plate in the x direction or z direction. In this manner, it is possible to develop a shear elongation without extending or warping the plate. Both the analytical and numerical analysis results presented in sections 4.2 and 6.3.3; respectively, prove this concept.

Along with the shear elongation of the plate, longitudinal elongation and contraction of the plate can be also achieved. If all of the elements are activated in extension, the plate will elongate along the x direction. Also, if all of the elements are activated in compression, the plate will contract along the x direction.

In order to induce bending into the plate, all elements on one side of the plate must induce positive strains while all of elements on the opposite side of the plate must induce negative strains. With this configuration, bending will be generated in the plate, resulting in a uniform edge displacement along the direction of the z axis. The displaced edge of the plate (free edge 1, Figure 4) remains parallel to the y axis. Again, both the analytical and numerical analysis results presented in sections 4.2 and 6.4.2; respectively, prove this concept.

3.2 Method of generating torque and twist using distributed piezoelectric elements

The elements are positioned along a helix, so that the direction of element extension and contraction is at an angle with respect to the generatrix. The twist of the structural member is caused by the simultaneous extension and contraction of piezoelectric elements that are mounted at different directions (as with the geometry of the piezoelements on the plate). This concept is valid for both composite and metal structures. Figure 6 is a graphical representation of a circular cross-section member made of composite material used to demonstrate the concept.

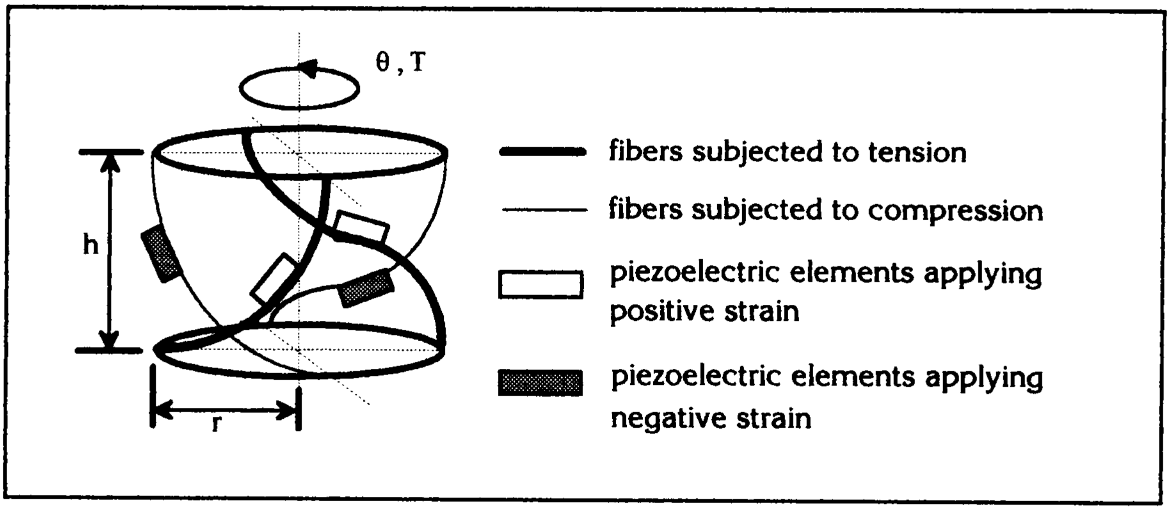

Figure 6 - Application of twist using piezoelecric actuators [20]

In the example, only four fibers are shown for the sake of the clarity of the drawing. Two of the fibers in Figure 6 represent the composite fibers wound counterclockwise (in view from above) and the other two fibers represent the composite fibers wound clockwise. The cylinder has height h and radius r. Assume that the top of the cylinder is free and the base of the cylinder is fixed. In Figure 6, the positive strain is applied to the entire length of fibers wound counterclockwise and the negative strain is applied to the entire length of fibers wound clockwise. The vertical components of the axial forces in the contracting and the expanding fibers will affect the height of the cylinder. The problem as stated is a statically indeterminate problem. It is simplified by assuming that the height of the cylinder is not affected by the changes in fiber lengths and remains constant. This assumption is based on the fact that there is an equal amount of contracting and expanding fibers. A counterclockwise rotation of the cylinder results from two actions: firstly, the horizontal displacements of the contracting fibers; and secondly, the horizontal displacements of the expanding fibers. Therefore, the resultants of the positive and negative strains applied in appropriate fibers, as shown in Figure 6, generate twist.

CHAPTER 4

ANALYTICAL FORMULATION

4.1 Magnitude of shear and bending displacements of a laminate plate generated using distributed piezoelements

The analytical formulation of the displacements of a plate subjected to loads imposed by piezoelectric actuators in this Thesis has been developed by [20]. The analytical formulation was done using the Classical Laminated Plate Theory (CLPT) [7], [16], [18], [21]. A modification to the CLPT method enables the strain transferred to the laminate by the piezoelectric actuator laminae to be modeled as thermally induced structural loads in the laminate [7], [16], 18], [21]. The modified CLPT method can be used to analyze a structure that has surface mounted elements on a metallic plate or both surface mounted and imbedded elements in a composite structure. For the modified CLPT method used here, the Kirchhoff hypothesis for plates and the Kirchhoff-Love hypothesis for shells are strictly adhered to. The assumptions for these hypothesis for the mechanical properties of the laminate are as follows [21];

1) The laminate is presumed to be made up of perfectly bonded laminae
2) The bonds are presumed to be infinitesimally thin as well as non-shear deformable (bonds between laminae do not deform)
3) Shear strains perpendicular to the middle surface are zero, that is, $\gamma_{xz} = \gamma_{yz} = 0$
4) Also, the normals do not deform (constant laminae thickness), so $\varepsilon_z = 0$

For an arbitrary laminate, the deformations due to external or internal loading are shown graphically in Figure 7.

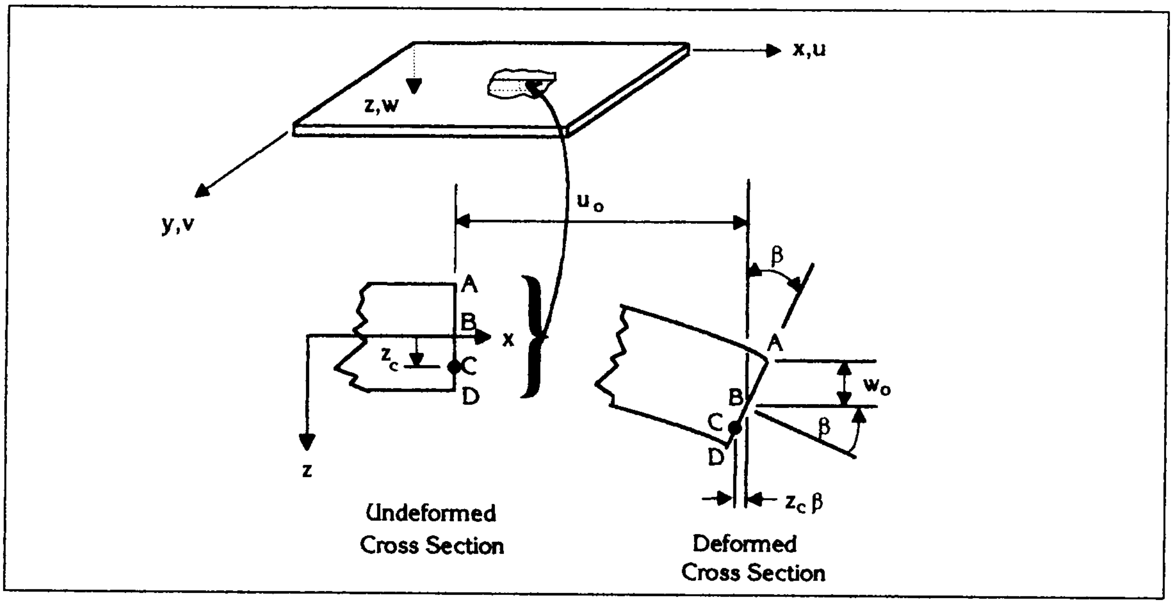

Figure 7 - Geometry of deformation in the xz plane of a laminate [21]

The implications of the above assumptions are as follows. All displacements across the laminae are continuous so that no laminae can slip relative to each other. Thus, the layers of bonded laminae act as one single layer. Also, referring to Figure 7, a line straight and perpendicular (ABCD) prior to a deformation of the laminate will remain straight and perpendicular after a deformation occurs. In addition to the above statement, the normals of the laminate do not compress or expand (the laminae keep constant thickness before and after deformation).

From Figure 7, the displacements of the laminate u, v, and w in the x, y, and z directions, respectively, are found by the laminate cross section in the xz plane. Upon substitution of the derived displacements u and v [21], and acknowledging that the strains in the laminate depend on the middle surface strains ε° and the middle surface curvatures k it is found that

$$\varepsilon = \varepsilon^\circ + zk \quad \text{where} \quad \varepsilon^\circ = \begin{Bmatrix} \varepsilon_x^o \\ \varepsilon_y^o \\ \gamma_{xy}^o \end{Bmatrix} = \begin{Bmatrix} \dfrac{\partial u}{\partial x} \\ \dfrac{\partial v}{\partial y} \\ \dfrac{\partial u}{\partial y} + \dfrac{\partial v}{\partial x} \end{Bmatrix}$$

$$\text{and } k = \begin{Bmatrix} k_{xx} \\ k_{yy} \\ k_{xy} \end{Bmatrix} = \begin{Bmatrix} -\dfrac{\partial^2 w}{\partial x^2} \\ -\dfrac{\partial^2 w}{\partial y^2} \\ -2\dfrac{\partial^2 w}{\partial x \partial y} \end{Bmatrix} \tag{2}$$

Now, the stress-strain relations for any k^{th} layer of a multilayered laminate in arbitrary coordinates is given by [21]

$$\{\sigma\}_k = \left[\bar{Q}\right]_k \{\varepsilon\}_k \tag{3}$$

In equation (3), $\left[\bar{Q}\right]_k$ is the transformed stiffness matrix. The transformed stiffness matrix is made up of the stiffness matrix of a laminae that lies at some arbitrary angle θ with respect to the other plies in the laminate. Therefore:

$$\left[\bar{Q}\right] = [T]^{-1}[Q][T]^{-T} \tag{4}$$

where $[Q]$ is the laminae stiffness matrix and $[T]$ is the transformation matrix given in [21]:

$$[T] = \begin{bmatrix} \cos^2\theta & \sin^2\theta & 2\sin\theta\cos\theta \\ \sin^2\theta & \cos^2\theta & -2\sin\theta\cos\theta \\ -\sin\theta\cos\theta & \sin\theta\cos\theta & \cos^2\theta - \sin^2\theta \end{bmatrix} \tag{5}$$

The resultant forces and moments acting on the laminate are given by

$$\{N\} = \int_{-t/2}^{t/2} \{\sigma\}_k dz = \sum_{k=1}^{N} \int_{z_{k-1}}^{z_k} \{\sigma\}_k dz \tag{6}$$

and

$$\{M\} = \int_{-t/2}^{t/2} \{\sigma\}_k z dz = \sum_{k=1}^{N} \int_{z_{k-1}}^{z_k} \{\sigma\}_k z dz \tag{7}$$

where z_k and z_{k-1} are defined in Figure 8.

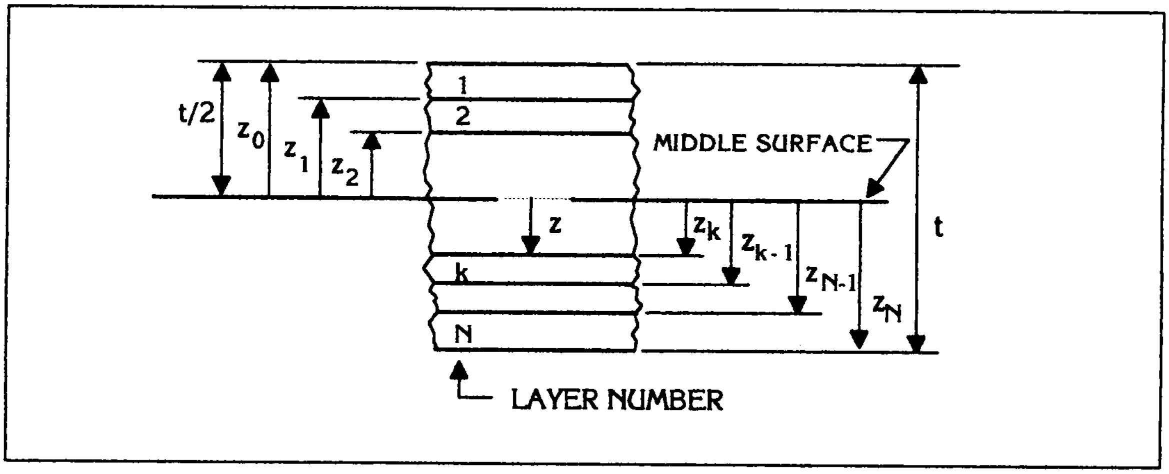

Figure 8 - Geometry on an n-layered laminate [21]

Knowing that the strains and curvatures are not functions of z but are middle surface values, they can be removed from under the summation signs. Therefore, equations (6) and (7) can be expressed in the form

$$\begin{Bmatrix} N \\ M \end{Bmatrix}_e = \begin{bmatrix} A & B \\ B & D \end{bmatrix}_l \begin{Bmatrix} \varepsilon^o \\ k \end{Bmatrix}_l - \begin{Bmatrix} N \\ M \end{Bmatrix}_a \quad (8)$$

where;

$A_{ij} = \sum_{k=1}^{N} \left(\bar{Q}_{ij}\right)_k (z_k - z_{k-1})$: extensional stiffnesses [21]

$B_{ij} = \frac{1}{2} \sum_{k=1}^{N} \left(\bar{Q}_{ij}\right)_k \left(z_k^2 - z_{k-1}^2\right)$: coupling stiffnesses [21]

$D_{ij} = \frac{1}{3} \sum_{k=1}^{N} \left(\bar{Q}_{ij}\right)_k \left(z_k^3 - z_{k-1}^3\right)$: bending stiffnesses [21]

$\bar{Q}_{ij}$: transformed stiffnesses [21]

Subscripts

a : piezoelectric actuator

l : laminate

e : external (resultant)

Equation (8) represents the modified CLPT method. In equation (8), the matrix with subscript a denotes the internal load developed by the actuator laminae. The laminate stiffness matrice as shown in equation (8) contains extensional stiffness (A), coupling stiffness (B) and the bending stiffness (D) of the laminate. The laminate stiffness matrice contains both the substructure stiffness and the stiffnesses due to the piezoelectric elements, whereas the actuator forcing vectors are dependent upon the stiffness of the piezoelectric elements [18].

The fully developed modified CLPT method equation follows

$$\begin{Bmatrix} N_x \\ N_y \\ N_{xy} \\ M_x \\ M_y \\ M_{xy} \end{Bmatrix}_e = \begin{bmatrix} A_{11} & A_{12} & A_{16} & B_{11} & B_{12} & B_{16} \\ A_{12} & A_{22} & A_{26} & B_{12} & B_{22} & B_{26} \\ A_{16} & A_{26} & A_{66} & B_{16} & B_{26} & B_{66} \\ B_{11} & B_{12} & B_{16} & D_{11} & D_{12} & D_{16} \\ B_{12} & B_{22} & B_{26} & D_{12} & D_{22} & D_{26} \\ B_{16} & B_{26} & B_{66} & D_{16} & D_{26} & D_{66} \end{bmatrix}_l \begin{Bmatrix} \varepsilon_X \\ \varepsilon_Y \\ \varepsilon_{XY} \\ k_X \\ k_Y \\ k_{XY} \end{Bmatrix}_l - \begin{Bmatrix} N_X \\ N_Y \\ N_{XY} \\ M_X \\ M_Y \\ M_{XY} \end{Bmatrix}_a \tag{9}$$

For the case where no external loads are applied to the laminate plate,

$$\begin{Bmatrix} N \\ M \end{Bmatrix}_e = \begin{Bmatrix} 0 \\ 0 \end{Bmatrix} = 0 \tag{10}$$

The models that this modified CLPT method is used to analyze all have the piezoelectric elements located symmetrically about the neutral plane of the substrate. The layout of a symmetrically oriented pair of elements is shown in Figure 9.

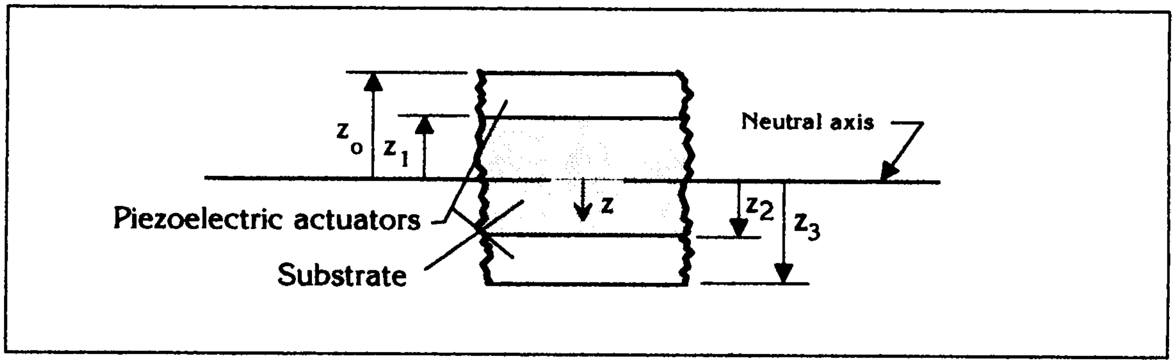

Figure 9 - Geometry of piezoelectric actuator pair

From Figure 9, it becomes apparent that the distance from the neutral axis to the outer face of each of the elements is equal, so $z_o = z_3$. Also, it is shown that the distance from the neutral axis to the bonded face of each of the elements is equal, therefore $z_1 = z_2$. From the definition of the coupling stiffnesses, the sum of the coupling stiffnesses from the substrate and elements that make up the laminate stiffness matrix is zero. Therefore, equation (8) can be reduced to

$$\begin{Bmatrix} N \\ M \end{Bmatrix}_a = \begin{bmatrix} A & 0 \\ 0 & D \end{bmatrix}_l \begin{Bmatrix} \varepsilon^o \\ k \end{Bmatrix}_l \tag{11}$$

The loads per unit length induced to the laminate by the piezoelectric elements are given by [18]

$N_a = \int_{-t/2}^{t/2} Q\Lambda dz$: the vector of piezoelectric element generated force

$M_a = \int_{-t/2}^{t/2} Q\Lambda z dz$: the vector of piezoelectric element generated moment

$\Lambda = \begin{bmatrix} \Lambda_x \\ \Lambda_y \\ \Lambda_{xy} \end{bmatrix}$: the vector of piezoelectric element generated strain

The strains and curvatures developed in the laminate due to the activation of the piezoelectric elements are found by using the following decoupled equations

$$\{\varepsilon^o\} = [A]^{-1}\{N_a\} \tag{12}$$

and

$$\{k\} = [D]^{-1}\{M_a\} \tag{13}$$

Equations (12) and (13) are based on several assumptions. The first is that the strain transferred to the laminate from the activated piezoelectric elements is equal in the x and y direction, therefore they are isotropic and $\Lambda_x=\Lambda_y=\Lambda$. The Poisson ratio for the piezoelectric elements is assumed to be equal to the substrate laminae, thus $\nu_{xya}=\nu_{yxa}=\nu_{xye}=\nu_{yxe}\nu$. The elastic modulus for the piezoelectric elements have been determined for the directional attachment of the elements to the substrate [6]. Figure 10 shows the details of directional attachment of the piezoelectric elements. In the model, the bond between the elements and the substrate is assumed to be perfect and of zero thickness.

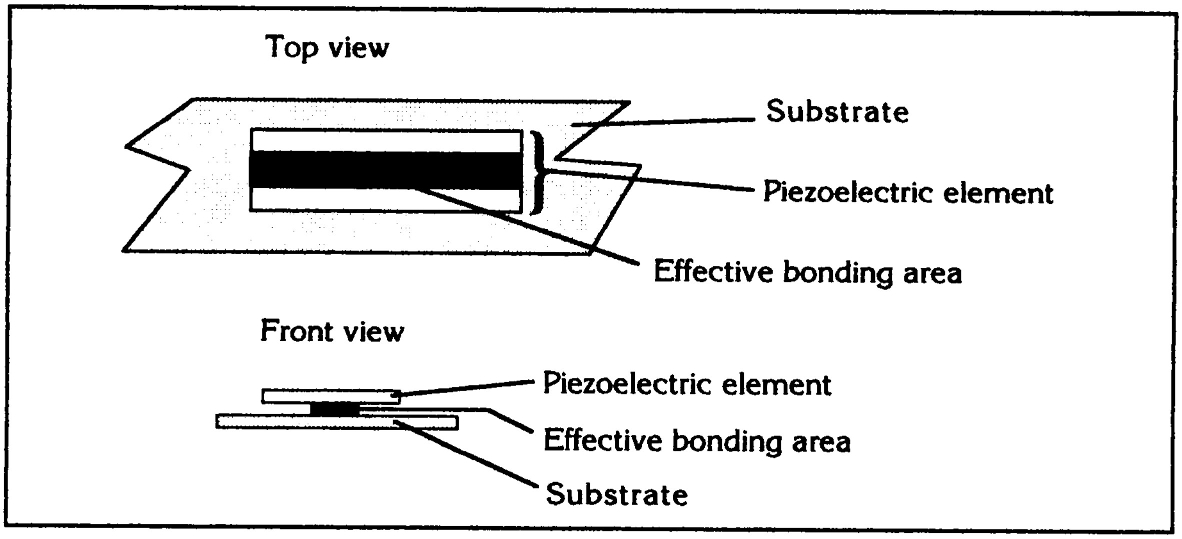

Figure 10 - Schematic of details of directional attachment of piezoelectric elements

The layout of piezoelectric elements on the substrate is shown in Figure 11.

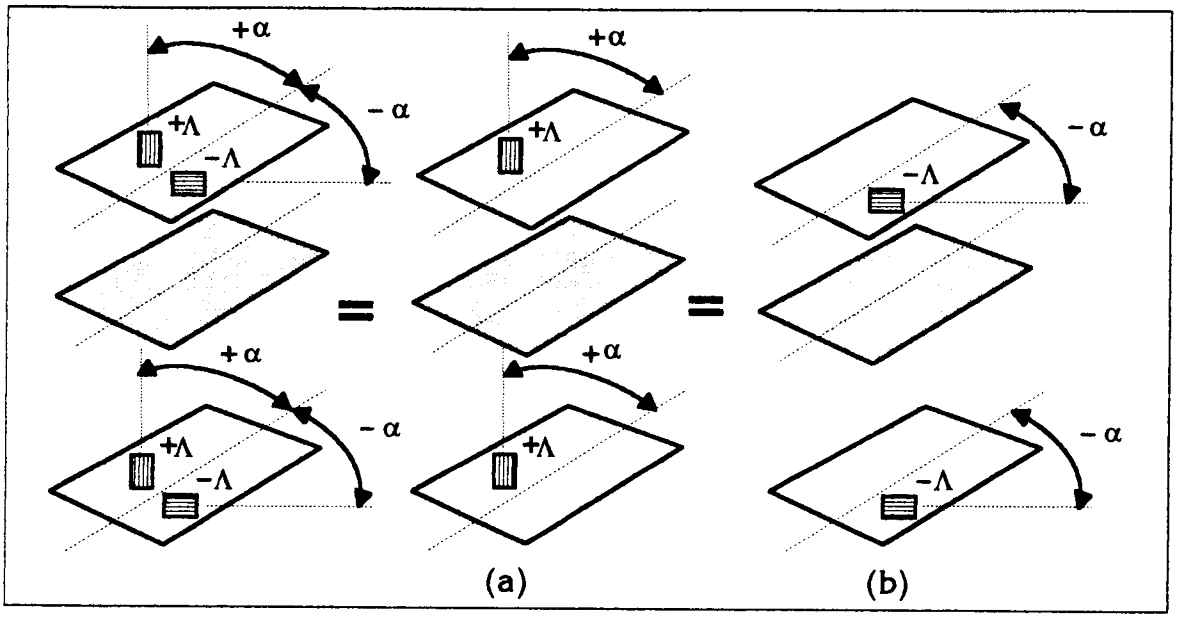

Figure 11 - Resolution of piezoelectric laminae into two components to generate a shear elongation [20]

The analytical model assumes that the piezoelectric elements consist of two components. For the case of shear elongation, component (a) in Figure 11 consists of piezoelectric elements bonded at $\alpha = +45°$ and generating tension. Component (b) consists of elements bonded at $\alpha = -45°$ and generating compression. Since the piezoelectric layer of elements is made up of discrete elements, they do not satisfy the criterion for a continuous laminae for the modified CLPT method. Therefore it is necessary to assume that the elements constitute a continuous laminae. With this assumption, the shear strain ε_{xy} due to both components (a) and (b) in Figure 11 are equal. However, the axial elongational strains ε_x and ε_y for component (a) are equal but opposite in magnitude to that of component (b). Therefore, the solution obtained upon solving equation (12) for the loading shown in Figure 11 for the expression for the shear strain is equal for both of the components (a) and (b). The correct solution for the shear elongation can be extracted from either the loading shown in component (a) or component (b) of Figure 11, knowing that any solution obtained for e_x and e_y of the plate are to be ignored. Validation of this concept is shown in the following section.

As for the shear elongation case, Figure 12 shows the geometrical layout for the analytical model for bending.

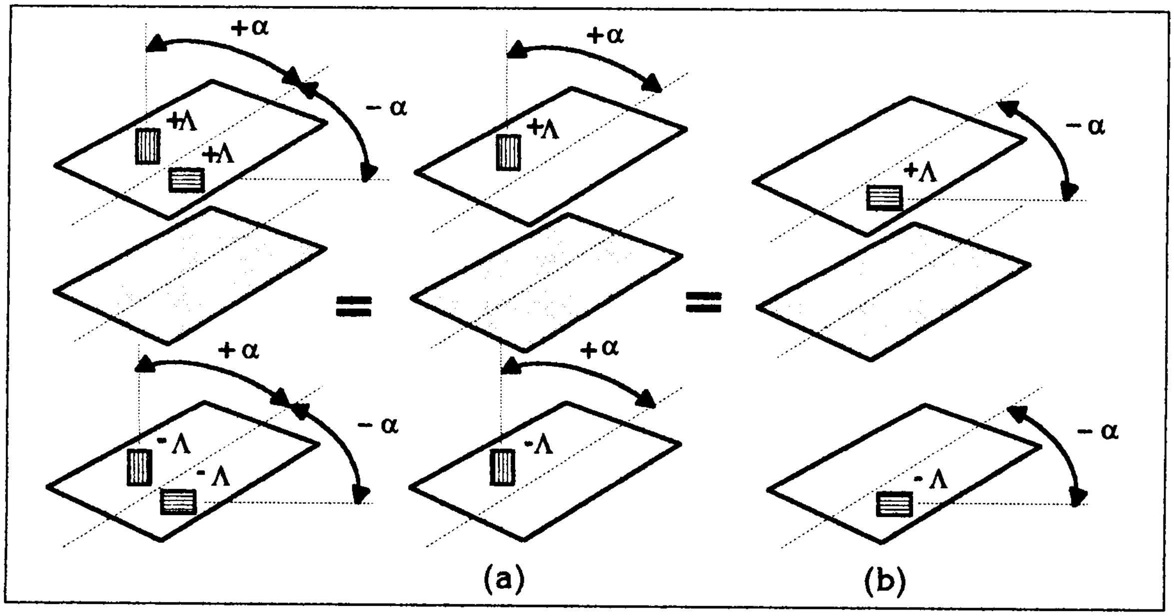

Figure 12 - Resolution of piezoelectric laminae into two components to generate bending [20]

From Figure 12, component (a) consists of piezoelectric elements bonded at α = 45° . For this component, all of the elements on upper surface of the substrate are generating tension, whereas all of the elements on the lower surface of the substrate are generating compression. Component (b) consists of elements bonded at α = -45° . For this component, all of the elements on upper surface of the substrate are generating tension, whereas all of the elements on the lower surface of the substrate are generating compression. As with the case of shear elongation, the curvatures of bending k_x and k_y due to both components (a) and (b) in Figure 12 are equal. However, the twisting curvature of bending strain k_{xy} for component (a) is equal but opposite in magnitude to that of component (b). Again, the solution obtained upon solving equation (13) for the curvatures of bending for the loading shown in Figure 12 requires this assumption for extracting the correct solution. The correct solution for the bending curvatures are extracted from either the loading shown in component (a) or component (b) of Figure 12, knowing that any solution obtained for k_{xy} is to be ignored. Again, validation of this concept is shown in the following section.

4.2 Analytical results of the magnitude of shear and bending displacements of a laminate plate generated using distributed piezoelements.

To solve equations (12) and (13), a symbolic mathematics software package known as MACSYMA (MAC's SYmbolic MAnipulation System) available on the University of Tennessee's VAX Cluster mainframe computing facilities was used. All pertinent data required to solve these equations was input into MACSYMA in the form of batch files. Each of the model's configurations required a separate data file, and they can be found in Appendix 1 of the Thesis. Equation (12) has been solved for the elongational strains for the loadings described in Figure 11. For component (a), the piezoelements generate strain in tension ($+\Lambda$) bonded at +45° ($+\alpha$).

Likewise, for component (b), the piezoelements generate strain in compression ($-\Lambda$) bonded at -45° ($-\alpha$). The results obtained are listed in Table 1.

Table 1 - Analytical solutions to the shear strains of a piezoelectricaly loaded plate

$$\varepsilon_x(+\Lambda,+45^o) = (\Lambda t_a(-4E_{1a}E_{2a}t_a-E_sE_{1a}t_s-E_sE_{2a}t_s+E_sE_{1a}t_s\nu-E_sE_{2a}t_s\nu +4E_{2a}^2t_a\nu^2+2E_sE_{2a}t_s\nu^2))/((2E_{2a}t_a+E_st_s)(-2E_{1a}t_a-E_st_s+2E_{2a}t_a\nu^2+E_st_s\nu^2))$$

$$\varepsilon_y(+\Lambda,+45^o) = (\Lambda t_a(-4E_{1a}E_{2a}t_a-E_sE_{1a}t_s-E_sE_{2a}t_s+E_sE_{1a}t_s\nu-E_sE_{2a}t_s\nu +4E_{2a}^2t_a\nu^2+2E_sE_{2a}t_s\nu^2))/((2E_{2a}t_a+E_st_s)(2E_{1a}t_a+E_st_s-2E_{2a}t_a\nu^2-E_st_s\nu^2))$$

$$\varepsilon_{xy}(+\Lambda,+45^o) = (2E_s(-E_{1a}+E_{2a})\Lambda t_at_s(1+\nu))/((2E_{2a}t_a+E_st_s)(-2E_{1a}t_a-E_st_s +2E_{2a}t_a\nu^2+E_st_s\nu^2))$$

$$\varepsilon_x(-\Lambda,-45^o) = (\Lambda t_a(-4E_{1a}E_{2a}t_a-E_sE_{1a}t_s-E_sE_{2a}t_s+E_sE_{1a}t_s\nu-E_sE_{2a}t_s\nu +4E_{2a}^2t_a\nu^2+2E_sE_{2s}t_a\nu^2))/((2E_{2a}t_a+E_st_s)(2E_{1a}t_a+E_st_s-2E_{2a}t_a\nu^2-E_st_s\nu^2))$$

$$\varepsilon_y(-\Lambda,-45^o) = (\Lambda t_a(-4E_{1a}E_{2a}t_a-E_sE_{1a}t_s-E_sE_{2a}t_s+E_sE_{1a}t_s\nu-E_sE_{2a}t_s\nu +4E_{2a}^2t_a\nu^2+2E_sE_{2a}t_s\nu^2))/((2E_{2a}t_a+E_st_s)(-2E_{1a}t_a-E_st_s+2E_{2a}t_a\nu^2+E_st_s\nu^2))$$

$$\varepsilon_{xy}(-\Lambda,-45^o) = (2E_s(-E_{1a}+E_{2a})\Lambda t_at_s(1+\nu))/((2E_{2a}t_a+E_st_s)(-2E_{1a}t_a-E_st_s +2E_{2a}t_a\nu^2+E_st_s\nu^2))$$

The variables in Table 1 have the following definitions:

$\Lambda = \frac{d_{31}V}{t_a}$: strain transfer to substrate due to piezo-actuation

t_a: piezoelectric actuator thickness

t_s: isotropic substrate thickness

E_{1a}: effective longitudinal modulus of directionally attached piezo-actuator

E_{2a}: effective transverse modulus of directionally attached piezo-actuator

E_s: elastic modulus of isotropic substrate

ν: Poisson ratio

From the results in Table 1, it is apparent that $\varepsilon_x(+\Lambda,+45°)=-\varepsilon_x(-\Lambda,-45°)$, $\varepsilon_y(+\Lambda,+45°)=-\varepsilon_y(-\Lambda,-45°)$ and $\varepsilon_{xy}(+\Lambda,+45°)=\varepsilon_{xy}(-\Lambda,-45°)$. Therefore, it has been shown analytically that the actuators bonded at an angle of $\alpha=+45°$ and generating extensional strains contribute an equal amount to the shear deflection as the actuators bonded at an angle of $\alpha=-45°$ and generating compressional strains. The strains generated by those two types of actuators along the longitudinal and lateral axes of the laminate cancel out each other. The main conclusion from these results is that the investigated layout of piezoelements eliminates the coupling between extensional and shear strains of the laminate.

As for the previous case, Equation (13) has been solved for the bending curvatures for the loadings described in Figure 12. For component (a), the piezoelements on the upper face generate strain in tension ($+\Lambda$) bonded at +45° ($+\alpha$) while the piezoelements on the lower face generate strain in compression ($-\Lambda$) bonded at +45° ($+\alpha$) . Likewise, for component (b), the piezoelements on the upper face generate strain in tension ($+\Lambda$) bonded at -45° ($-\alpha$) while the piezoelements on the lower face generate strain in compression ($-\Lambda$) bonded at -45° ($-\alpha$). The results obtained are listed in Table 2.

Table 2 - Analytical solutions to the curvatures of bending of a piezoelectricaly loaded plate

$$\begin{aligned}k_x(upper,+\Lambda,+45^\circ;\, lower,-\Lambda,+45^\circ) = {} & (6\Lambda t_a(t_a+t_s)(2E_sE_{2a}t_s^3v^2 + 12E_{2a}^2t_at_s^2v^2\\ & +24E_{2a}^2t_a^2t_sv^2 + 16E_{2a}^2t_a^3v^2 - E_sE_{2a}t_s^3v + E_{1a}E_st_s^3v - E_sE_{2a}t_s^3 - E_{1a}E_st_s^3\\ & -12E_{1a}E_{2a}t_at_s^2 - 24E_{1a}E_{2a}t_a^2t_s - 16E_{1a}E_{2a}t_a^3))/((E_st_s^3 + 6E_{2a}t_at_s^2\\ & +12E_{2a}t_a^2t_s + 8E_{2a}t_a^3)(E_st_s^3v^2 + 6E_{2a}t_at_s^2v^2 + 12E_{2a}t_a^2t_sv^2 + 8E_{2a}t_a^3v^2\\ & -E_st_s^3 - 6E_{1a}t_at_s^2 - 12E_{1a}t_a^2t_s - 8E_{1a}t_a^3))\end{aligned}$$

$$k_y(upper,+\Lambda,+45^\circ;\, lower,-\Lambda,+45^\circ) = k_x(upper,+\Lambda,+45^\circ;\, lower,-\Lambda,+45^\circ)$$

$$\begin{aligned}k_{xy}(upper,+\Lambda,+45^\circ;\, lower,-\Lambda,+45^\circ) = {} & (12\Lambda E_s(E_{2a}-E_{1a})t_at_s^3(t_a+t_s)(v+1))/\\ & ((E_st_s^3 + 6E_{2a}t_at_s^2 + 12E_{2a}t_a^2t_s + 8E_{2a}t_a^3)(E_st_s^3v^2 + 6E_{2a}t_at_s^2v^2\\ & +12E_{2a}t_a^2t_sv^2 + 8E_{2a}t_a^3v^2 - E_st_s^3 - 6E_{1a}t_at_s^2 - 12E_{1a}t_a^2t_s - 8E_{1a}t_a^3))\end{aligned}$$

Table 2 only shows the results from the α=+45° piezoelectric orientation. The solutions to the α=-45° orientation are as follows:

$$k_x(upper,+\Lambda,-45^\circ;\, lower,-\Lambda,-45^\circ) = k_x(upper,+\Lambda,+45^\circ;\, lower,-\Lambda,+45^\circ)$$

$$k_y(upper,+\Lambda,-45^\circ;\, lower,-\Lambda,-45^\circ) = k_y(upper,+\Lambda,+45^\circ;\, lower,-\Lambda,+45^\circ)$$

$$k_{xy}(upper,+\Lambda,-45^\circ;\, lower,-\Lambda,-45^\circ) = -k_{xy}(upper,+\Lambda,+45^\circ;\, lower,-\Lambda,+45^\circ)$$

Following the same reasoning for the previous case, any twisting of the plate due to the κ_{xy} component is canceled out. Therefore, the induced bending caused by the piezo-actuators in the prescribed layout causes no twisting of the plate under symmetric loading. Under the assumption that the plate is clamped along the y-axis, the only bending curvature that results are that of κ_x. Again, as with the previous case, either the $\alpha=+45°$ or $\alpha=-45°$ solutions are valid for the analysis.

The computed displacements for both the shear and bending cases for the actual model built and tested will be reported in Chapter 6 for comparison with the numerical models and the experimental plate.

CHAPTER 5

NUMERICAL ANALYSIS

The numerical analysis of the displacements of a laminate plate generated using distributed piezoelements was done with the use of a commercially available finite element package. The finite element package used was Integrated Design Engineering Analysis Software (I-DEAS^{TM}) from Structural Dynamics Research Corporation (SDRC). The versions of I-DEAS^{TM} used were VI and VII.

5.1 Magnitude of shear and bending displacements of a laminate plate generated using distributed piezoelements

Finite element models have been designed to numerically model two piezo-actuator loaded plates. Two distinct piezo-actuator layouts have been modeled; each of the finite element models correspond corresponding with the actual aluminum plate specimens built for testing.

5.1.1 Finite element modeled characteristics of the activated piezoelement

Several important assumptions have been made when modeling the characteristics of the strain transfer from the activated piezoelement to the substrate. First, a perfect bond between the piezoelectric element and the substrate was assumed. This was equivalent to the assumption that either the shear modulus of the bonding material between the actuator and the substrate approached infinity, or that the bonding layer thickness approached zero [1]. Referring to Figure 13, the direction of strain transfer from the piezo-actuator to the substrate was assumed to be parallel to the x-coordinate. The strains generated by the directionally attached piezoelectric elements in the local y and z-coordinate directions were negligible .

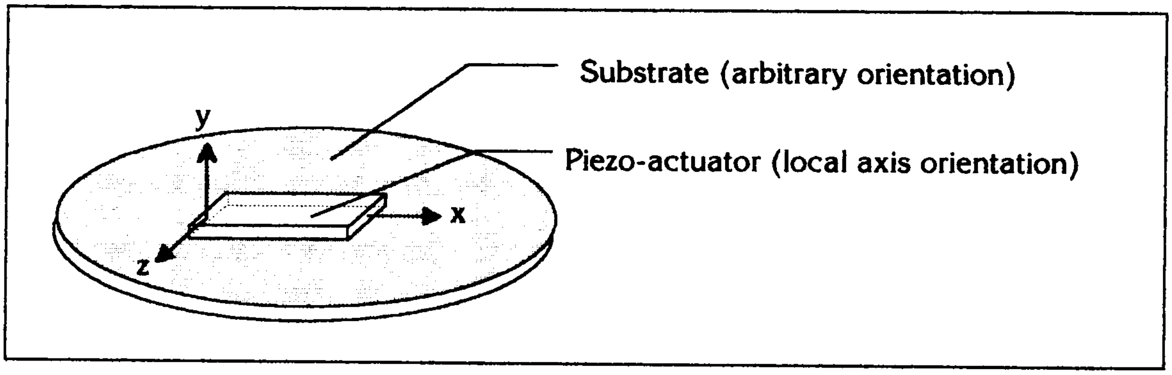

Figure 13 - Piezoelectric element local axis geometry

The actual strain transferred to the substrate was modeled by assuming that the strain transfer was due to forces applied on the edges of the activated piezo-actuator. Three different models of this equivalent force were investigated: that of the strain-energy model [14]; next, the pin-force model [1], and lastly the Linear Shear Stress Model (LSSVM) [13]. The first two cases modeled the strain transferred to the substrate from an activated piezo-actuator pair with constant forces. Please refer to Table 3 for a comparison between the two constant force models.

Table 3 - Comparison between strain-energy and pin-force methods

Case 1	Case 2	strain-energy	pin-force
Pure Bending [13] 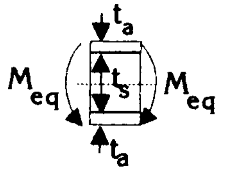	Pure Bending 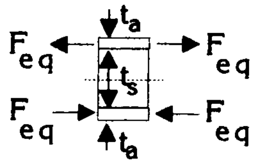	$M_{eq} = \frac{t_s^2 E_s}{6+\Psi} s\Lambda$ $F_{eq} = \frac{M_{eq}}{t_s}$	same $\left(\Psi = \frac{t_s E_s}{t_a E_a}\right)$
Pure extension [13] 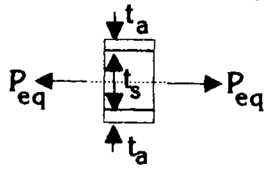	Pure extension 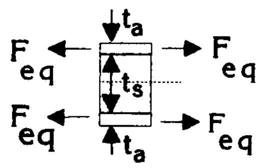	$P_{eq} = \frac{2t_s E_s}{6+\Psi} s\Lambda$ $F_{eq} = \frac{t_s E_s}{6+\Psi} s\Lambda$	$P_{eq} = \frac{2t_s E_s}{2+\Psi} s\Lambda$ $F_{eq} = \frac{t_s E_s}{2+\Psi} s\Lambda$

For the case of pure bending, the expression for the equivalent moment (M_{eq}) for both cases was equal. The equivalent moments used for the numerical models presented within this thesis have been broken down to their equivalent forces (F_{eq}). The geometrical applications of the equivalent forces are shown in Table 3. For the case of pure extension, the expressions for P_{eq} for the pin-force model and the strain-energy model differed. Again, the numerical models presented here use the equivalent forces in given Table 3.

The LSSVM model for the effective axial forces acting on the plate can be expressed as:

$$F_s(x) = \frac{-abE_aE_sh(\lambda_t+\lambda_b-2\Lambda)}{2K_1}\left(K_{10} + K_{11}\frac{\cosh(\eta_1 x)}{\cosh(\eta_1 l)}\right) \tag{14}$$

$$M_s(x) = \frac{-2ab^3E_aE_sh(\lambda_t+\lambda_b)}{6K_0}\left(K_8 + K_9\frac{\cosh(\eta_2 x)}{\cosh(\eta_2 l)}\right) \tag{15}$$

where

$K_{0,1,8,9,10,11}$ are functions of the material and geometrical properties of the plate.

The geometry of the LSSVM analytical model is shown in Figure 14.

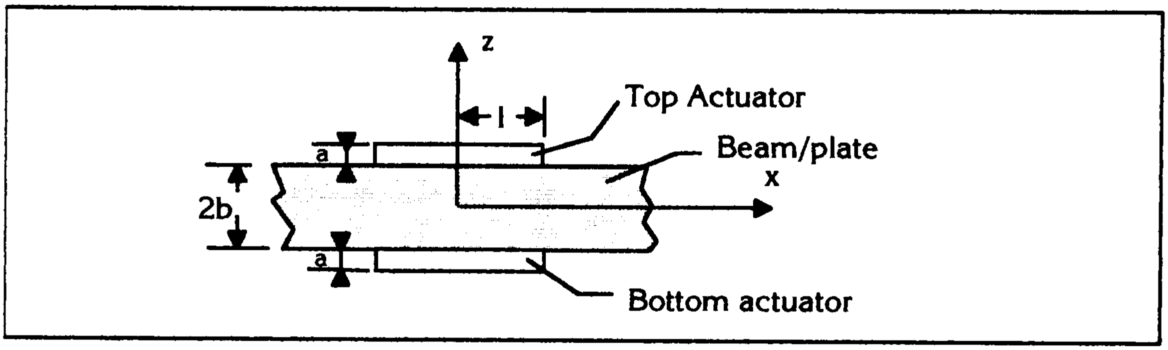

Figure 14 - Geometry of the analytical model [13]

The free-body diagrams of the LSSVM model forces expressed by equations (14) and (15) are shown in Figure 15.

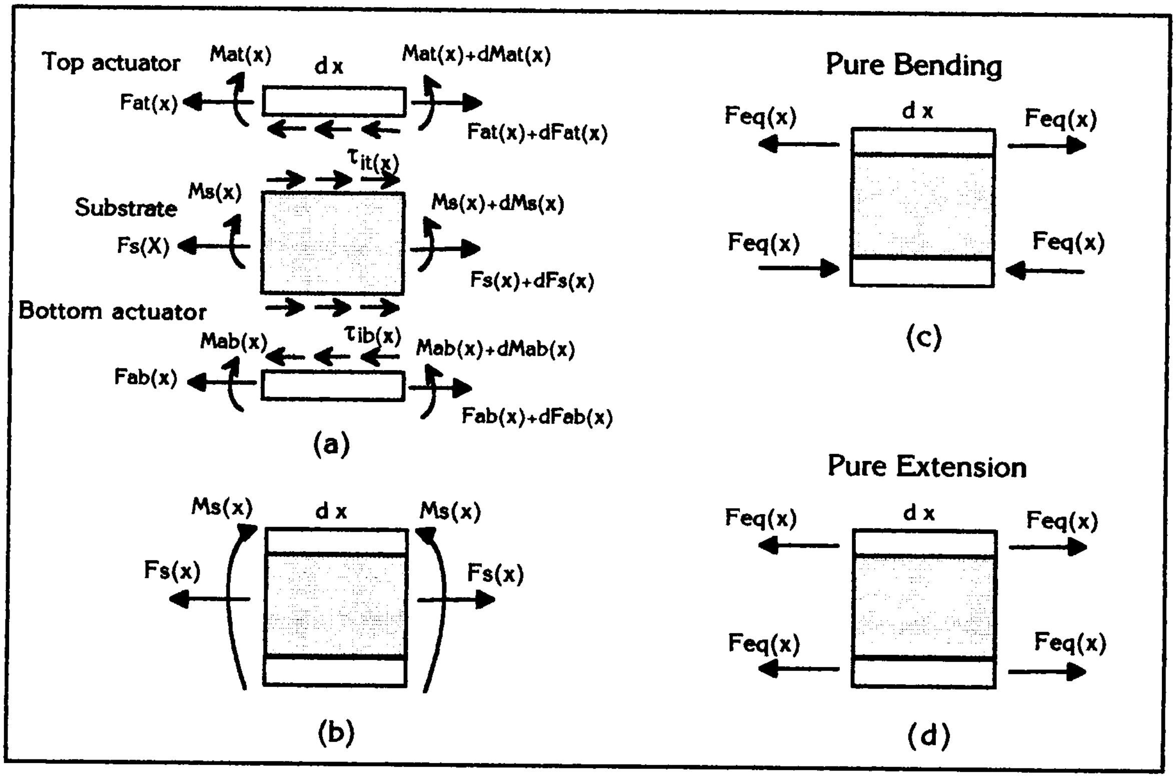

Figure 15 - Free-body diagram: (a) constituent, (b) integrated actuator/beam [13] (c) equivalent forces for pure bending, (d) equivalent forces for pure extension

Figure 15 presents a comparison between the magnitudes of equivalent force among the pin-force, strain-energy, and LSSVM models for an actuator pair activated in pure extension. The calculations used for the comparison are found

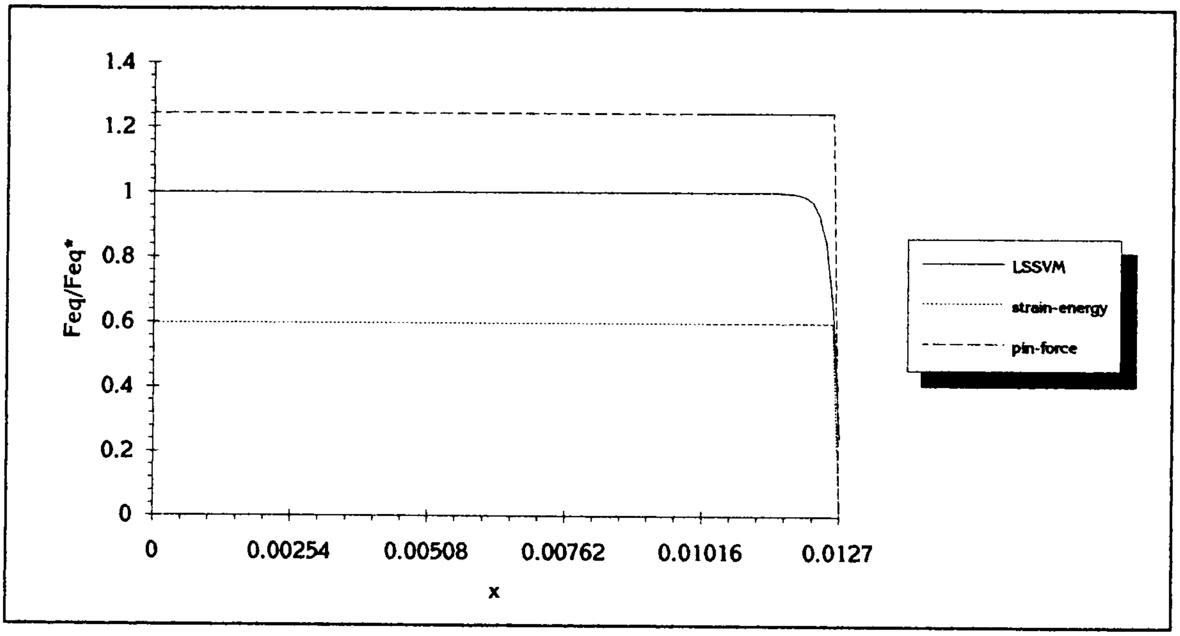

Figure 16 - Comparison between pin-force, strain-energy, and LSSVM equivalent forces under pure extension

in Appendix 2. In Figure 16, all equivalent force values for the calculated pin-force, the strain-energy, and the LSSVM models have been normalized by Feq*. Feq* is the force level at x=0, which corresponds to the center of the activated element(refer to Figure 14) for the LSSVM model. The geometry of the numerical models have been used for the comparisons made in Figure 16 .

A comparison between the magnitudes of equivalent force between the pin-force, strain-energy, and LSSVM models for an actuator pair activated in pure bending was not possible due to the low aspect ratio of actuator thickness to plate thickness [22]. Since the magnitude of equivalent forces for the pure extension case for the LSSVM model falls between that of the pin-force and strain-energy models, the latter two cases will give a sufficient representation of F_{eq} for the numerical models here.

5.1.2 Description of the finite element models for the plate with piezoelements

All of the finite element models in this section are three dimensional. The properties of the finite element models are listed in Table 4.

Table 4 - Properties of finite element models

Specimen	Material properties of elements	Physical properties of elements
Aluminum plate	Modulus of elasticity : 63 E+9 Pa Shear modulus : 23.684 E+9 Pa Poissons ratio : .33	Order : linear Family : solid bricks
Steel beams	Modulus of elasticity : 63 E+12 Pa Shear modulus : 23.684 E+12 Pa Poissons ratio : .33	Order : linear Family : solid bricks

For each of the two piezo-actuator layouts, two finite element models were built. For each of the layouts, one model had a restraining rigid steel bar mounted to the plate, and the other model had this edge free (see Figure 17 for details).

The actual finite element models with their equivalent force loadings for shear displacement are shown in Figures 18,19,20, and 21.

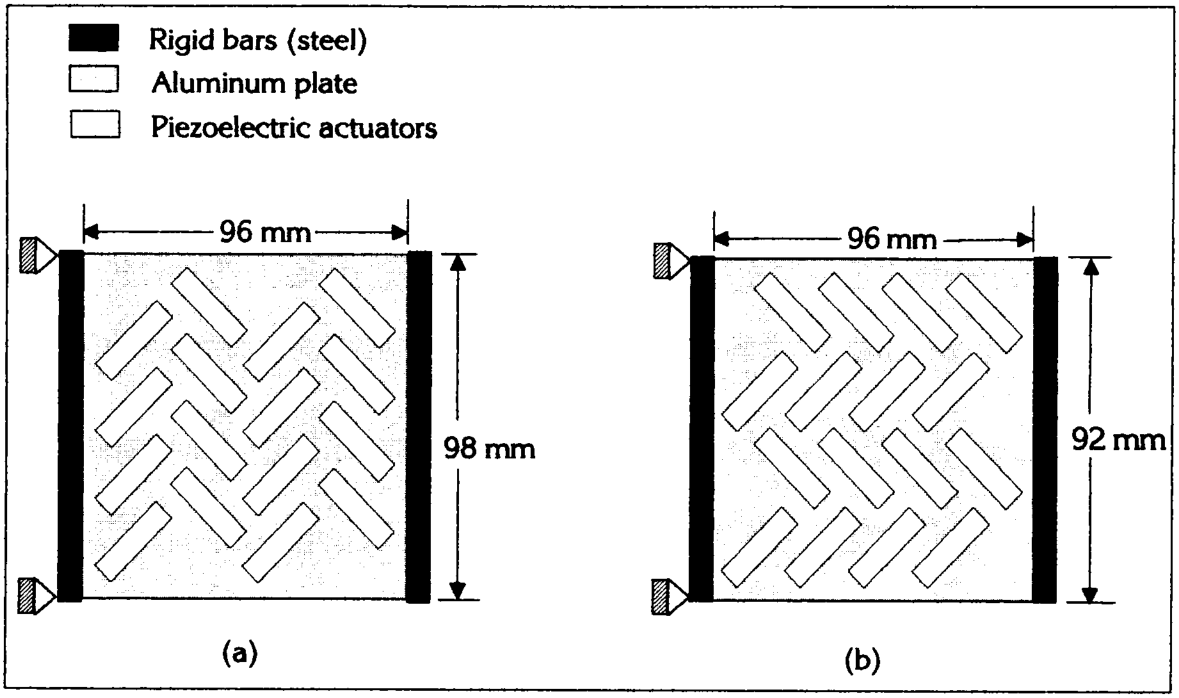

Figure 17 - Diagram of both plate/actuator geometries: (a) layout one, (b) layout two

Figure 18 is a picture of the finite element model for piezo-actuator/plate layout one (with rigid steel bar). The aluminum plate for layout one had dimensions of 0.096 m by 0.098 m by 2.794 E-4 m. The model consisted of 48 finite elements by 49 finite elements, where each element had dimensions of 2 E-3 m by 2 E-3 by 2.794 E-4 m. The free rigid steel beam was modeled by the last column of finite elements opposite to the supported edge of the plate. The finite elements for the bar had the same dimensions as the finite elements for the aluminum plate. The properties for the finite elements are listed in Table 4. The properties of the rigid bar were made based on the assumption that no strains induced to the bar from the plate will cause any deformations of the bar. Therefore, the modulus of elasticity for the rigid bar has been increased to ensure that no deformations will occur. The

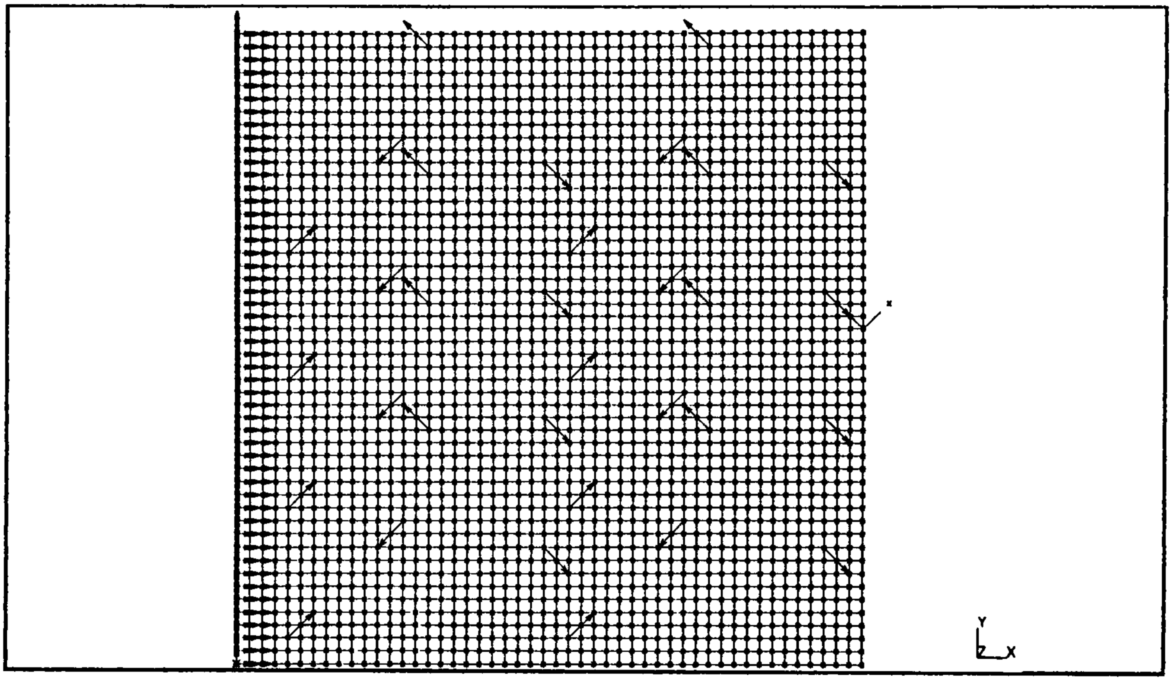

Figure 18 - Finite element model for layout one, with rigid steel bar, loaded for shear displacement

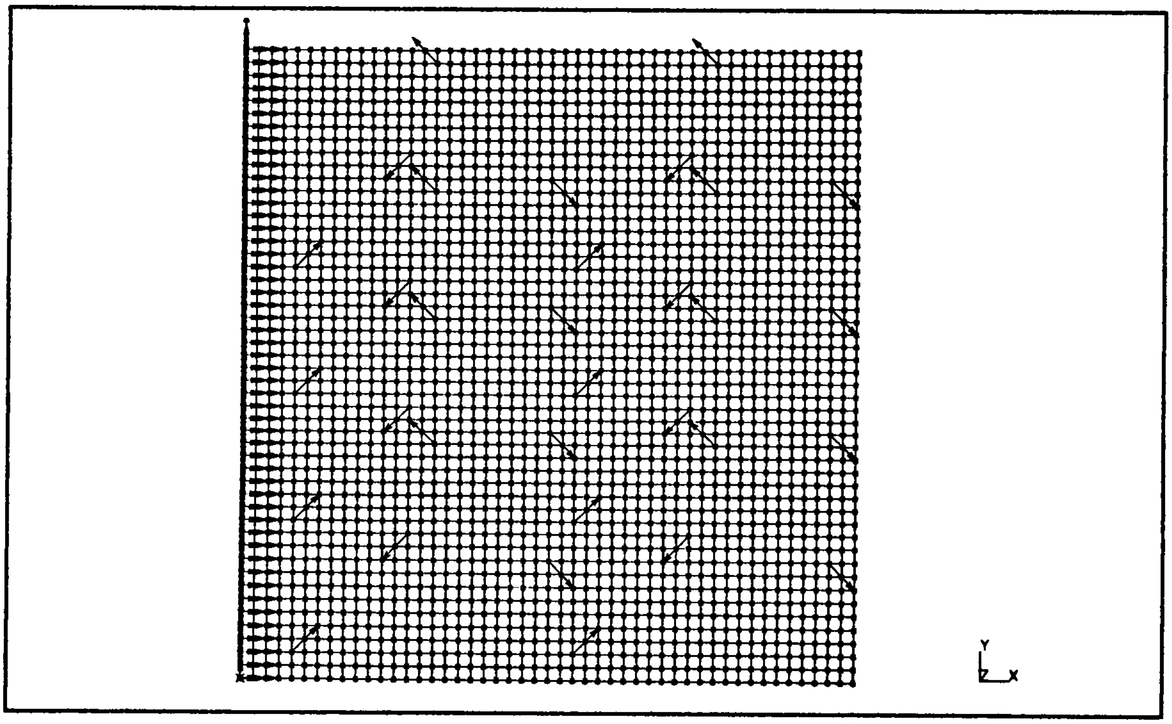

Figure 19 - Finite element model for layout one, no rigid steel bar, loaded for shear displacement

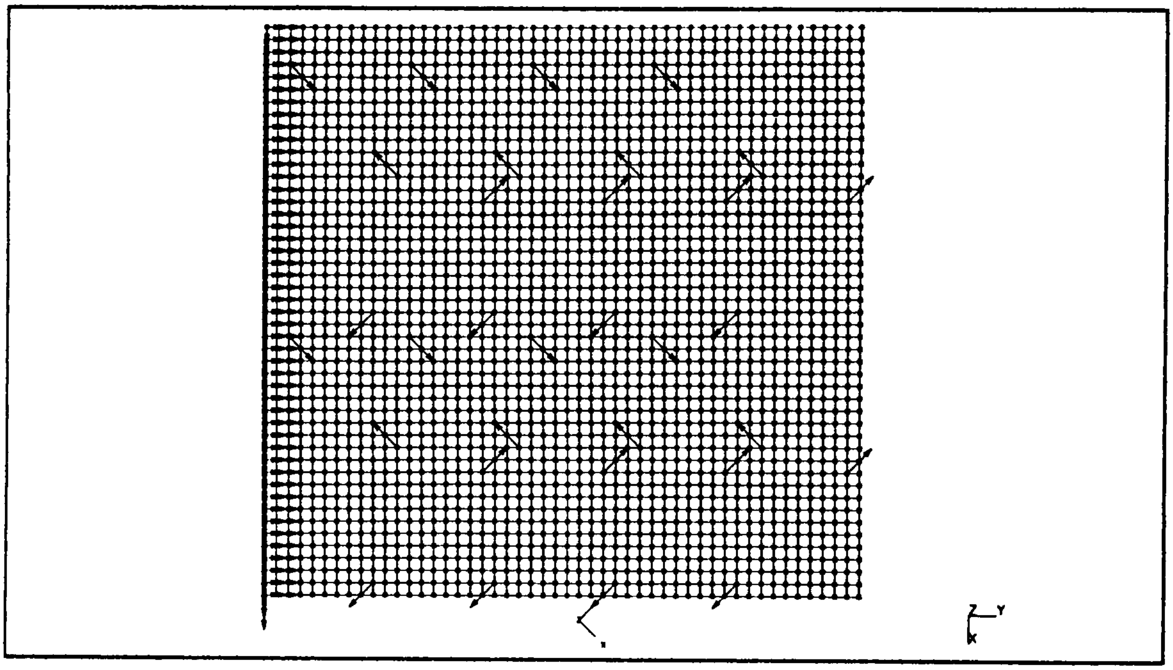

Figure 20 - Finite element model for layout two, with rigid steel bar, loaded for shear displacement

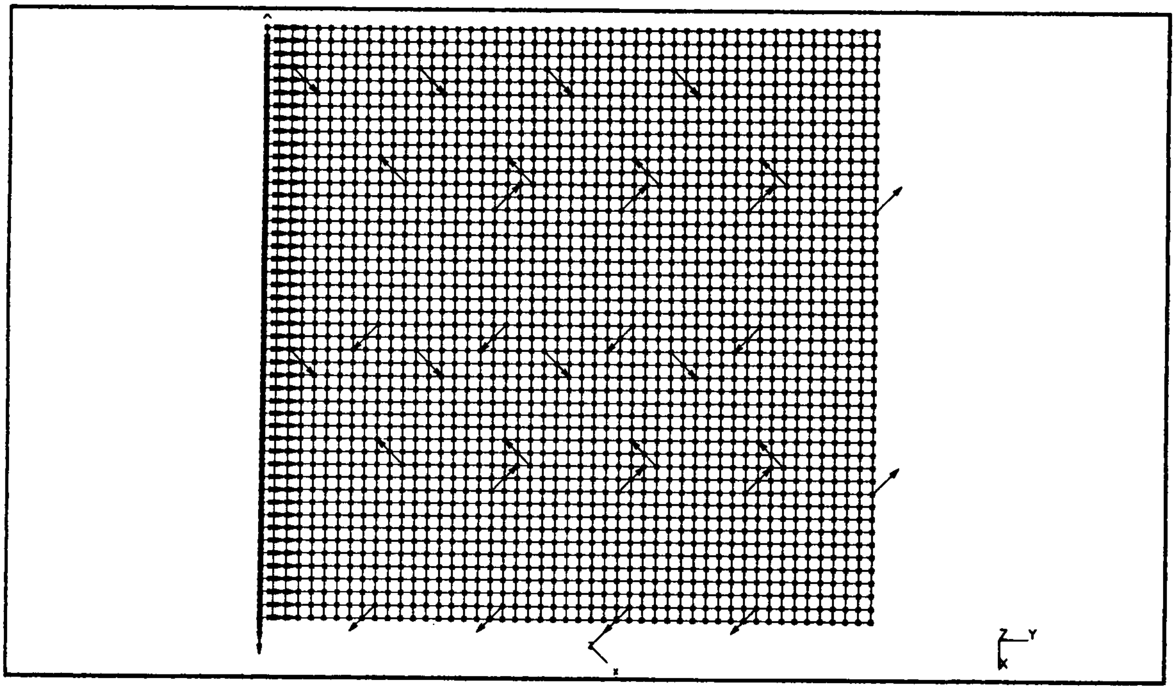

Figure 21 - Finite element model for layout two, no rigid steel bar, loaded for shear displacement

clamped rigid bar was replaced with zero degree of freedom restraints applied to nodes along the edge of the beam. The equivalent forces were modeled as nodal forces corresponding to the center of the edges of the activated piezo-actuators. The only difference between the models for the plate with rigid bar and the plate with no rigid bar (Figure 19) was that the last column of finite elements was removed for the latter case.

Figure 20 shows the finite model for piezo-actuator/plate layout two (with rigid steel bar). The aluminum plate for layout two had dimensions of 0.096 m by 0.092 m by 2.794 E-4 m. The model consisted of 48 finite elements by 41 finite elements, where each finite element had dimensions of 2 E-3 m by 2 E-3 by 2.794 E-4 m. Again, the free rigid steel beam was modeled by the last column of finite elements opposite to the supported edge of the plate. The assumptions for the boundary conditions and the rigid bar characteristics were the same as those for layout one. As with layout one, the only difference between the models of the plate with rigid bar and the plate with no rigid bar was that the last column of finite elements was removed for the latter case.

The finite element models for the case of bending of the plate due to the piezoelements were the same as those for the shear displacement cases. The only change for the bending displacement case was that the equivalent forces were applied to nodes in order to produce the equivalent moments required.

The results of the numerical analysis will be presented in Chapter 6 of the Thesis for comparison with the analytical model and the experimental plate.

CHAPTER 6

ALUMINUM PLATE TESTING

6.1 Aluminum plate fabrication

An aluminum plate with surface mounted piezoelectric elements was fabricated to correlate the numerical and analytical model data. The plate was used to show the shear inducing capability of the proposed layouts of piezoelements (Figure 17). The general steps for manufacturing the plate model are shown in Figure 22.

6.1.1 Description of piezoceramic elements used to induce shear displacement and bending displacements in the plate

The piezoelectric elements used in this study were PZT G1195 lead zirconate titanate, with nickel full coating on the top and bottom faces of the piezoelements. The elements were purchased from PIEZO SYSTEMS, INC., precut and pre-poled. The electro-mechanical properties of the G1195 piezoelements are listed in Table 5.

Table 5 - Electro-mechanical properties of G1195 piezoceramic

Curie temperature............................T_c	~360	°C
Coercive field.................................E_c	1.2 E6	V/m
Density..ρ	7650	Kg/m^3
Piezoelectric charge coefficient.......d_{31}	190 E-12	m/V
Piezoelectric voltage coefficient......g_{31}	11E-3	V-m/N
Elastic moduli..................................E	63 E+9	N/m^2
Maximum Actuation Potential......ε_{MAX} [24]	(1.968 to 2.362)E+6	V/m

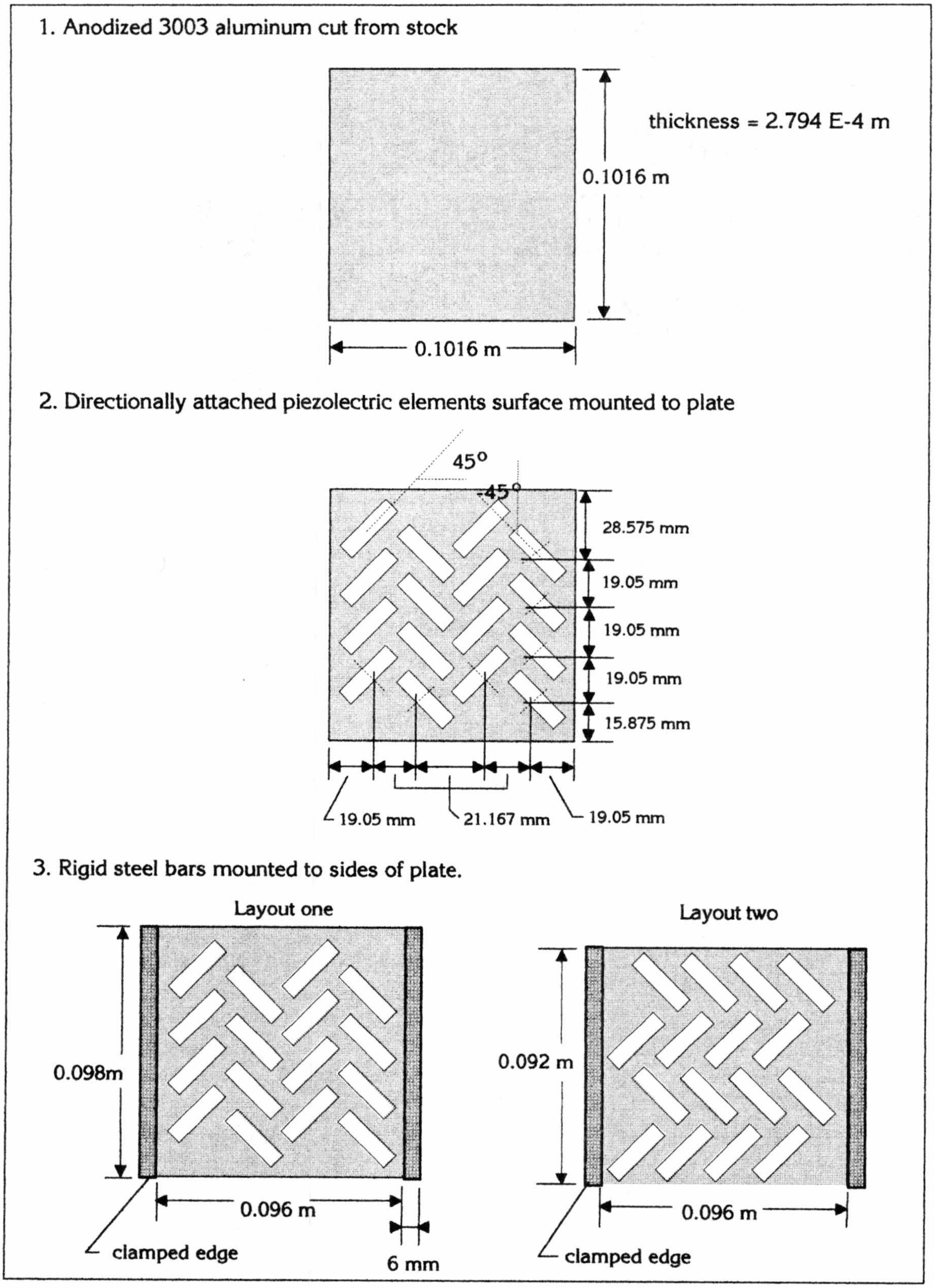

Figure 22- General steps for manufacturing the plate

The elements have dimensions of 0.0254 m 6.35 E-3 m by 1.905 E-4 m. For designation of the poling direction, the high voltage face of the elements were marked with a red stripe by the manufacturer. The response of a piezoelement to an activation potential (V) through its thickness with respect to the elements' poling

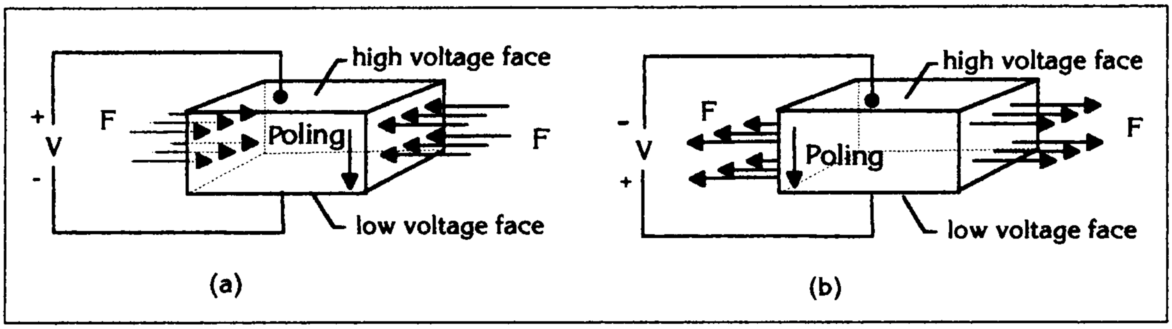

Figure 23 - Piezoelectric activation voltage responses: (a) compression, (b) extension

direction are shown in Figure 23. Figure 23 (a) shows the response of a directionally attached piezoelectric element to a voltage applied through the piezoelement in the poling direction. Figure 23 (b) shows the response of a directionally attached piezoelectric element to a voltage applied through the piezoelement in the opposite direction to the poling direction.

6.1.2 Details of the preparation of the piezoelectric elements for directional attachment

The first step of preparing the elements for directional attachment to the plate. The low voltage face the of the elements were prepared to be bonded to the plate. This side was first sanded with 600 grit paper, then cleaned with Blue Shower cleaner/degreaser. Next, a solder dot was made on the middle of the edge of the element. A 25 watt soldering iron and 60/40 tin/lead solder were used for all soldering. Approximately 30.5 cm of 32 gage teflon coated thermocouple wire, purchased from OMEGA Engineering, Inc. was tined and soldered to the element. A multimeter circuit tester was then used to ensure a good solder connection had been made. The solder flux was then removed with solder flux remover. The solder dot was then filed and/or sanded with 400 grit paper to 2.03 E-4 m or less. The element was again cleaned with the cleaner/degreaser, making sure not to touch the cleaned face with anything that could contaminate it. Next, two layers of 6.35 E-5 m thick 3M Scotch tape were applied to the soldered face and trimmed. The arrangement of the tape was such that the directional attachment properties of the element would be maximized. The final step included one more check for a good connection between the wire and element, as well as one last cleaning and degreasing. This concluded the preparations of the low voltage poled face of the elements for directional attachment. These elements were then stored until needed.

The aluminum used for the plate was donated by the Aluminum Company of America (Alcoa) in Alcoa, Tennessee. The aluminum chosen was 3.048 E-4 m thick 3003 aluminum. The aluminum was anodized by prior to being cut to size , as well as before mounting the prepared piezoelements. The properties of the anodized aluminum plate are shown in Table 6.

After the aluminum plate was anodized, the aluminum was cut to the dimensions shown in Figure 22. The next step was to drill a series of 0.41275 mm holes through the plate to accommodate the solder dots on the low voltage poled face of the prepared piezoelements. Extreme caution was taken to avoid any

Table 6 - Properties of anodized aluminum

Modulus of elasticity	: 63 E+9 Pa
Shear modulus	: 23.684 E+9 Pa
Poissons ratio	: .33
Thickness	: 2.794 E-4 m

bending or warping of the plate. After the holes were drilled, the plate was ready for the attachment of the prepared piezoelements.

6.1.3 Piezoelement bonding procedure

The prepared piezoelements were bonded to the plate with Eccobond LV-45 two part epoxy resin, purchesed from EMERSON & CUMMING Inc. This epoxy exhibits a high shear strength adhesive recommended for joining dissimilar materials. The epoxy resin was prepared by mixing four parts by weight of Eccobond LV-45 epoxy resin with one part by weight of Eccobond LV-45 catalyst. This composition of the two parts resulted in a rigid bonding layer with the properties stated in Table 7.

Table 7 - Properties of cured Eccobond LV-45 bonding layer

Physical properties		Thermal properties		Electrical properties	
Tensile Lap Shear Strength		Service temperature		Dielectic strength	
25 °C	1.643 E+6 Pa	Upper limit	95 °C	1.458 E+7 to	V/m
65 °C	8.902 E+5 Pa	Lower Limit	-55 °C	1.574 E+7	

Prior to bonding the prepared elements, the plate was marked off with guide lines to ensure that the elements were to be mounted at the proper angle. The α=+/-45° layout of the elements on the plate is shown in Figure 22. Note that sixteen element pairs of elements were bonded to the plate. The exact specifications of a bonded pair of piezoelements is described in Figure 24.

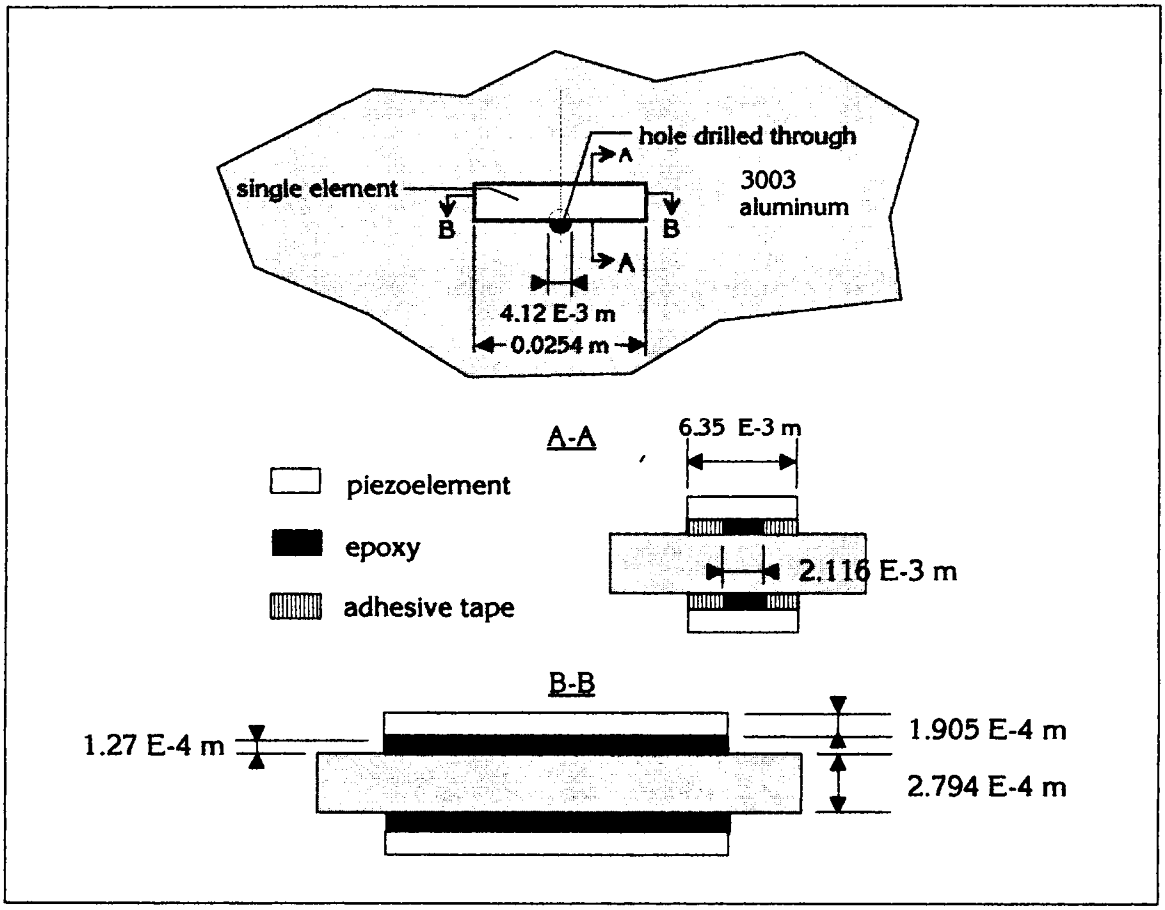

Figure 24 - Details of bonding geometry for a directionally attached piezoelement pair

Before the elements were bonded, the bond area of the plate and the prepared elements were cleaned and degreased. The epoxy was then applied to the element along the gap between the strips of tape (see Figure 24) on the low voltage face of the element. Then, the element was placed in its proper orientation and held in place with tape. This process was repeated until one entire side of the plate had all of its sixteen elements mounted. The bonds of the elements were allowed to cure for 24 hours at room temperature before removing the mounting tape. After the 24 hour cure, the tape was removed and the side of the plate with the elements was once again cleaned and degreased. Next, the plate was turned over and rested upon a 0.0254 m thick piece of foam rubber to protect the bonded elements. Figure 25 is a photograph of the plate to this stage.

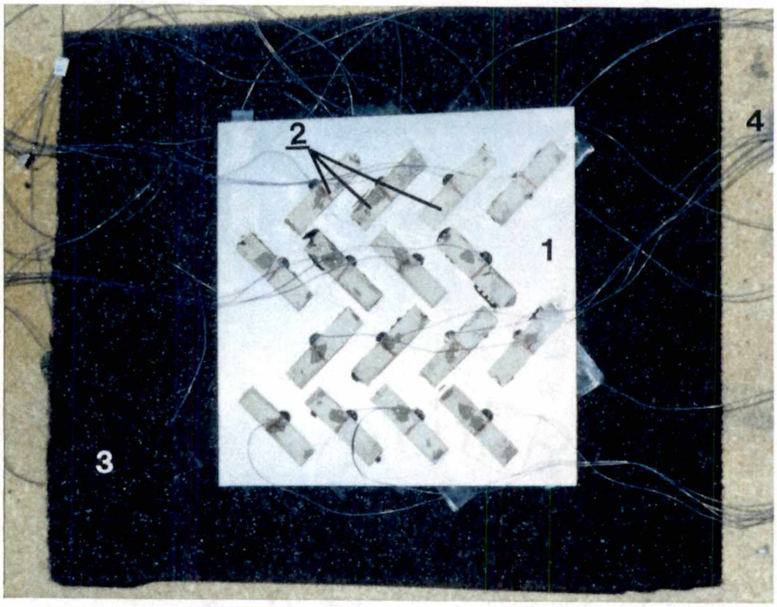

Figure 25 - Photograph of intermediate step in plate fabrication

Referring to Figure 25, the labeling of the plate corresponds to:

1. Aluminum plate
2. Piezoelectric elements
3. Foam rubber protective matting
4. Low voltage face 32 gage teflon wire leads

Now, the entire process described for mounting the piezoelements was repeated on the opposite side of the plate

6.1.4 Finishing procedures of plate manufacturing

The next step in the fabrication of the plate was the mounting of the two rigid steel bars to the sides of the plate, as previously shown in Figure 22. The steel bars had a channel cut into them so that an edge of the plate would fit snugly. Figure 22 shows the steel bar that was used as the clamped support during the plate experiments. It was used for mounting the plate in the stand designed for the plate experiments. The other steel bar served as a guide for the plate . The guide on the plate was sandwiched between a set of four sealed bearings mounted on the shear plate displacement testing stand. After the epoxy used to bond the bars to the edges of the plate was allowed to cure for 24 hours, the wire leads to the high voltage poled faces of the piezoelements were soldered. 30 gage teflon coated copper wire was used for the leads. Here, the high voltage face was prepared for a solder dot in the same manner as for the low voltage poled face. The placement of the solder dot was in the exact center of the high voltage poled face. Approximately 30.5 cm of the 30 gage teflon copper wire was then tinned and soldered to the bonded elements. The solder dots were not filed or sanded. The remaining step to the fabrication of the plate involved labeling the wires (thus the elements) for identification and preparing the plate to be mounted in the test stand. The labeling of the wires and elements is shown graphically in Figures 26 and 27.

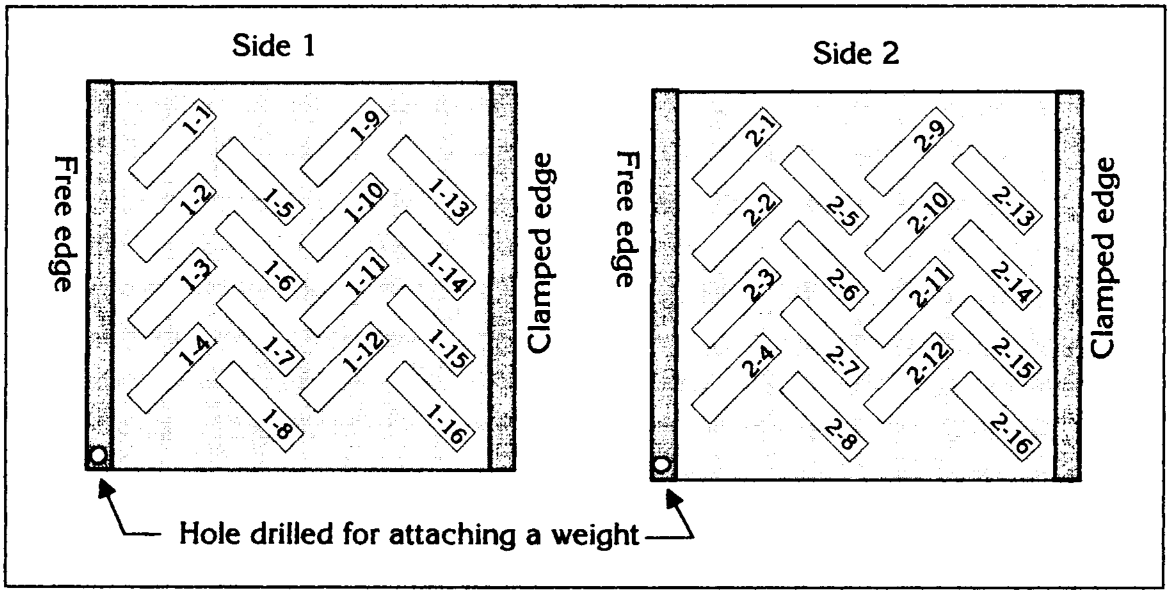

Figure 26 - Details of element labeling, layout one

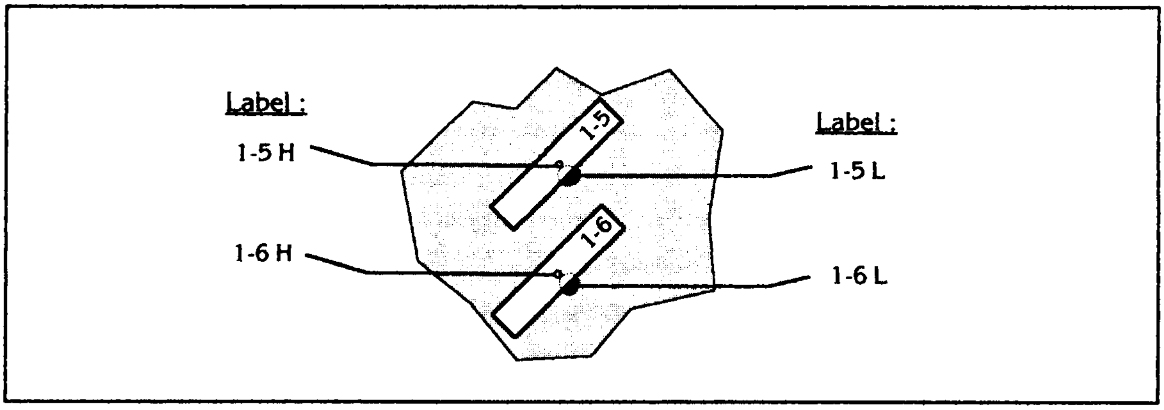

Figure 27 - Details of wire labeling

After the wires were labeled they were wound to connect together by each bank (column) of four elements. This left only eight bundles of wires leaving the plate for easier manageability. A photograph of the completed plate model is shown in Figure 28. Referring to Figure 28, the labeling of the plate corresponds to:

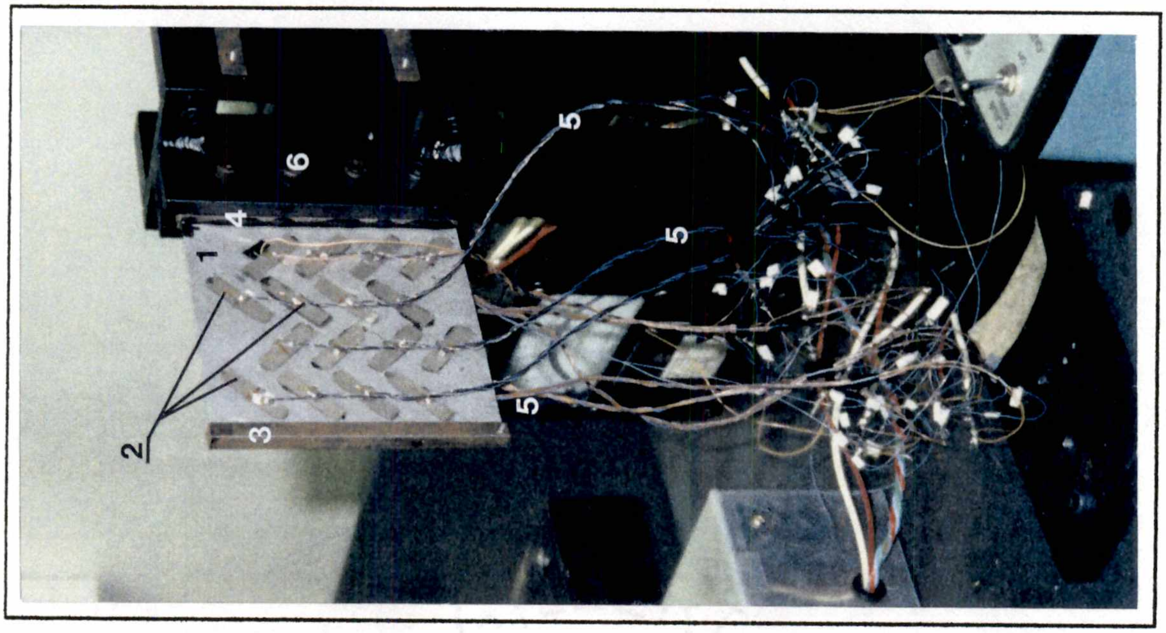

Figure 28 - Photgraph of completed plate with piezoelements, layout one

1. Aluminum plate
2. Piezoelectric elements
3. Free edge rigid steel bar
4. Clamped edge rigid steel bar
5. Bundle of wire leads
6. Plate testing stand

The completed plate was then ready to be mounted into the plate test stand.

6.2 Investigation of the shear modulus and bending rigidity of the plate with piezoelements

No theory on the effect to the shear modulus and bending rigidity of a plate due to discretely attached piezoelements exist.. Therefore, a comparison between the shear modulus and the bending rigidity of the plate before and after the addition of the surface mounted piezoelectric elements was done. This test was performed in order to calculate the effect upon the shear modulus and bending rigidity due to the addition of the piezoelements. Since the test required shearing and bending the plate by an external force, which in turn could damage some of the piezo-actuator bonds, this test was the final experiment performed on the plate. Therefore, the values for the shear modulus as well as for the bending rigidity of the plate were calculated for the piezo-actuator layout two only.

6.2.1 Experimental investigation of the shear modulus of the plate with piezoelements

The schematic of the experimental setup for the investigation of the shear modulus of the plate is shown in Figure 29. The actual experimental set-up for the experiment is shown in Figure 30. To insure true shear displacement for the experiment, the top, bottom, and center of the plate was restrained from any bending displacements. To help ensure that a vertical displacement of the plate was maintained, the rigid bar opposite to the clamped end of the plate was sandwiched between a set four sealed bearings on the testing stand. The bearing guide was not

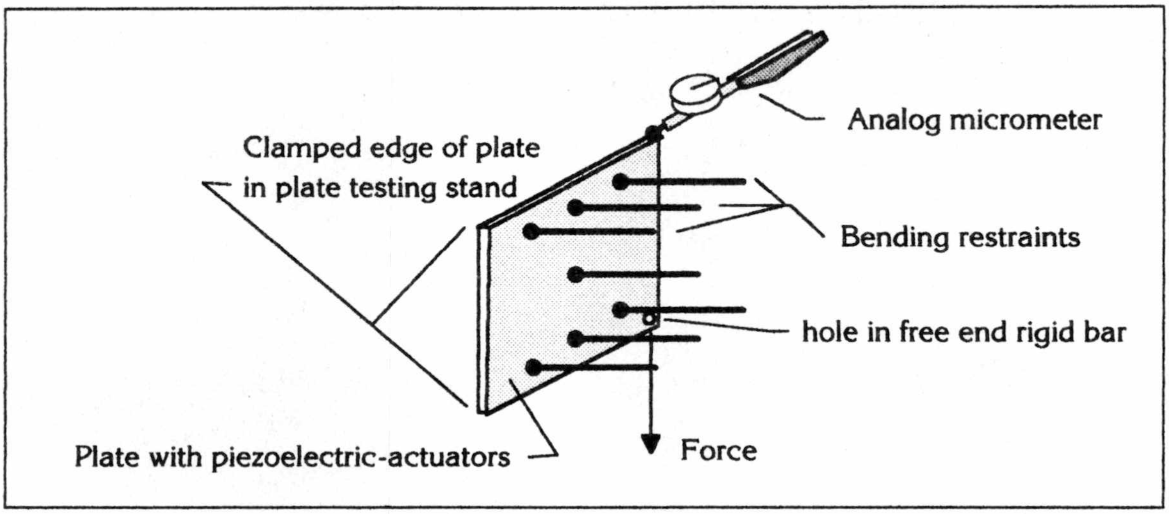

Figure 29 - Experiment set-up for shear modulus of plate measurement

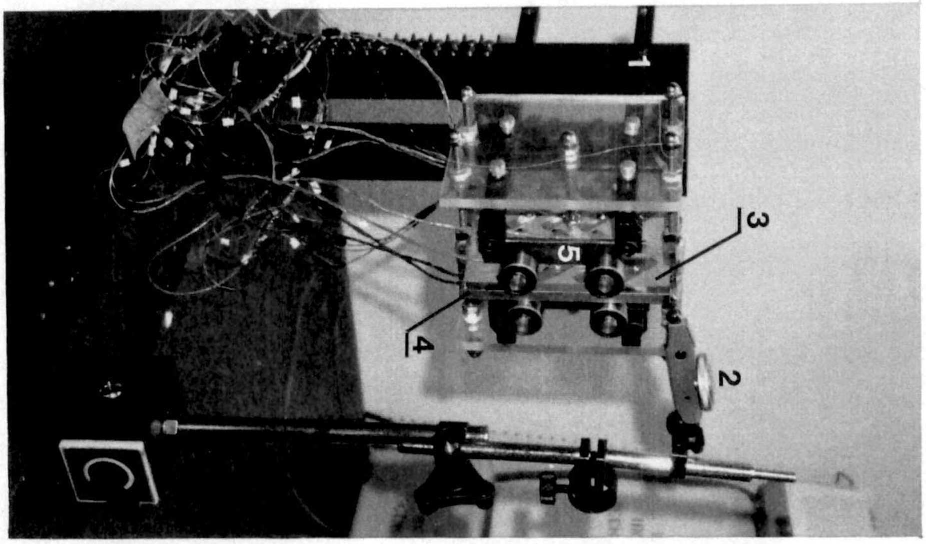

Figure 30 - Photograph of the experimental plate mounted in testing stand

shown in Figure 29 for the sake of clarity of the drawing. To induce shear displacements, masses were suspended from the hole in the free end of the rigid steel bar. The shear displacements were measured with an analog micrometer placed on the top of the free edge rigid bar as shown in Figure 29. The micrometer used was a Scherr Tumico 50-5077 analog micrometer. The least count of the micrometer was 2.54 E-6 m. Referring to Figure 30, the labeling of the plate corresponds to:

1. Plate testing stand
2. Analog micrometer
3. Plate with piezoelements
4. Free end rigid steel bar
5. Sealed bearing guide for the free end rigid steel bar

The results for the shear displacement versus force of the loading described above are plotted in Figure 31. The plot shows that the shear displacement versus force was very linear; therefore, an arbitrary force and displacement from the best fit line was chosen for the calculation of the shear modulus. The details for the calculation can be found in Appendix 3.

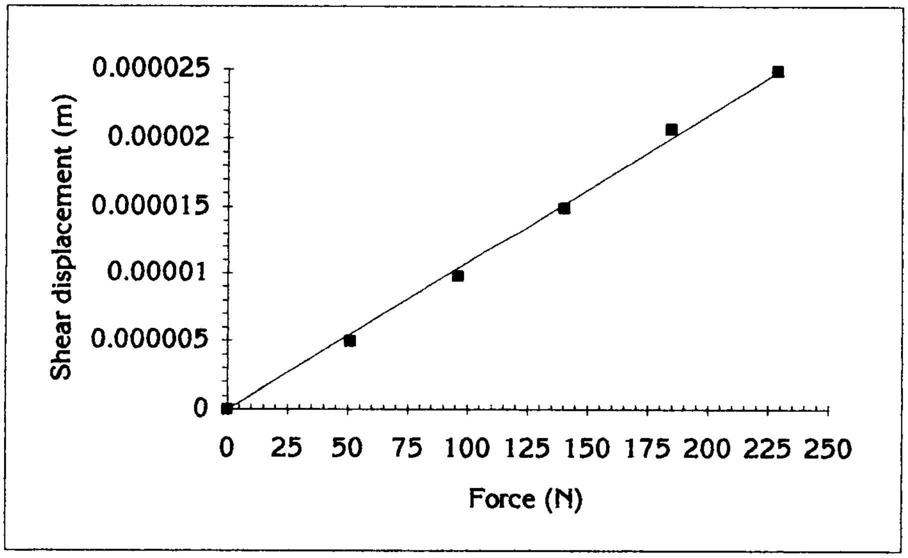

Figure 31- Shear displacement of plate versus applied force

The calculated experimental value for the shear modulus of the plate with the piezoelements arranged in layout two was 34.4E+9 Pa. The aluminum (no piezoelements) plate has the value of shear modulus of 23.68 E+9 Pa (Table 6). This coincides with a 10.72 E+9 Pa increase between the experimental value and the aluminum (no piezoelements) plate (Table 6). This showed that the addition of the piezoelements had the net effect of increasing the shear modulus of the aluminum plate by 45.25%.

6.2.2 Experimental investigation of the bending rigidity of the plate with piezoelements

The experimental setup for the bending rigidity of the plate is shown in Figure 32. The actual experimental set-up for the experiment is shown in Figure 33. No additional restraints were placed on the plate. Masses were suspended to provide a force on the free end rigid steel bar to induce bending displacements. The bending

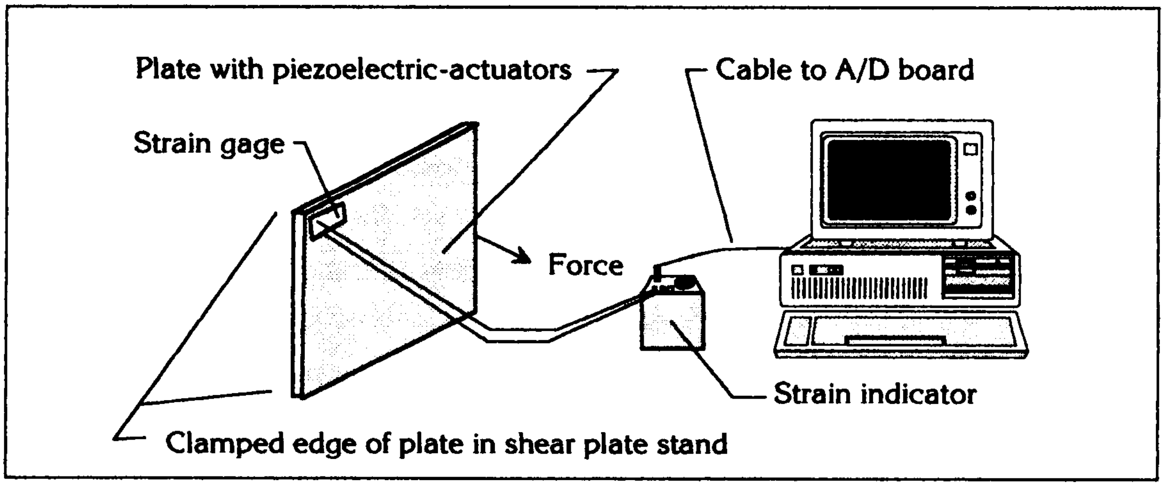

Figure 32 - Experiment set-up for bending rigidity of the plate

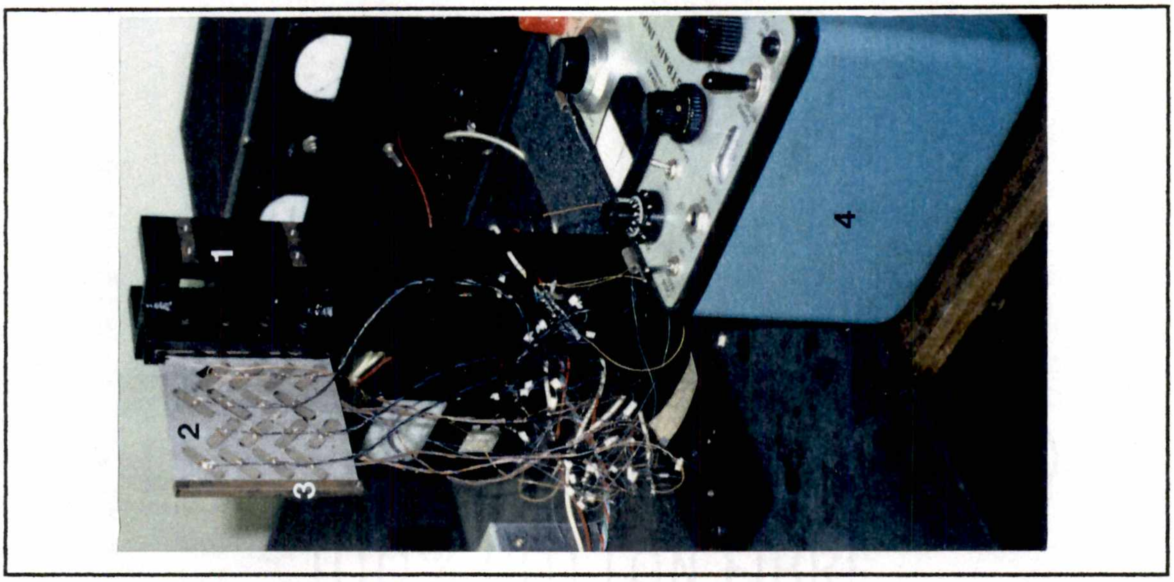

Figure 33 - Photograph of the experimental plate mounted in testing stand for bending rigidity test

displacements were measured with one strain gage mounted in the upper corner of the test plate. A Model P-350 A Vishay Instruments strain indicator was used. The analog signal output of the strain indicator was linear to +/- 250 mV DC. The output from the strain indicators were fed into a 16 channel CIO-AD16 analog to digital converter from Computer Boards, Inc.. The A/D converter was connected to an IBM PC-8088 computer. The resolution of the A/D board was 12 bit corresponding to a full scale range setting of +/- 500 mV DC. Referring to Figure 33, the labeling of the plate corresponds to:

1. Plate testing stand
2. Plate with piezoelements
3. Free end rigid steel bar
4. Strain indicator

Before the experimental data was taken, it was necessary to show that the strains measured by the strain gage/indicator set-up was a valid method to collect the bending displacement data. Through a series of tests, it was shown that the method did represent an accurate and repeatable means to measure the bending displacement of the plate.

The results for the bending displacement versus force of the loading described above are plotted in Figure 34. This bending displacement of the plate was calibrated using a known displacement of the plate and its corresponding voltage output from the strain indicator. The data for the calibration and remaining test runs was collected on the computer by the A/D board. The plot shows that the bending displacement versus force was close to linear; therefore, an arbitrary force and displacement from the best fit line was chosen for the calculation of the bending rigidity. The details for the calculation can be found in Appendix 4.

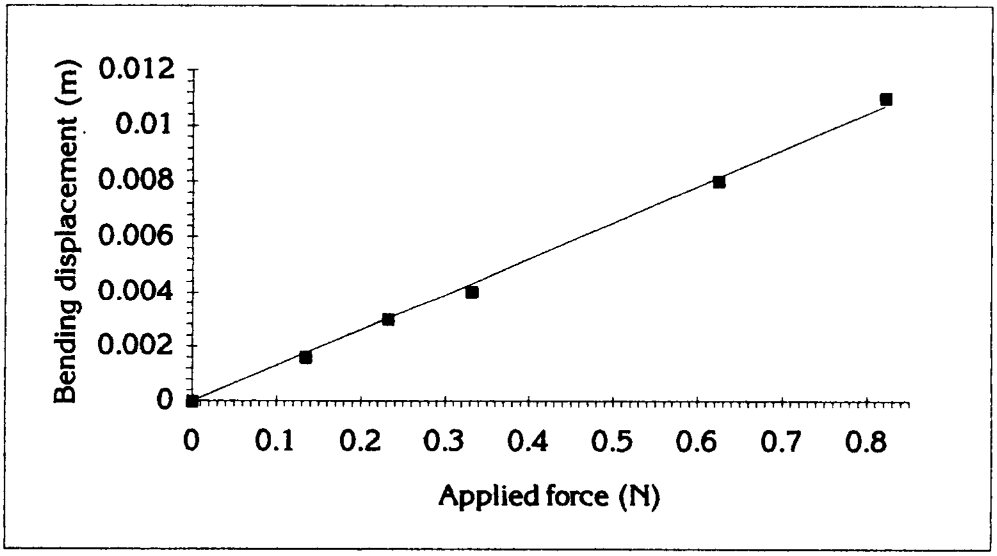

Figure 34 - Bending displacement of plate versus force for bending rigidity calculation

The calculated experimental value for the elastic modulus of the plate with the piezoelements arranged in layout two was 135.3 E+9 Pa. This experimental value for the elastic modulus gave a value of 0.0226 Nm^2 for the bending rigidity. The aluminum (no piezoelements) plate has the value of bending rigidity of 0.015 Nm^2 (Table 6). This value coincides with a 0.076 Nm^2 increase between the experimental value and aluminum (no piezoelements) plate (Table 6). This showed that the addition of the piezoelements had the net effect of increasing the bending rigidity of the aluminum plate by 114.75%.

6.3 Experimental investigation of induced shear displacement of the plate with piezoelements in layout one and two

The experimental set-up for the induced shear displacement due to the activation of the piezo-actuators for both of the layouts is shown in Figure 35. The

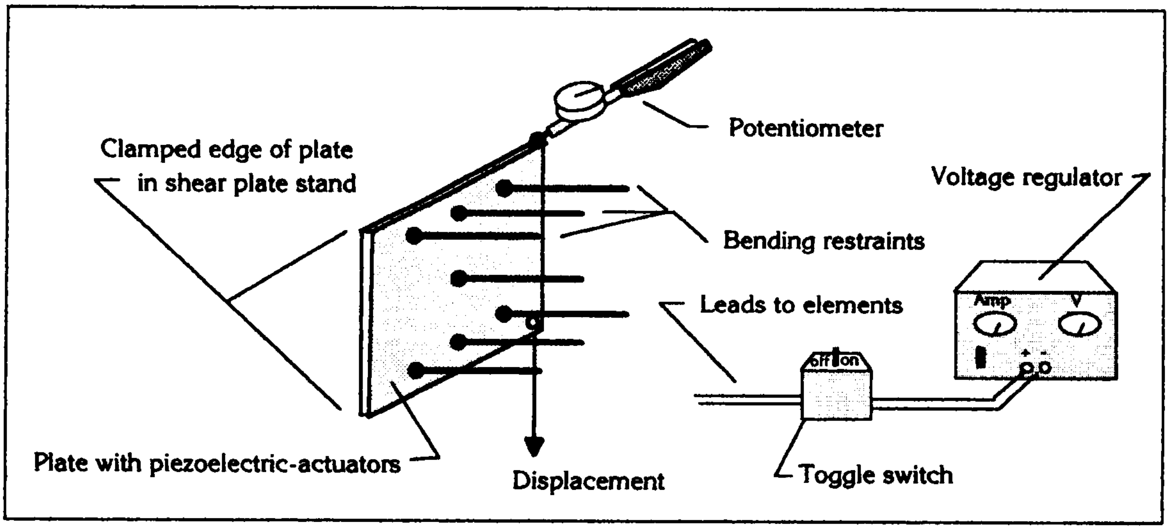

Figure 35 - Experiment set-up for shear displacement of plate

physical set-up of the experiment for the measurement of the shear displacement of the plate was similar for that in Section 6.2.1. The only difference was that the shear displacement of the plate was generated by the activation voltage provided by a DC voltage regulator. The DC voltage regulator used for all static measurements of experimental models was a Variable Voltage Regulated Power Supply from Oregon Electronics. The voltage output of the regulated power supply was +/-300 volts DC. A toggle switch was placed between the elements on the plate and the voltage supply.

6.3.1 Details of piezoelement activation potential sequence for shear displacement of plate, layout one

In order to induce the desired shear displacement of the plate, the elements must be activated in the proper sequence. For the piezo-actuator plate, layout one, the elements were given the activation voltages listed in Table 8 (please refer to Figure 26 for details of element labeling). In Table 8, the negative direction of activation potential resulted in the expansion of the piezo-actuator (voltage direction opposite of poling direction). Likewise, the positive direction of activation potential resulted in the compression of the piezo-actuator (voltage direction in same direction of poling direction).

Table 8 - Activation potential details for shear displacement, layout one

Side 1		Side 2	
Element no.	Direction of activation potential (Volts)	Element no.	Direction of activation potential (Volts)
1 to 4	(-)	1 to 4	(-)
5 to 8	(+)	5 to 8	(+)
9 to 12	(-)	9 to 12	(-)
13 to 16	(+)	13 to 16	(+)

6.3.2 Determination of maximum activation potential for the directionally attached piezoelectric elements

Depoling of an element occurs when too large a voltage is passed through a piezoelectric element. When an element becomes depoled, the reaction of the element to a positive or negative activation voltage is indistinguishable. It is possible to re-pole the element by the application of a very high voltage in the direction of the original positive poling direction, but the effectiveness of the re-poled element is greatly reduced.

The depoling voltage is a function of the mounting geometry of the piezoelement [23]. It was experimentally determined that depoling of directionally attached elements surface mounted to aluminum occurs at approximately 190 volts. Therefore; the maximum activation voltage to be applied through the piezoelements has been chosen to be 150 v. This value ensures a safety margin of 26.66%.

6.3.3 Data correlation for the shear displacement of the plate, layout one

When the maximum activation potential was applied through the elements to generate the shear displacement of the plate (layout one), a vertical deflection of 7.62 E-6 m +/-1.27 E-6 m was measured. Only one data point (150 V) was collected due to the limitations of the measuring device.

The analytical expression for the shear strain of the laminate plate was $\varepsilon_{xy}(+\Lambda,+45°)=\varepsilon_{xy}(-\Lambda,-45°)=\varepsilon_{xy}$ (laminate plate) from Table 1. The expression for the shear strain was solved for differing values of the activation potential (see Appendix

1 for details). The relation of the shear strain to the shear displacement of the plate comes from equation (2) and is as follows

$$\varepsilon_{xy} = \frac{\partial u}{\partial y} + \frac{\partial \upsilon}{\partial x} \tag{16}$$

It was shown that u is zero for both of the piezoelement layouts, so

$$\frac{\partial u}{\partial y} = 0 \tag{17}$$

Integrating equation (16) with respect to x leads to the expression for the shear displacement of the laminate

$$\upsilon = \varepsilon_{xy} x + C \tag{18}$$

The boundary condition for the plate is $\upsilon(0)=0$, thus solving equation (18) for v yields

$$\upsilon = \varepsilon_{xy} x \tag{19}$$

The shear displacements for the plate were found by solving equation (19). The results for the analytical analysis of the plate are shown in Table 9.

Table 9 - Analytical results of shear displacements of plate, layout one

Activation voltage	Shear strain of plate	Shear displacement (m)
150	7.317E-05	7.02E-06
125	6.098E-05	5.85E-06
100	4.878E-05	4.68E-06
75	3.659E-05	3.51E-06

Table 10 shows the numerical results for the shear displacement computation of the plate. The results in Table 10 were for an activation voltage of 150 volts through the elements activated in the sequence detailed in Table 8. The graphical results of the shear displacements of the two equivalent force models are shown in Figures 36 to 37.

Table 10 - Finite element results of shear displacement, layout one

	Vertical displ. (y)		Horizontal displ. (x)		Transverse displ. (z)		Rot. (x.y.z)
	upper rt. (m)	lower rt. (m)	upper rt. (m)	lower rt. (m)	upper rt. (m)	lower rt. (m)	(deg)
Strain-energy model							
Restrained plate	-1.76E-06	-1.76E-06	1.42E-07	-2.70E-07	1.78E-12	1.60E-12	0.0
Unrestrained plate	-1.65E-06	-1.89E-06	1.12E-07	-4.33E-07	-6.68E-16	-9.83E-16	0.0
Pin-force model							
Restrained plate	-3.64E-06	-3.66E-06	3.05E-07	-5.35E-07	6.76E-12	1.60E-12	0.0
Unrestrained plate	-3.42E-06	-3.93E-06	2.32E-07	-8.99E-07	-1.39E-15	-2.04E-15	0.0

Figure 36 shows the results of the strain-energy equivalent force induced shear displacement of the plate with the rigid steel bar mounted on the free end. The finite element model for this case is presented in Figure 18. The exact displacements of two nodes that represent the upper and lower locations of the free end rigid bar are listed in Table 10. Referring to Figure 36 and Table 10, the characteristics of the shear deformations of the plate are as follows:

1. The vertical displacement of the rigid bar remained virtually parallel to the y axis (resulting in shear elongation with no axial elongation).

2. The plate did not undergo any transverse deformations out of the y axis, or any rotations about the x, y or z axis. (the plate remains flat)

The results of the strain-energy equivalent force induced shear displacement of the plate with no rigid steel bar are shown in Figure 37. The finite element model for this case is presented in Figure 19. The exact displacements of two nodes that represent the upper and lower positions of the free end of the plate are listed in Table 10.

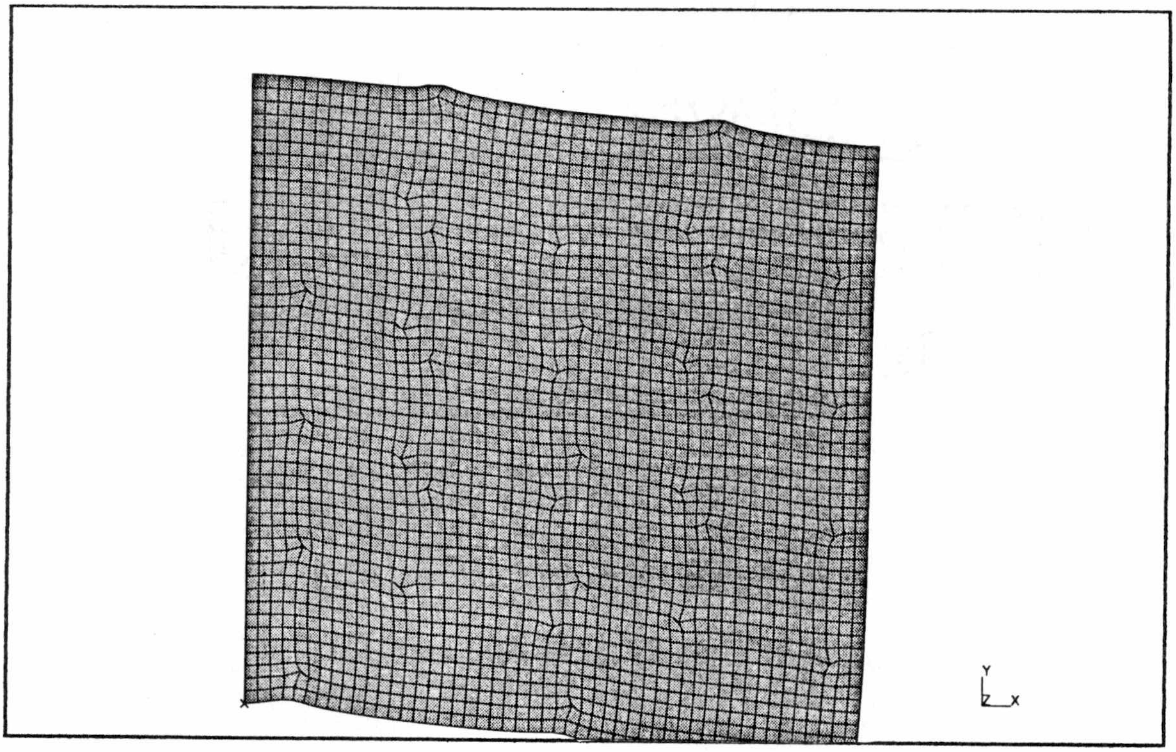

Figure 36 - Finite element analysis results of shear displacements for layout one, with rigid steel bar

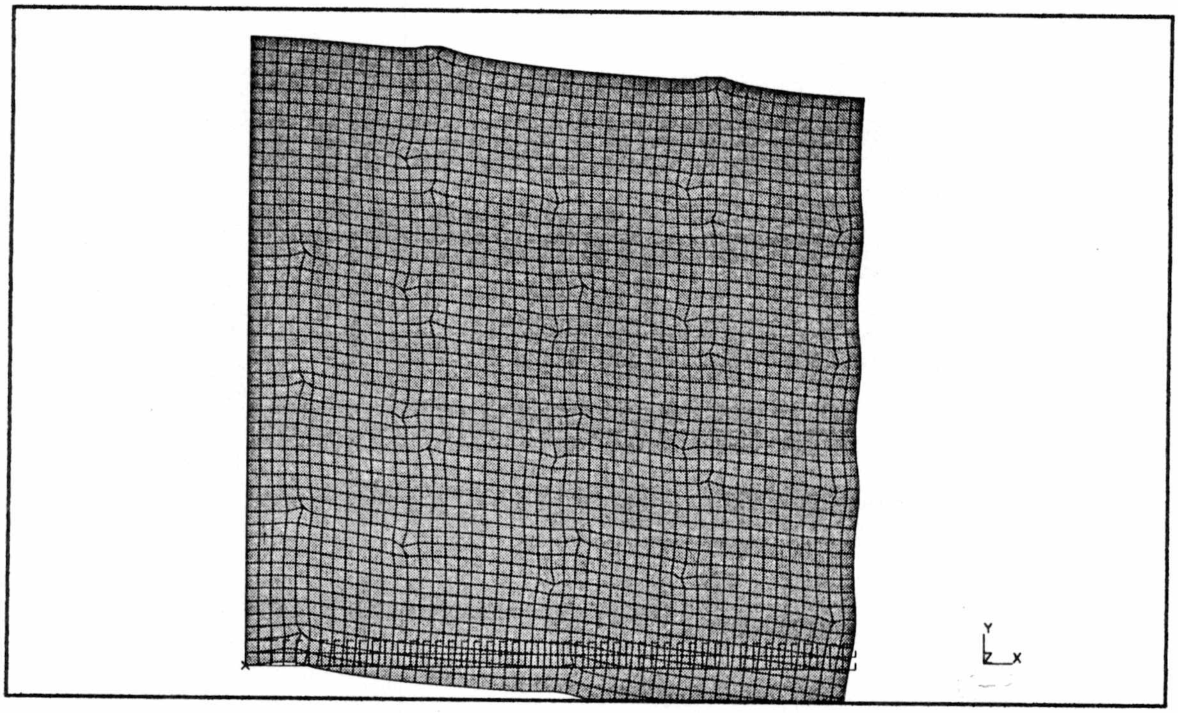

Figure 37 - Finite element analysis results of shear displacements for layout one, no rigid steel bar

Referring to Figure 37 and Table 10, the characteristics of the shear displacements of the plate with no rigid steel bars are as follows:

1. The free edge of the plate undergoes very slight deformations, indicating very small axial (x-axis direction) displacements .

2. The axial deformations are approximately one order of magnitude less than that of the vertical displacements of the plate, so the assumption of non-coupled shear deformations can be held for this case as well.

3. The plate does not undergo any transverse deformations out of the y axis, or any rotations about the x, y or z axis (the plate remains flat).

The pin-force equivalent force induced shear displacement of the plate with rigid steel bars is also shown in Figure 36. This was due to the fact that the physical characteristics of the induced deformation of the plate are the same, the only difference being the magnitude of deformation. The finite element model for this case is presented in Figure 18. The exact displacements of two nodes that represent the upper and lower locations of the free end rigid bar are listed in Table 10. The characteristics of the shear deformations of the plate are the same as the strain-energy equivalent force model.

The pin-force equivalent force induced shear displacement of the plate with no rigid steel is also shown in Figure 37. The finite element model for this case is presented in Figure 19. The exact displacements of two nodes that represent the upper and lower positions of the free end of the plate are listed in Table 10. The characteristics of the shear deformations of the plate are the same as the strain-energy equivalent force model.

A comparison among the data generated for the magnitude of the shear displacement of the plate induced by the piezoelements in layout one is listed in Table 11. Table 11 showed that the analytical model provided the most accurate

Table 11 - Data correlation for shear displacement, layout one

Test run	Shear displacement (m)	% difference
Experimental	7.62E-06	0.00
Analytical	7.02E-06	-7.87
Numerical (av)		
Strain-energy		
with rigid bar	1.76E-06	-76.90
no rigid bar	1.77E-06	-76.77
Pin-force		
with rigid bar	3.65E-06	-52.10
no rigid bar	3.36E-06	-55.91

calculation for the shear displacement. The percent difference between the actual and analytical shear displacement was only 7.87%. It was shown that the shear displacement for the plate predicted by the numerical analysis varies from 52.10 % to 76.90% smaller than the experimental result.

Although the results of the numerical modeling did not match the experimental shear displacement, they do provide a look at the physical deformation characteristics of the plate. These differences in the magnitudes of shear displacements may be attributable the equivalent force models used. Accurate experimental and theoretical data correlation for all of the models has been observed for various beam geometries [1], [13, [14]. But none of the afore mentioned experimental models incorporated a pattern of discretely attached piezoelements capable of inducing non-coupled displacements. Therefore, some of the discrepancy of the numerical analysis could be inherent to the physical geometry of piezoelements presented in this Thesis. Another source of error in the numerical analysis could be due to the modeling of the equivalent forces as nodal point forces. A direct consequence to modeling the equivalent forces as single nodal forces was the generation of relatively large deformations in the model in the immediate area of the force application (please refer to Figures 36 and 37). An alternative method would been to distribute the equivalent force evenly over several nodes representative of the width of the piezoelement bond area and modifying the mesh.

6.3.4 Details of piezoelement activation potential sequence for shear displacement of plate, layout two

For the piezo-actuator plate, layout two, the elements were labeled in the sequence in Figure 38. In order to induce the desired shear displacement of the plate, the piezoelements were activated by the activation voltages listed in Table 12 (please refer to Figure 38 for details of element labeling). As shown in Table 12, the negative direction of activation potential resulted in the expansion of the piezo-actuator (voltage direction opposite to direction of poling direction). Likewise, the positive direction of activation potential resulted in the compression of the piezo-actuator (voltage direction in same direction of poling direction).

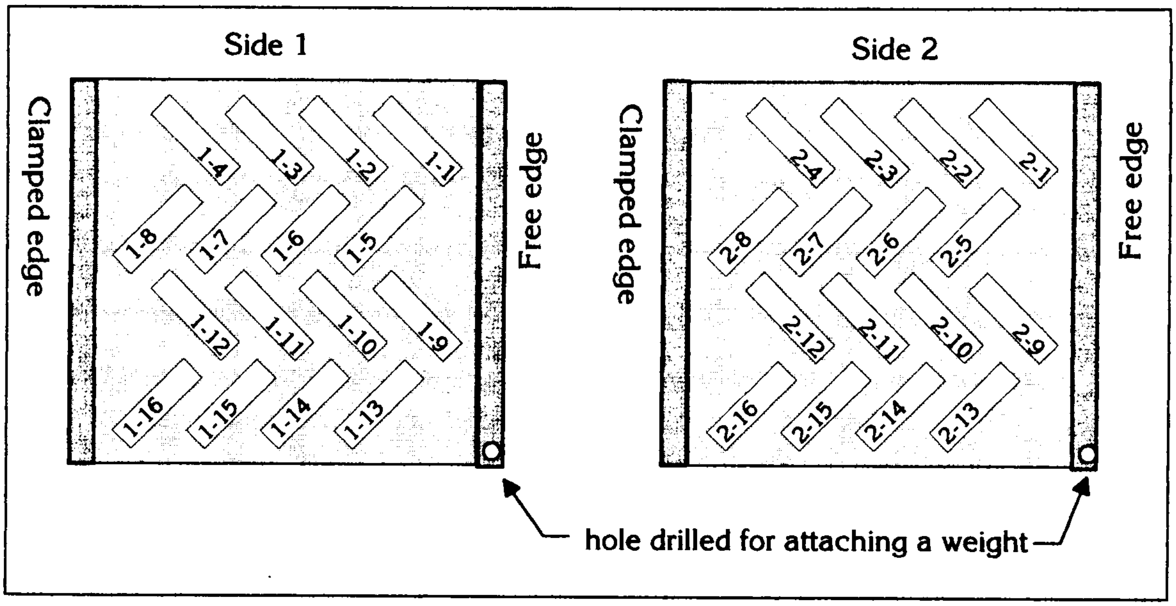

Figure 38 - Details of element labeling, layout two

Table 12 - Activation potential details for shear displacement, layout two

Side 1		Side 2	
Element no.	Direction of activation potential (Volts)	Element no.	Direction of activation potential (Volts)
1 to 4	(+)	1 to 4	(+)
5 to 8	(-)	5 to 8	(-)
9 to 12	(+)	9 to 12	(+)
13 to 16	(-)	13 to 16	(-)

6.3.5 Data correlation for the shear displacement of the plate, layout two

When the maximum activation potential was applied through the elements to generate shear displacement in the plate (layout two) a vertical deflection of 8.0 E-6 m +/-1.27 E-6 m was measured. Again, only one experimental data point (150 V) was collected due to the limitations of the measuring device.

The analytical expressions for the shear strain of the laminate plate were the same as for the plate layout one. The expression for the shear strain was obtained for the differing values of the activation voltage presented in the data files in Appendix 1. The results for the analytical analysis of the plate for layout two are the same as for layout one (please refer to Table 9). This phenomenon was due to the fact that the shear displacement values obtained from the analytical analysis were only dependent on the length of the laminate in the x direction.

The numerical results of the shear displacement of the plate for an activation voltage of 150 volts through the elements activated in the sequence detailed in Table 12 are shown in Table 13. The graphical results of the shear displacements of the two equivalent force models are shown in Figures 39 to 40.

Table 13 - Finite element results of shear displacement, layout two

	Vertical displ. (y)		Horizontal displ. (x)		Transverse displ. (z)		Rot. (x.y.z)
	upper rt. (m)	lower rt. (m)	upper rt. (m)	lower rt. (m)	upper rt. (m)	lower rt. (m)	(deg)
Strain-energy model							
Restrained plate	-1.90E-06	1.90E-06	3.15E-07	-2.43E-07	1.55E-12	1.13E-12	0.0
Unrestrained plate	-1.92E-06	-1.80E-06	4.18E-07	-2.18E-07	-1.83E-15	-1.47E-15	0.0
Pin-force model							
Restrained plate	-3.95E-06	-3.95E-06	7.25E-07	-5.06E-07	3.21E-12	2.35E-12	0.0
Unrestrained plate	-4.00E-06	-3.74E-06	8.69E-07	-4.54E-07	-3.73E-15	-2.95E-15	0.0

The results of the strain-energy equivalent force induced shear displacement of the plate with the rigid steel bar mounted on the free end are shown in Figure 39. The finite element model for this case is presented in Figure 20. The exact displacements of two nodes that represent the upper and lower locations of the free end rigid bar are listed in Table 13. It was found that the deformations of the plate with rigid bar due to the activated piezoelements matched the induced deformations for the plate with piezoelements in layout one with rigid bar (see section 6.3.2)

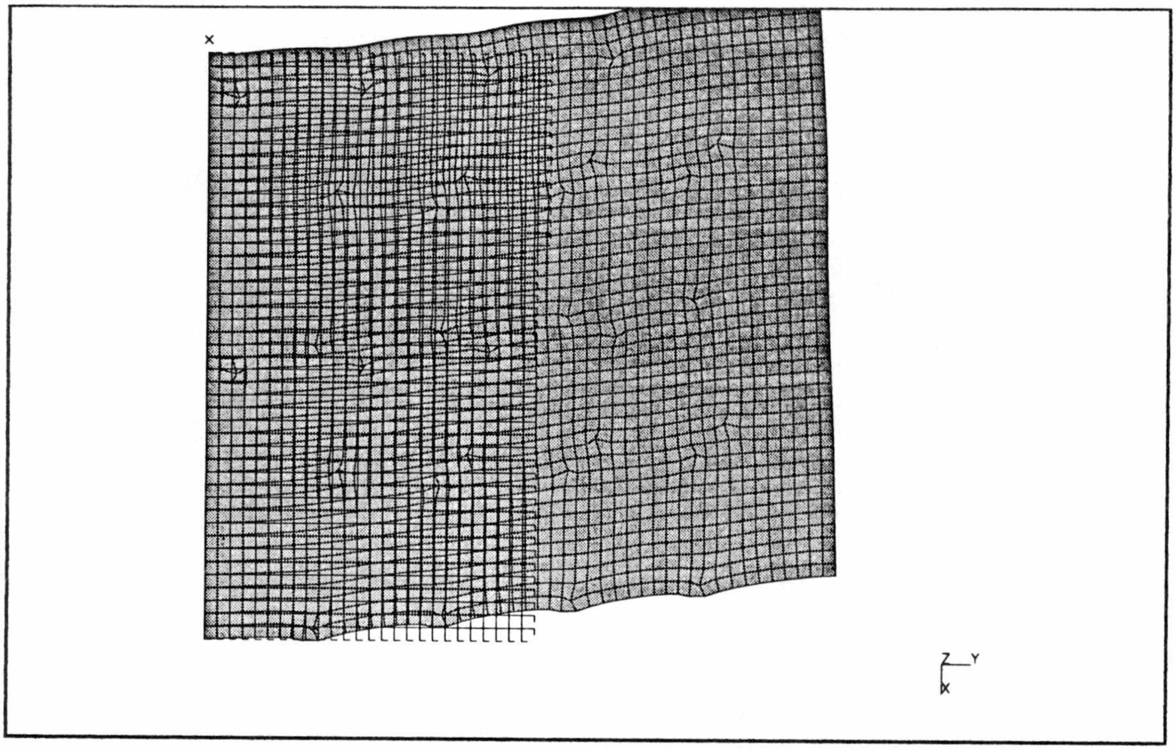

Figure 39 - Finite element analysis results of shear displacement for layout two, with rigid steel bar

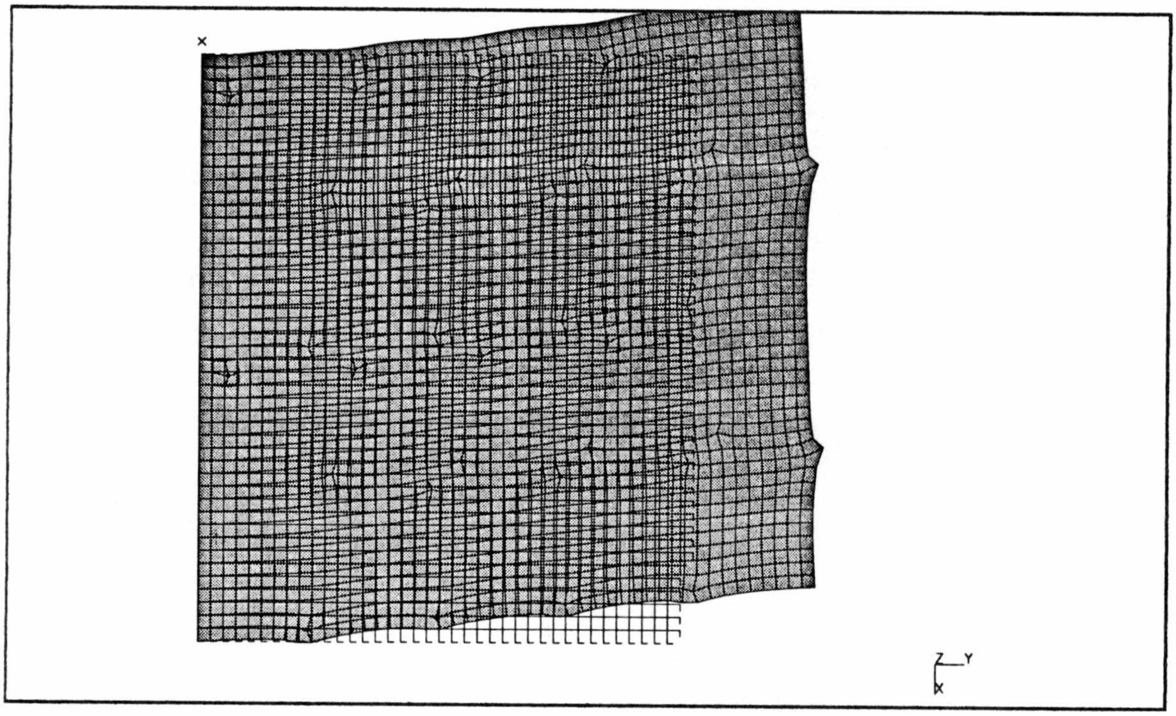

Figure 40 - Finite element analysis results of shear displacement for layout two, no rigid steel bar

Figure 40 shows the results of the strain-energy equivalent force induced shear displacement of the plate with no rigid steel bar. The finite element model for this case is presented in Figure 21. The exact displacements of two nodes that represent the upper and lower positions of the free end of the plate are listed in Table 13. It was found that the deformations of the plate with no rigid bar due to the activated piezoelements matched the induced deformations for the plate with piezoelements in layout one with no rigid bar (see section 6.3.2 for details).

The pin-force equivalent force induced shear displacement of the plate with rigid steel bar is also represented by Figure 39. This is due to the fact that the induced deformations of the plate due to the activated piezoelements similar, the only difference being the magnitude of deformation. The finite element model for this case is shown in Figure 20. The exact displacements of nodes that represent the upper and lower locations of the free end rigid bar are listed in Table 13. The characteristics of the shear deformations of the plate are the same as the strain-energy equivalent force model (see section 6.3.2 for details).

The pin-force equivalent force induced shear displacement of the plate with no rigid steel bar is also represented by Figure 40. The finite element model for this case is presented in Figure 21. Again, the exact displacements of two nodes that represent the upper and lower positions of the free end of the plate are listed in Table 13. the conclusions for the induced deformations of the plate due to the activated piezoelements are the same as the strain-energy equivalent force model (see section 6.3.2 for details).

A comparison among the data points generated for the magnitude of the shear displacement of the plate induced by the piezoelements in layout two is listed in Table 14. In Table 14 it was shown that the analytical model provided the most

Table 14 - Data correlation for shear displacement, layout two

Test run	Shear displacement (m)	% difference
Experimental	8.00E-06	0.00
Analytical	7.02E-06	-12.25
Numerical (av)		
Strain-energy		
with rigid bar	1.90E-06	-76.25
no rigid bar	1.86E-06	-76.75
Pin-force		
with rigid bar	3.95E-06	-50.63
no rigid bar	3.87E-06	-51.63

accurate calculation for the shear displacement (as for the plate, layout one). The percent difference between the actual and analytical shear displacement was only 12.25 %. It was shown that the shear displacement for the plate predicted by the numerical analysis varies from 52.10 % to 76.90 % smaller than the experimental result. Although the results of the numerical modeling did not match the experimental shear displacement, they do provide a look at the physical deformation characteristics of the plate. (see section 6.3.3 for possible sources of error in the numerical model)

It was shown that the analytical model had less accuracy for the plate with piezoelements in layout two versus that of layout one. This was due to the fact that the actual dimensions for the two plate layouts. As stated earlier, the plate with layout two was made from the plate with layout one. This required the rigid steel bars to be removed from the plate with layout one. When the new rigid bars were attached to the plate in the geometry for layout two, the effective surface area of the aluminum plate reduced. In essence, the piezoelements in layout one had to transfer more strain to the aluminum plate in order to match the shear displacement capabilities of the piezoelements in layout two. The differences between the analytical results with that of the actual experimental values comes from the fact that the length of the experimental plate for both of the piezoelement layouts did not change.

However, it was shown that the relative inaccuracies of numerical analysis for both of the layouts almost remained constant. This was due to the fact that the finite elements take into account the varying geometries of the plates.

Figure 41 is a photograph of the experimental plate with piezoelement layout one in the plate testing stand. The plate was set-up for shear displacement measurement.

Referring to Figure 41, the labeling of the plate corresponds to:

1. Plate testing stand
2. Analog Micrometer
3. Experimental plate with piezoelements, layout one
4. Free end rigid steel bar
5. Sealed bearing guide for the free end rigid steel bar
6. Piezoelement lead bus
7. DC voltage regulator

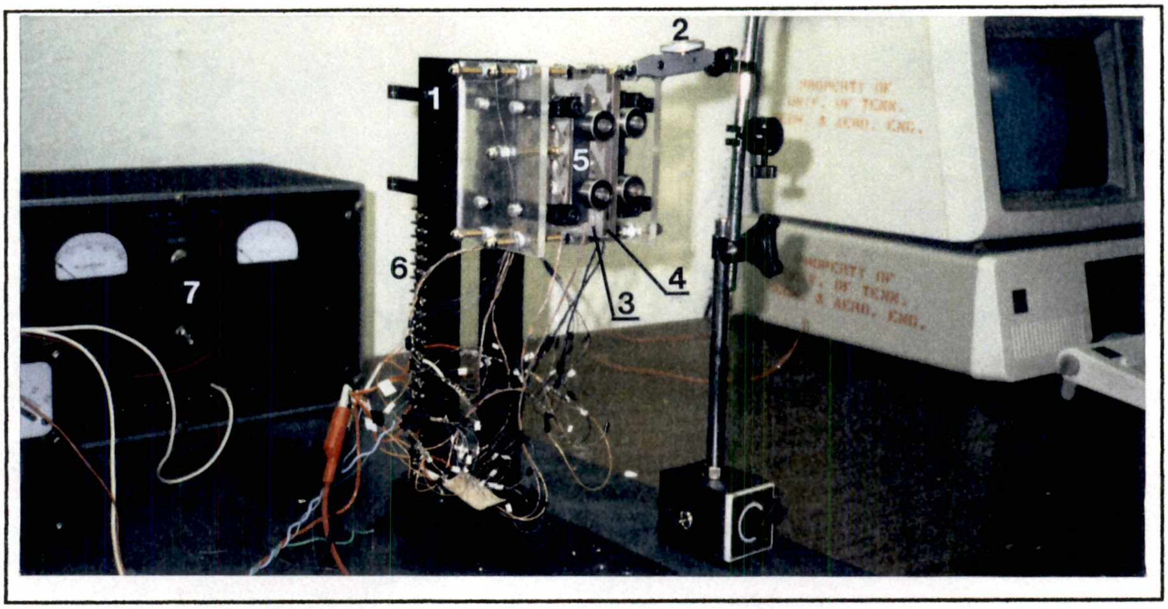

Figure 41 - Photograph of the experimental plate with piezoelement layout one, mounted in plate testing stand

6.4 Experimental investigation of induced bending displacement of the plate with piezoelements

The experimental set-up for the induced bending displacement due to the activation of the piezo-actuators for both of the layouts is shown in Figure 42. The physical set-up of the experiment for the measurement of the shear displacement of the plate was the same as that described in section 6.2.2. The only difference was that the bending displacement of the plate was generated by the activation voltage provided by the DC voltage regulator.

Before the experiments were run with for this configuration, it was necessary to show that an accurate strain/bending measurement could be made. This was done to make sure that the strain measured by the strain gage/indicator

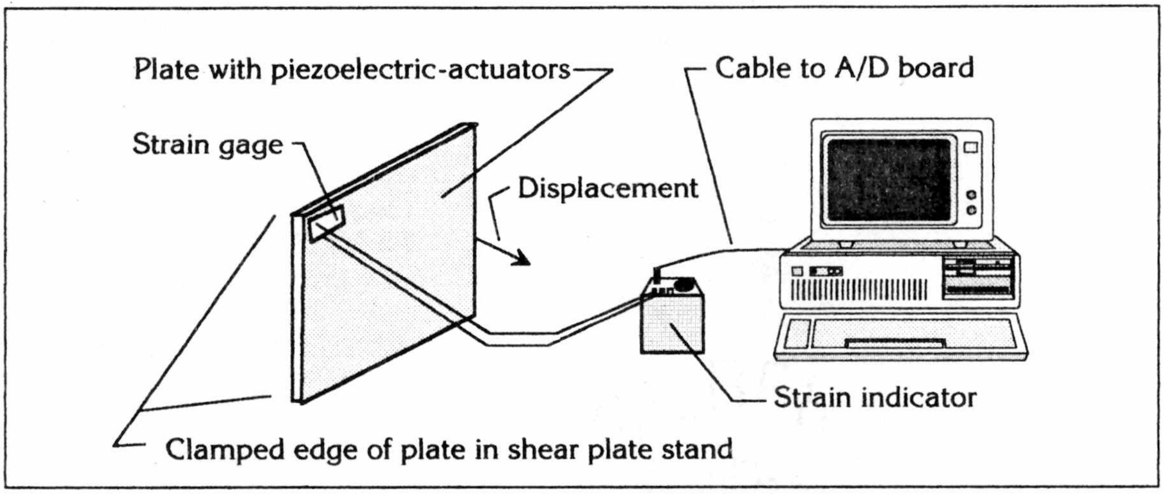

Figure 42 - Experiment set-up for bending displacement of plate

configuration was that of the plate, not a combination of the bending strain of the plate and a strain field generated by the activated piezo-actuators. Therefore, the effect of the far strain field generated by the activated piezoelements upon the strain measured by the strain gage was analyzed. The results of this test showed that the effect of the far strain field from the piezo-actuators had no effect on the strain measured by the strain gage. This showed that the strain measured by the strain gage was that due to the bending displacement of the plate only (see section 6.2.2).

6.4.1 Details of piezoelement activation potential sequence for bending displacement of plate

In order to induce the desired bending displacement of the plate, the elements must be activated in the proper sequence. For the piezo-actuator plate, both layouts of the elements were given the activation voltages listed in Table 15 (please refer to Figures 26 and 38 for details of element labeling). In Table 15, the

Table 15 - Activation potential details for bending displacement, both layouts

Side 1		Side 2	
Element no.	Dierection of activation potential (Volts)	Element no.	Direction of activation potential (Volts)
1 to 4	(-)	1 to 4	(+)
5 to 8	(-)	5 to 8	(+)
9 to 12	(-)	9 to 12	(+)
13 to 16	(-)	13 to 16	(+)

responses of the piezoelements follow those described in section 6.3.1. As can be seen from Table 15, to induce bending of the plate, all actuators on one side of the plate were activated in compression, while all actuators on the opposite side of the plate were activated in extension.

6.4.2 Data correlation for the bending displacement of the plate, layout one

To generate bending displacements, values for the activation potential of 75, 100, 125, and 150 volts were applied through the elements on the experimental plate (layout one) . The data collected with the A/D board for the strain indicator output versus activation voltage is listed in Table 16. Figure 43 shows the plot of bending displacement versus activation voltage.

Table 16 - Bending displacements for plate, layout one

Activation potential (v)	Delta mV	Bending displacement (m)
0	0	0
75	-175.77	1.11E-03
100	-232.28	1.46E-03
125	-291.76	1.84E-03
150	-352.66	2.22E-03

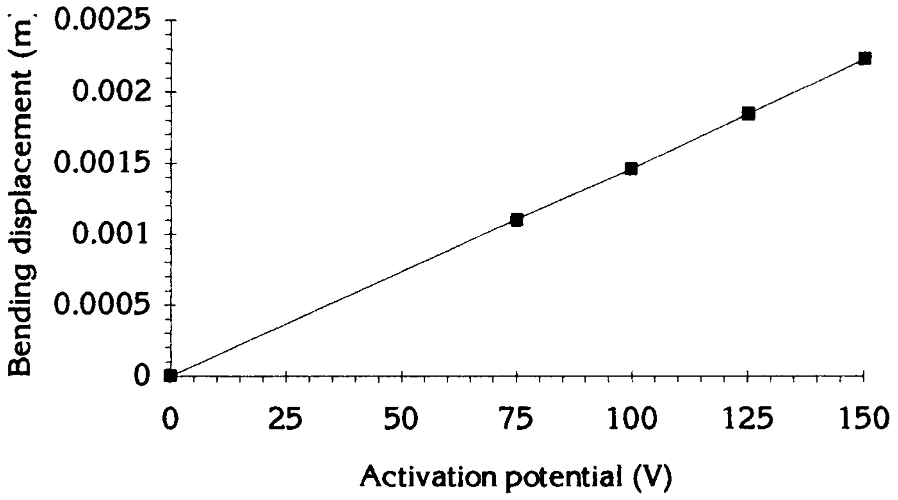

Figure 43 - Bending displacement versus activation potential for plate, layout one

The analytical result for the bending curvature of the laminate plate is the expression for k_x from Table 2. The expression for k_x is:

$k_x(upper, +\Lambda, -45°; lower, -\Lambda, -45°) = k_x(upper, +\Lambda, +45°; lower, -\Lambda, +45°) = k_x$

The expression for the bending curvature was solved for the differing values of the activation potential (see Appendix 1 for calculations). The relation of the curvature to the shear displacement of the plate is as follows

$$k_x = \frac{\partial^2 w_o}{\partial x^2} \tag{20}$$

Integrating equation (20) twice with respect to x leads to the expression for the bending displacement of the laminate

$$w = \frac{k_x x^2}{2} + C_1 x + C_2 \tag{21}$$

The boundary conditions for the plate are

$$w(0) = 0 \text{ and } \frac{dw}{dx}(0) = 0 \qquad 22$$

Solving equation (21) for the above boundary conditions for w yields

$$w = \frac{k_x x^2}{2} \qquad 23$$

The bending displacements for the plate were found by solving equation (23). The results for the analytical analysis of the plate are shown in Table 17. Figure 44 shows the plot of bending displacement versus activation voltage.

Table 17 - Analytical results of bending displacements of plate, layout one

Activation voltage	Curvature of bending	Bending displacement (m)
150	0.443414	2.04E-03
125	0.369512	1.70E-03
100	0.295609	1.36E-03
75	0.221707	1.02E-03

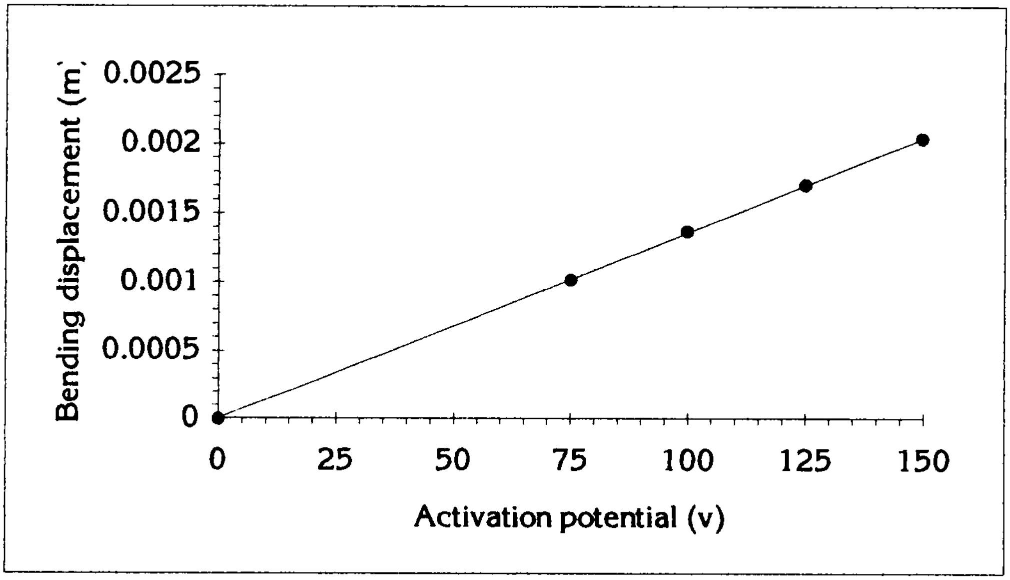

Figure 44 - Analytical result of bending displacement versus activation potential for plate, layout one

The numerical results of the bending displacements of the plate for an activation voltage through the elements activated in the sequence detailed in Table 15 are shown in Table 18. A plot of the average bending displacements of the upper and lower right nodes of the plate versus the activation potentials of the piezoelements is shown in Figure 45.

Table 18 - Finite element results of bending displacement, layout one

Strain-energy model	Vertical displ. (x)		Horizontal displ. (y)		Transverse displ. (z)		Rot. (x.y.z)
& Pin-force model	upper rt. (m)	lower rt. (m)	upper rt. (m)	lower rt. (m)	upper rt. (m)	lower rt. (m)	(deg)
150 volts							
Restrained plate	0.0	1.42E-14	7.11E-15	7.11E-15	-4.41E-04	-4.60E-04	0.0
Unrestrained plate	0.0	0.0	0.0	0.0	-3.70E-04	-5.08E-04	0.0
125 Volts							
Restrained plate	0.0	1.18E-14	5.92E-15	5.92E-15	-3.68E-04	-3.83E-04	0.0
Unrestrained plate	0.0	0.0	0.0	0.0	-3.08E-04	-4.24E-04	0.0
100 Volts							
Restrained plate	0.0	9.47E-15	4.74E-15	4.74E-15	-2.94E-04	-3.07E-04	0.0
Unrestrained plate	0.0	0.0	0.0	0.0	-2.47E-04	-3.39E-04	0.0
75 Volts							
Restrained plate	0.0	7.11E-15	3.55E-15	3.55E-15	-2.21E-04	-2.30E-04	0.0
Unrestrained plate	0.0	0.0	0.0	0.0	-1.85E-04	-2.54E-04	0.0

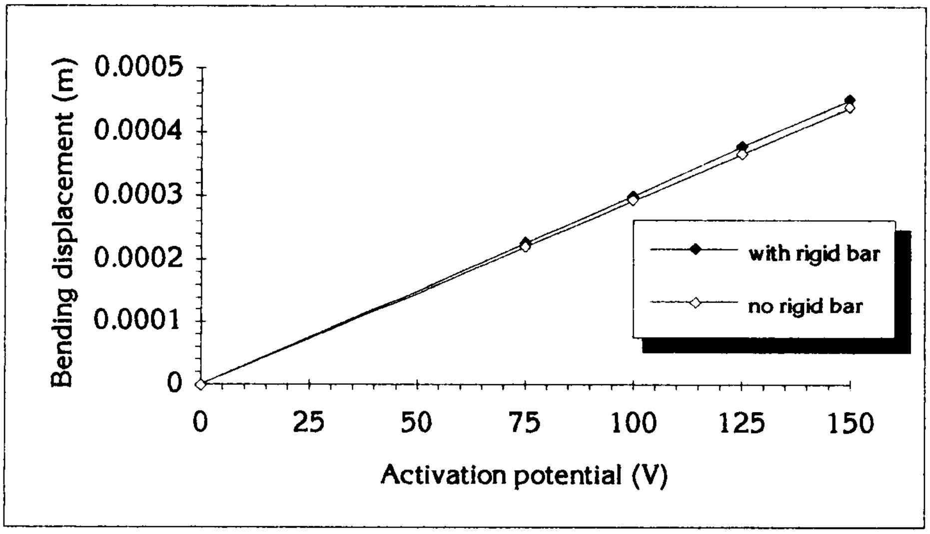

Figure 45 - Numerical result of bending displacement versus activation potential for plate, layout one

Since the equivalent forces for the pure bending case for both the strain-energy and pin-force models are equal, the following results are simply referred to as the equivalent force model. The graphical results of the bending displacements for the equivalent force model are shown in Figures 46 and 47.

The results of the equivalent force induced bending displacements of the plate with the rigid steel bar mounted on the free end are shown in Figures 46 and 47. The finite element model for this case is presented in Figure 18. The only change in Figure 18 for the bending displacement case was the geometry of the applied nodal forces (see section 5.1.2 for details). Figure 46 shows the side view of the plate under bending deformation. This plot shows that all of the finite elements in the model retained their original geometrical attributes, thus, no shearing of the plate was generated. Figure 47 shows the top view of two representative rows of elements. The bending displacements of the top row of elements (a) and the bottom row of elements (b) are almost identical in shape and magnitude. These observations along with the exact displacement data of two nodes that represent the upper and lower locations of the free end rigid bar (Table 18) lead to the following conclusions:

1. The plate experienced smooth, even bending.
2. The top and bottom edges of the plate remained virtually parallel to the y axis.
3. The plate did not undergo any rotations about the x, y or z axis.

The results of the equivalent force induced bending displacements of the plate without the rigid steel bar are shown in Figure 48. The finite element model for this case is presented in Figure 19. The only change in Figure 19 for the bending

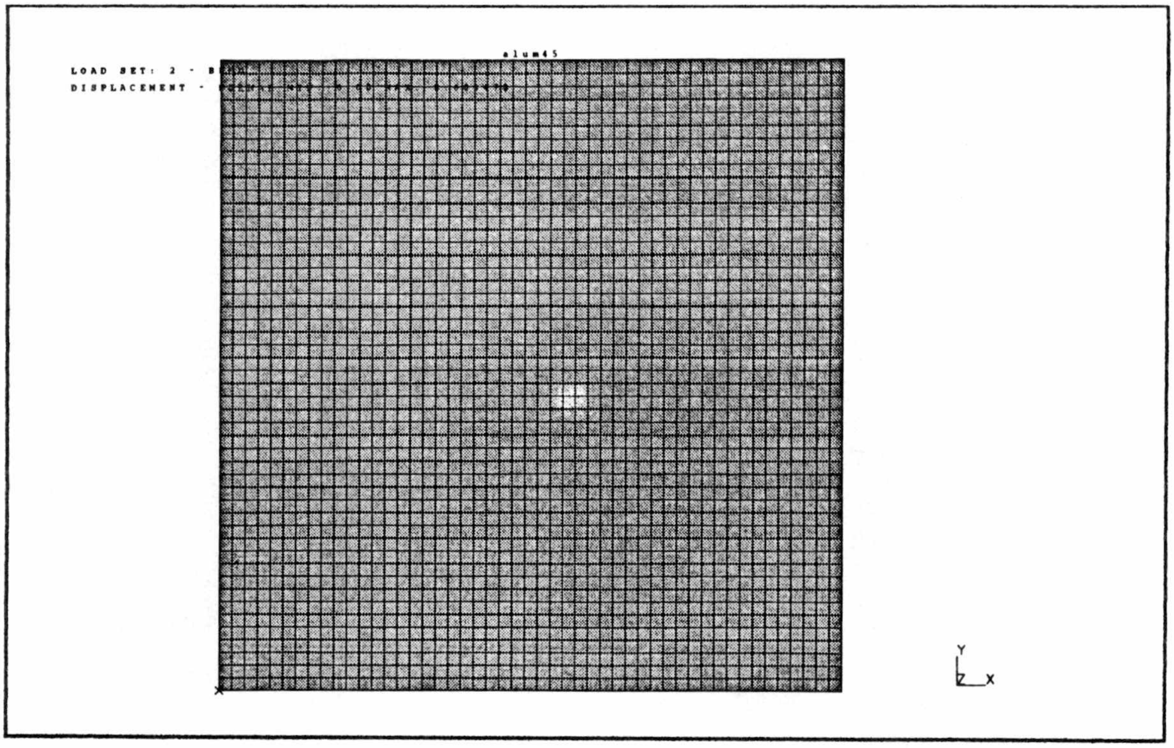

Figure 46 - Finite element analysis results of bending displacements for layout one, with rigid steel bar, side view of entire plate

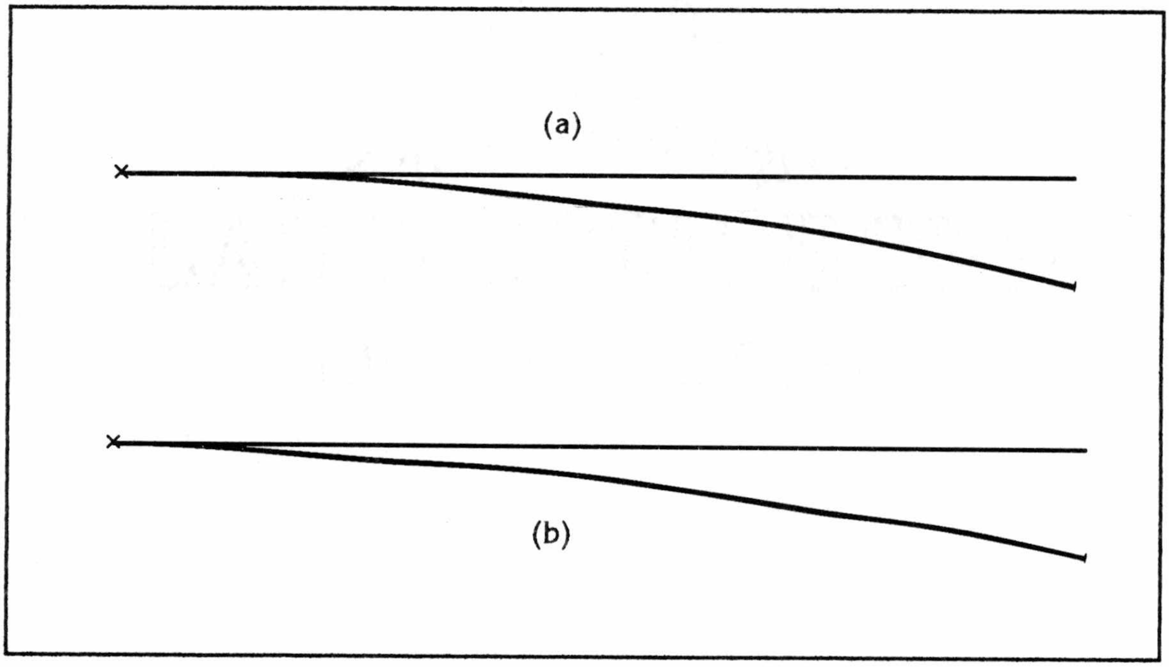

Figure 47 - Finite element analysis results of bending displacements for layout one, with rigid steel bar, top view: (a) top row of elements

(b) bottom row of elements

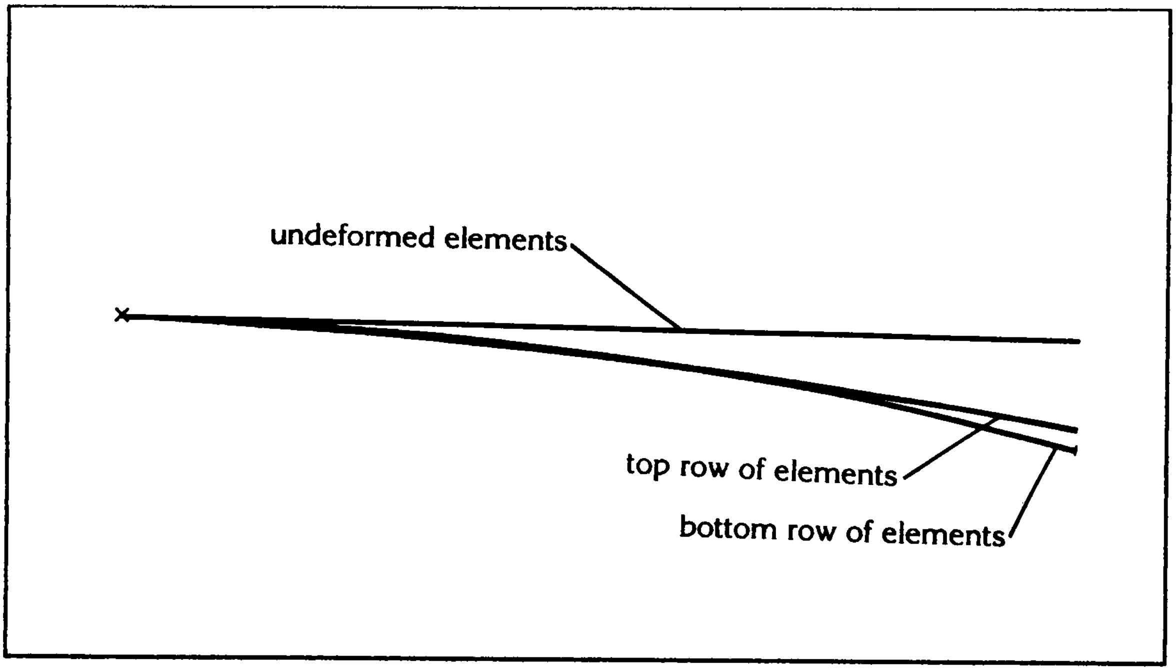

Figure 48 - Finite element analysis results of bending displacements for layout one, with rigid steel bar, top view

displacement case was the geometry of the applied nodal forces (see section 5.1.2 for details). The side view of the plate deformed in bending was the same for the case with the rigid steel bar (please refer to Figure 46). Figure 48 shows the top view of two representative rows of elements. The magnitude of the bending displacements of the top row of elements was slightly less than that of the bottom row of elements. These observations along with the exact displacement data of two nodes that represent the upper and lower locations of the free end rigid bar (Table 18) lead to the following conclusion:

1. The free edge condition (no bar) on the plate ensures no deformations parallel to the y axis.

2. The free edge condition (no bar) ensures no elongation in the y axis.

3. The rigid steel bar maintains an edge displacement parallel to x axis, whereas the free edge condition (no bar) does not.

A comparison among the data generated for the magnitude of the bending displacement of the plate induced by the piezoelements in layout one is plotted in Figure 49. Since all of the data was close to being linear, a comparison between the data for the value for the bending displacement versus an activation potential of 100 volts.

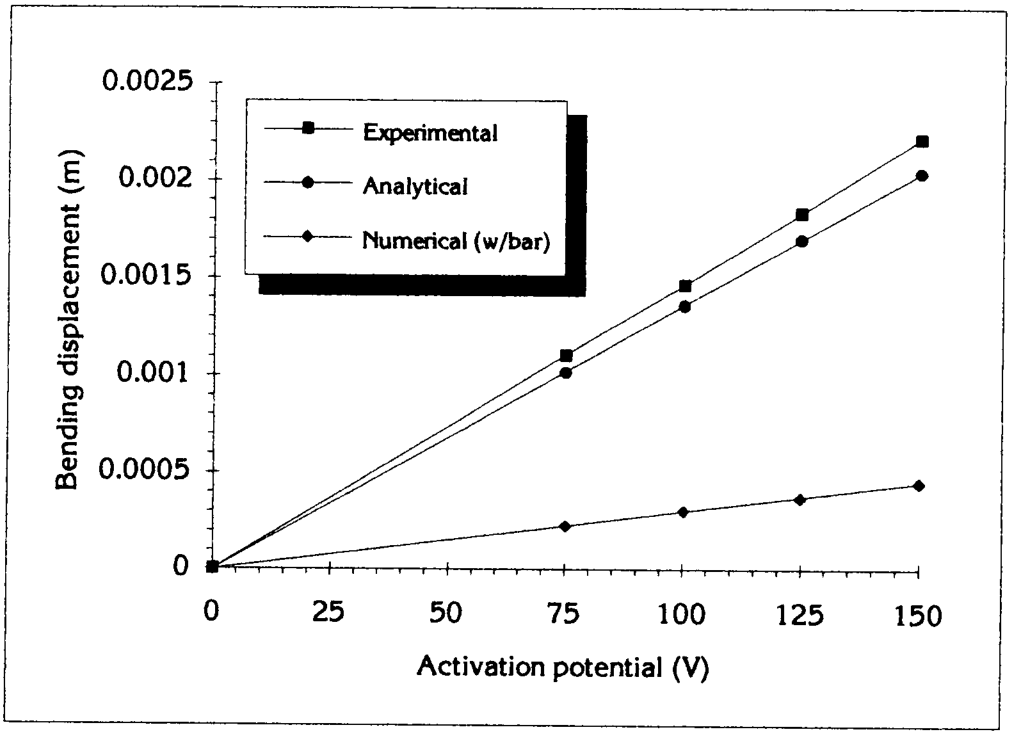

Figure 49 - Comparison of experimental, analytical, and numerical results for bending displacement of plate, layout one

The percent difference between the actual and analytical bending displacement was only 7.0167%. It was shown that the shear displacement for the plate predicted by the numerical analysis (with rigid bar) was 77.944% less than the actual displacement.

Although the results of the numerical modeling did not match the experimental bending displacement, they do provide a look at the physical deformation characteristics of the plate. These differences in the magnitudes of bending for the numerical model are the same for those of the shear displacement model (please refer to section 6.3.5).

6.4.3 Data correlation for the bending displacement of the plate, layout two

To generate bending displacements for the plate with piezoelements in layout two, the same activation potential sequence and magnitudes were used as for the plate with piezoelements in layout one (please refer to Table 15). The data collected with the A/D board for the strain indicator output versus activation voltage is listed in Table 19. Figure 50 shows the plot of bending displacement versus activation voltage.

Table 19 - Bending displacements for plate, layout two

Activation potential (v)	Delta mV	Bending displacement (m)
0	0	0
75	-182.103	1.15E-03
100	-238.377	1.50E-03
125	-298.257	1.88E-03
150	-365.067	2.30E-03

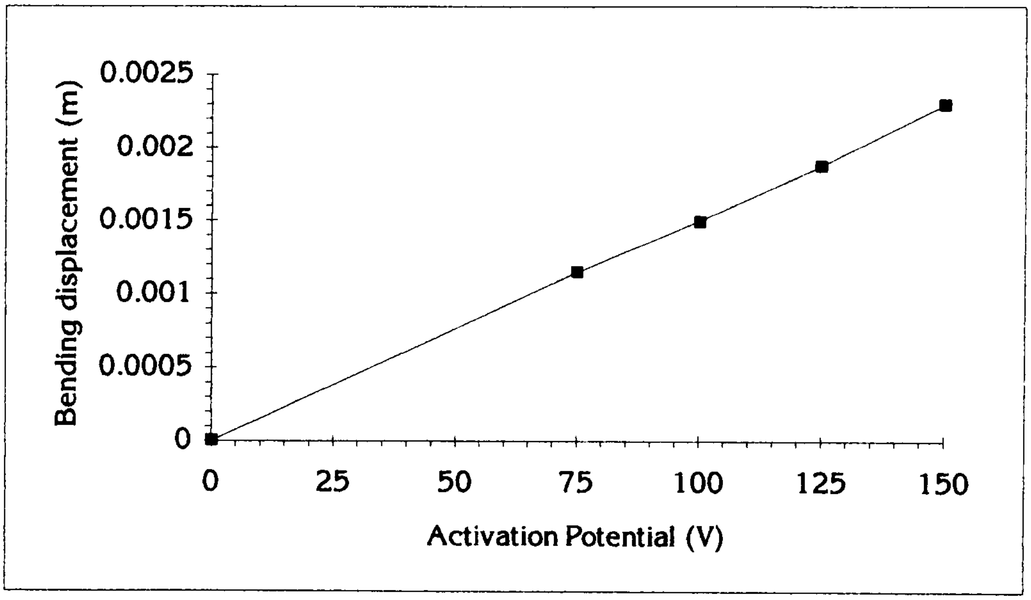

Figure 50 - Bending displacement versus activation potential for plate, layout two

average bending displacements of the upper and lower right nodes of the plate versus the activation potentials of the piezoelements is shown in Figure 51.

The analytical results for the beam displacement are the same as the results for layout 2 (see section 6.3.3). Table 20 shows the numerical results of the bending displacements computation of the plate. The results are for plate layout two for an

Table 20 - Finite element results of bending displacement, layout two

Strain-energy model	Vertical displ. (x)		Horizontal displ. (y)		Transverse displ. (z)		Rot. (x.y.z)
& Pin-force model	upper rt. (m)	lower rt. (m)	upper rt. (m)	lower rt. (m)	upper rt. (m)	lower rt. (m)	(deg)
150 volts							
Restrained plate	-5.77E-15	-5.33E-15	0.0	0.0	-4.78E-04	-4.78E-04	0.0
Unrestrained plate	1.11E-16	0.0	0.0	0.0	-4.88E-04	-3.90E-04	0.0
125 Volts							
Restrained plate	0.0	-4.44E-15	0.0	0.0	-3.98E-04	-3.98E-04	0.0
Unrestrained plate	0.0	0.0	0.0	0.0	-4.07E-04	-3.25E-04	0.0
100 Volts							
Restrained plate	0.0	-3.55E-15	0.0	0.0	-3.19E-04	-3.19E-04	0.0
Unrestrained plate	0.0	0.0	0.0	0.0	-3.26E-04	-2.60E-04	0.0
75 Volts							
Restrained plate	0.0	-2.66E-15	0.0	0.0	-2.39E-04	-2.39E-04	0.0
Unrestrained plate	0.0	0.0	0.0	0.0	-2.44E-04	-1.95E-04	0.0

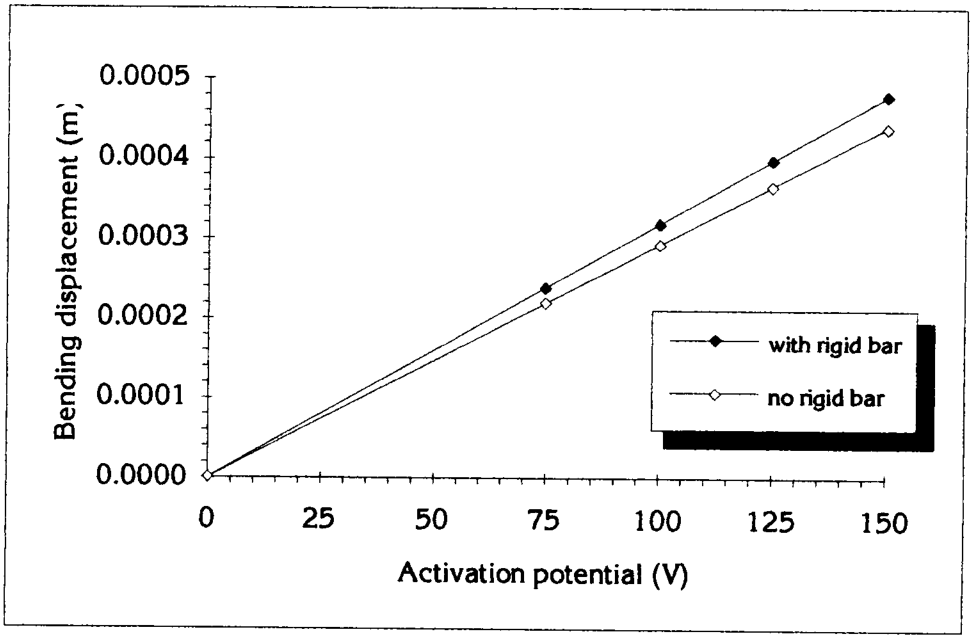

Figure 51 - Numerical result of bending displacement versus activation potential for plate, layout two

activation voltage through the elements in the sequence detailed in Table 15. A plot of the displacements for the equivalent force model are shown in Figure 52.

Since the equivalent forces for the pure bending case for both the strain-energy and pin-force models are equal, the following results are simply referred to as the equivalent force model.

Figure 52 shows the results of the equivalent force induced bending displacements of the plate with the rigid steel bar mounted on the free end. The finite element model for this case is presented in Figure 20. The only change in Figure 20 for the bending displacement case was the geometry of the applied nodal

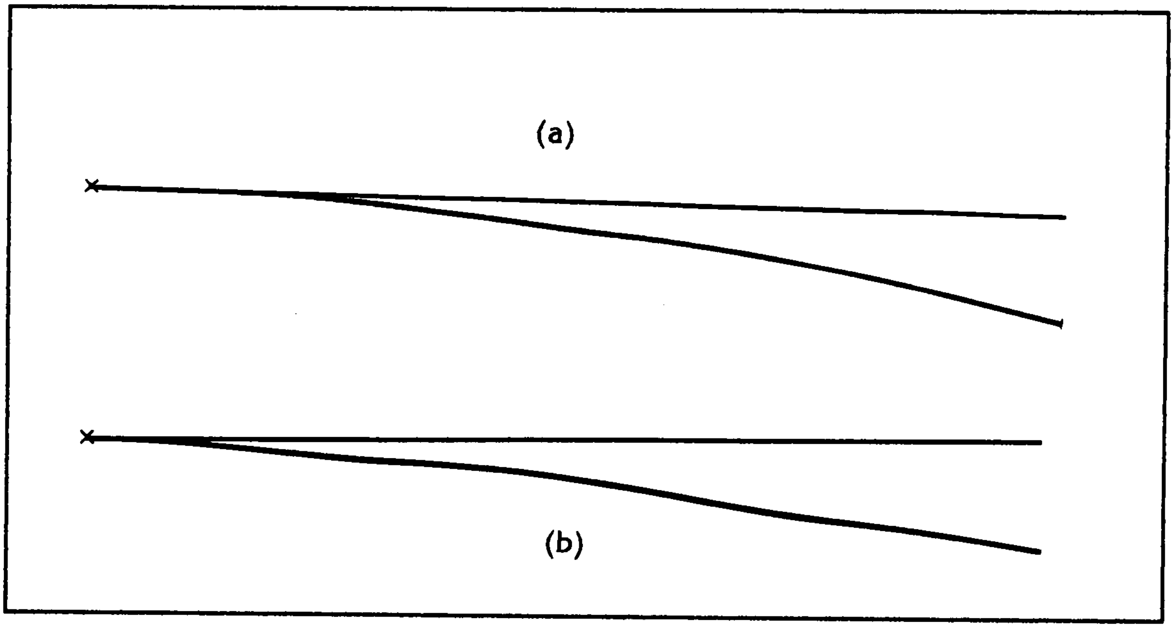

Figure 52 - Finite element analysis results of bending displacements for layout two, with rigid steel bar, top view: (a) top row of elements
(b) bottom row of elements

forces (see section 5.1.2 for details). Figure 46 is a representation of the side view of the plate under bending deformation. This plot shows that all of the finite elements in the model retained their original geometrical attributes, thus, no shearing of the plate was generated. Figure 52 shows the top view of two representative rows of elements. The bending displacements of the top row of elements (a) and the bottom row of elements (b) are almost identical in shape and magnitude. These observations along with the exact displacement data of two nodes that represent the upper and lower locations of the free end rigid bar lead to the same conclusions for the plate layout two as the plate layout one (section 6.4.2)

The results of the equivalent force induced bending displacements of the plate without the rigid steel bar are shown in Figure 53. The finite element model for this case is presented in Figure 21. The only change in Figure 21 for the bending displacement case was the geometry of the applied nodal forces (see section 5.1.2 for details). The side view of the plate deformed in bending was the same for the case with the rigid steel bar (please refer to Figure 46). Figure 53 shows the top view of two representative rows of elements.

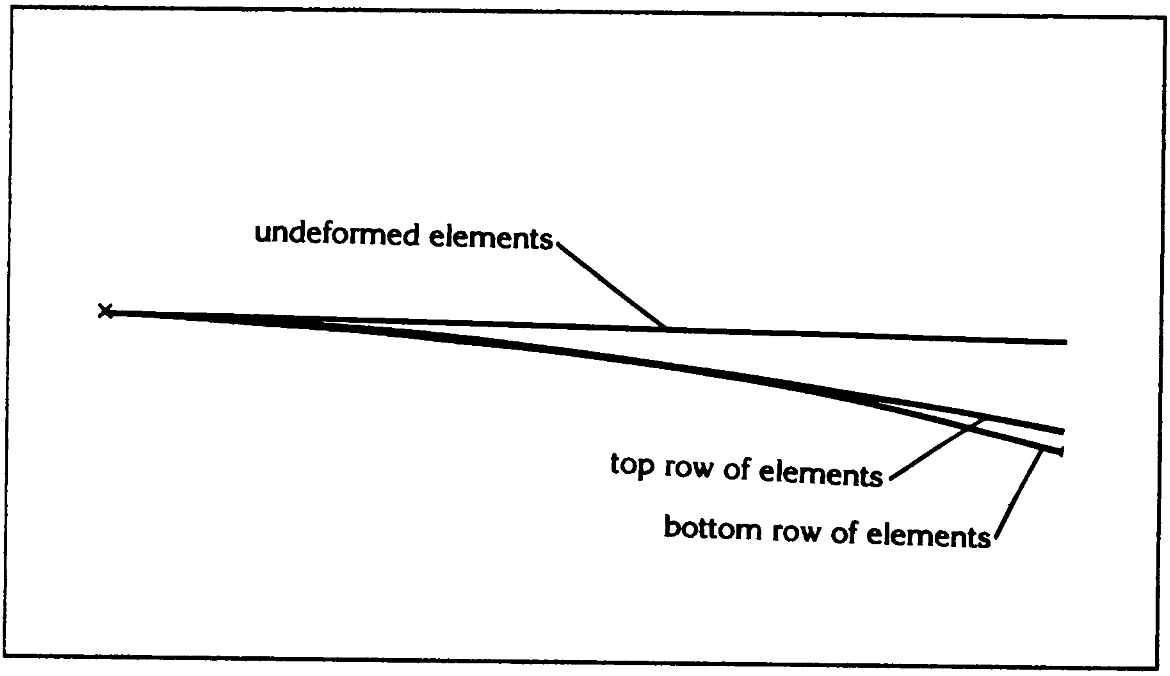

Figure 53 - Finite element analysis results of bending displacements for layout two, no rigid steel bar, top view

The magnitude of the bending displacements of the top row of elements was slightly less than that of the bottom row of elements. These observations along with the exact displacement data of two nodes that represent the upper and lower locations of the free end rigid bar lead to the same conclusions for the plate layout two as the plate layout one (section 6.4.2).

A comparison among the data generated for the magnitude of the bending displacement of the plate induced by the piezoelements in layout one is plotted in Figure 54. Since all of the data was very linear, a comparison between the data for the value for the bending displacement verse an activation potential of 100 volts.

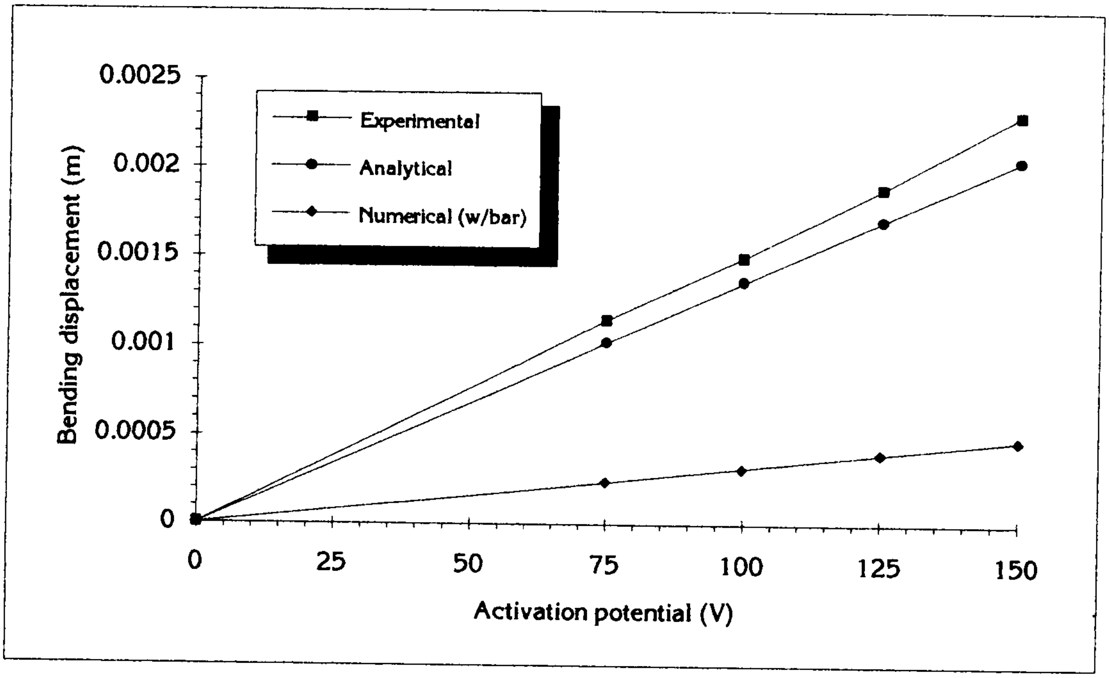

Figure 54 - Comparison of experimental, analytical, and numerical results for bending displacement of plate, layout two

The percent difference between the actual and analytical bending displacement was only 10.294%. It was shown that the shear displacement for the plate predicted by the numerical analysis (with rigid bar) was 78.7% less than the actual displacement. It was shown that relative differences between the experimental and numerical model displacements for both of the piezoelement layouts are very close. But, the relative differences between the experimental and analytical model displacements increase between the plates with piezoelement layout one and two. This is attributable to the inherent characteristics of each of the methods please refer to section 6.3.5 for details).

Although the results of the numerical modeling did not match the experimental bending displacement, they do provide a look at the physical deformation characteristics of the plate.

Figure 55 is a photograph of the experimental plate with piezoelement layout one installed in the plate testing stand. The plate was set-up for bending displacement measurement.

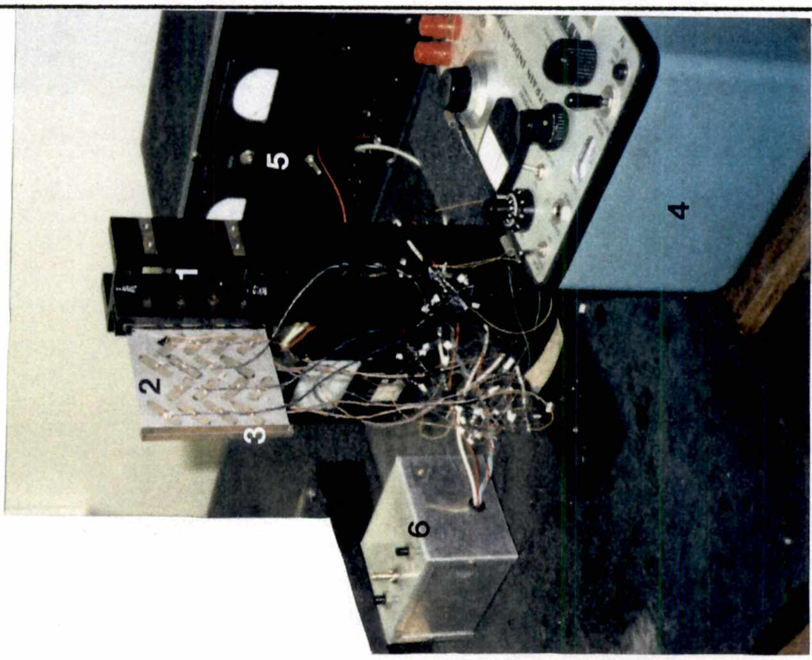

Figure 55 - Photograph of the experimental plate with piezoelement layout one, mounted in plate testing stand

Referring to Figure 55, the labeling of the plate corresponds to:

1. Plate testing stand
2. Plate with piezoelements
3. Free end rigid steel bar
4. Strain indicator
5. DC voltage regulator
6. On/Off Toggle switch

CHAPTER 7

COMPOSITE BEAM TESTING

7.1 Fabrication of composite beam with piezoelectric elements

A fiberglass beam with surface mounted piezoelectric elements was fabricated in order to study the non-coupled torsional and bending characteristics of a closed section thin-walled structure.

7.1.1 Composite beam fabrication

The general steps for the manufacture of the composite beam are shown in Figure 56. The first step of fabrication of the composite beam was the production of a foam core. The foam core served to maintain the desired geometry of the composite beam during the curing process of the composite. The foam core was cut from a block and shaped to the desired size with a low voltage high current non insulated steel wire [24], [25]. The cross-sectional dimensions for the core matched the desired internal cross-sectional area of the composite beam (please refer to Figure 56). Next, one ply of style #120 fiberglass cloth saturated with plast #88/87 laminating epoxy resin was wrapped around the foam core [24], [25]. The fiberglass and epoxy resin was obtained from Fibre Glast Developments Corporation. The specifications for the style #120 fiberglass were as follows: 3 oz. fabric, 8.89E-5 m thick, and 4 harness satin weave. The plast #88 epoxy resin was mixed with plast

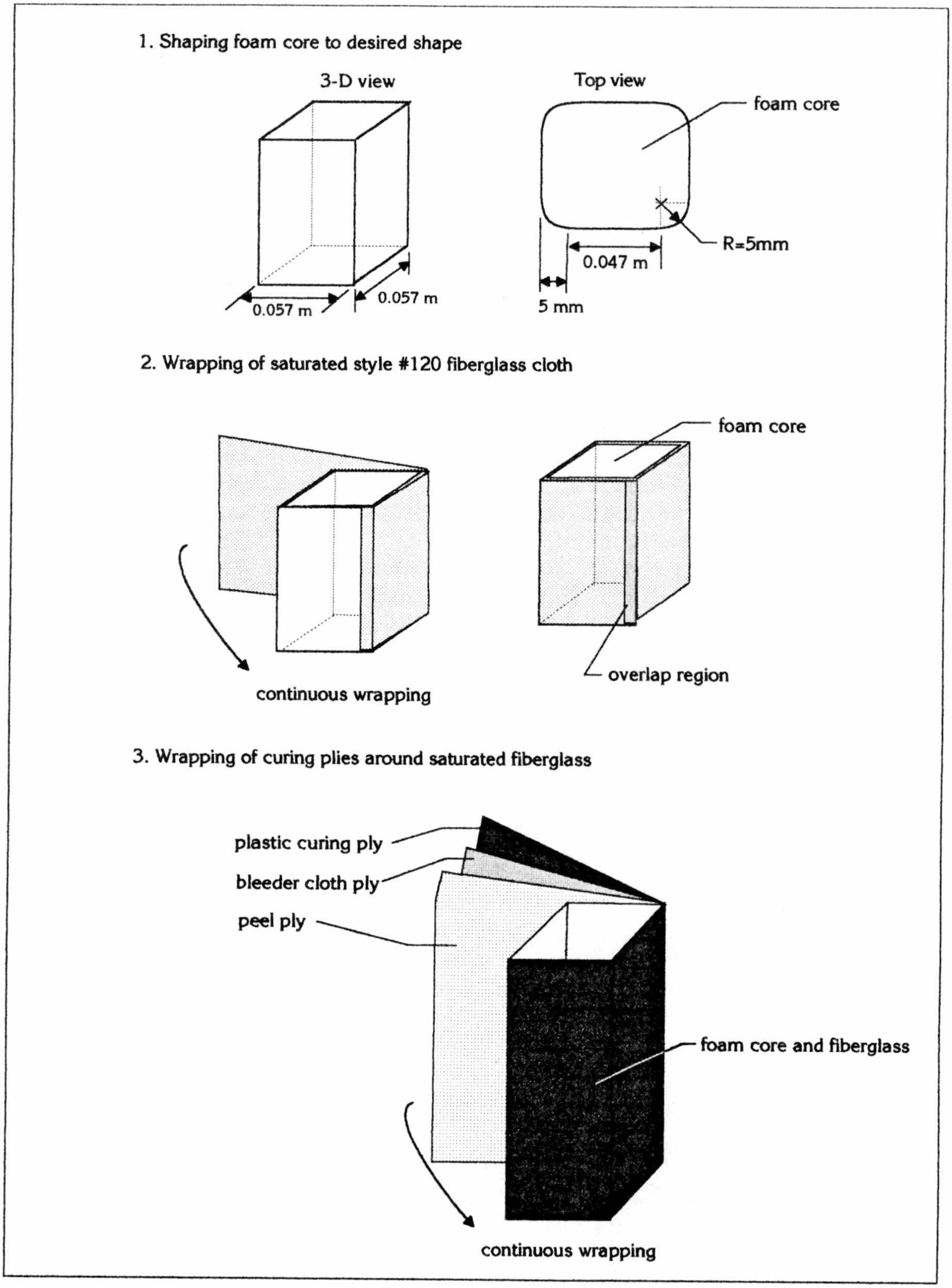

Figure 56 - General steps for manufacturing the composite beam

#87 epoxy resin curing agent. The ratio of 5 parts #88 resin with 1 part #87 by weight or volume resulted in a gel time of 15-90 minutes, with full cure in 5-7 days at room temperature.

The seam of the overlapped composite was positioned along a corner of the beam [24], [25] (please refer to Figure 56). This was done to minimize deformities of the beam walls where the piezoelements were to be mounted. Care was taken to ensure that the seam of the composite was as small and as uniform as possible. The orientation of the glass fibers in the composite were [+45°/-45°] with respect to the longitudinal axis of the composite beam. The details of the orientation of the glass fibers with respect to the longitudinal axis of the beam are shown in Figure 57. With this configuration, the axial strains transferred from the piezoelements to the composite beam were parallel to the fibers in the composite. Care was taken to minimize distortion of the fibers and to maintain fiber orientation.

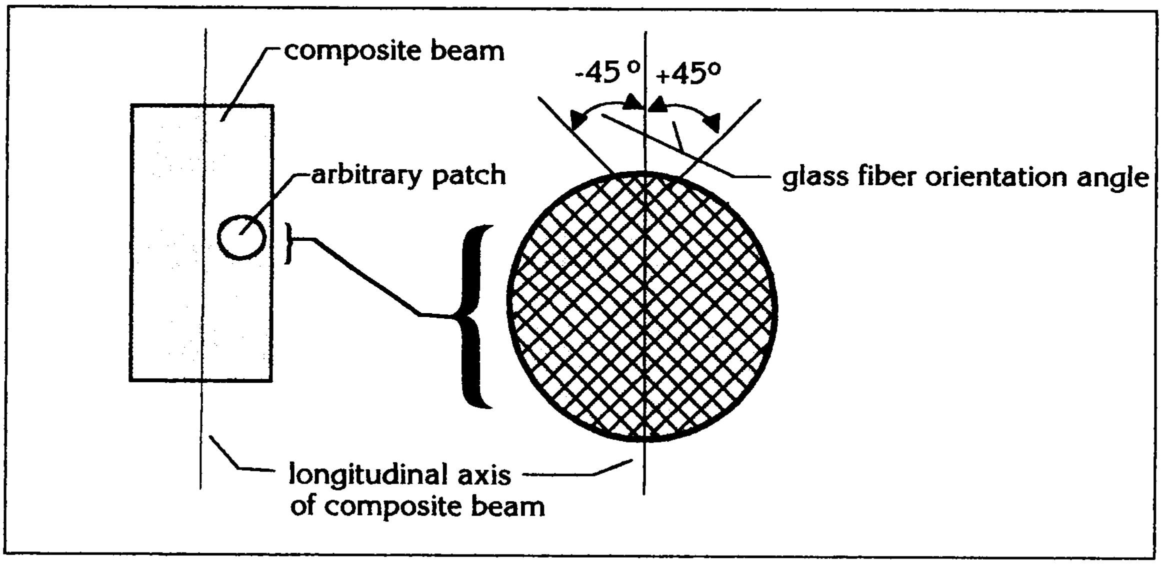

Figure 57 - Glass fiber orientation with respect to the longitudinal axis of the composite beam

After the saturated fiberglass cloth was positioned around the foam core, it was tightly wrapped with a peel ply. The peel ply served as a semi-permeable membrane to allow excess resin to flow out of the fiberglass cloth. A layer of bleeder cloth was tightly wrapped around the peel ply. The bleeder cloth served to dissipate the excess resin content in the fiberglass. The last curing ply was a layer of plastic wrapped around the entire specimen [24], [25]. The plastic ply served two purposes: firstly, it maintained the desired shape of the beam by maintaining even tension on the two inner curing plies; secondly, it enabled the beam to be handled without getting excess resin everywhere. Then entire assembly was cured for 24 hours at room temperature. After the 24 hour room cure, the composite beam specimen was removed from the curing plies so that an inspection of the quality of the composite beam could be made. After a composite beam was fabricated to this point, it was allowed to fully cure for an additional 4 days at room temperature with no curing plies. When the composite beam was fully cured, it was cut to its desired length using a ban saw. The final step was the application of acetone to dissolve the foam core [24].

Several composite beams were fabricated with slight variations in the manufacturing process for each case before acceptable parameters were obtained [24]. The fabrication steps listed above were those for the composite beam specimen chosen for the experimental model. All of the desired physical qualities discussed in the fabrication process were achieved in that specimen. The dimensions of the composite beam used for the experimental model are shown in Figure 58.

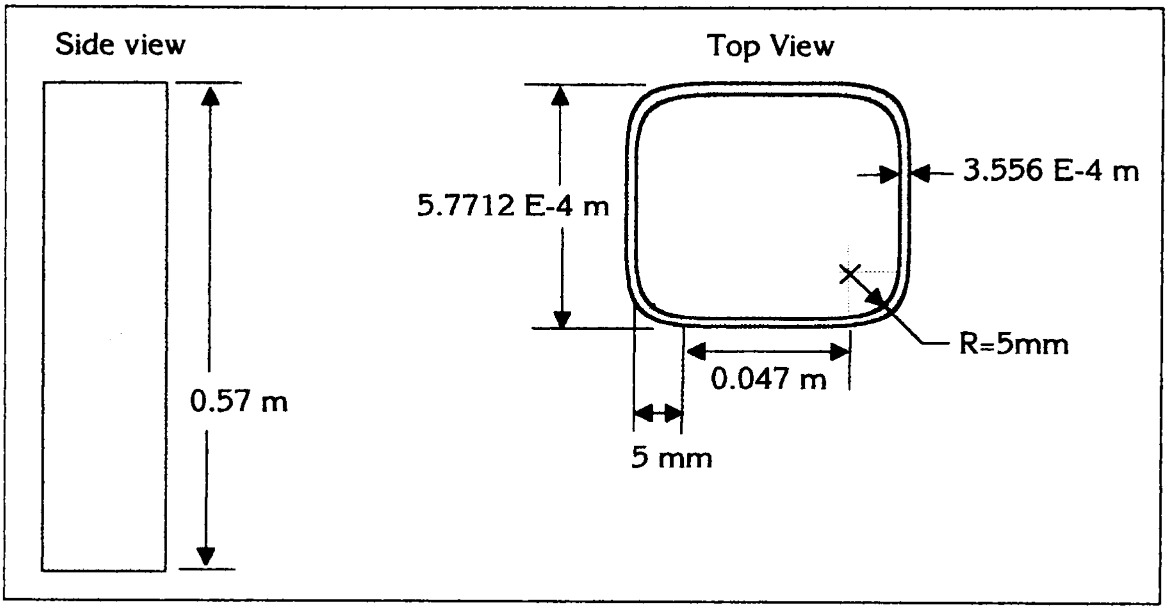

Figure 58 - Dimensions of composite beam

7.1.2 Piezoelements bonding procedure

The steps for the preparation of the piezoelements for directional attachment to the composite beam were the same as for the aluminum plate model (section 6.1.2). The piezoelement layout on the composite beam is shown in Figure 59. The diagram of the piezoelement layout in Figure 59 shows the surface mounted elements on the beam. Each element depicted in Figure 59 represents a piezoelement pair (please refer to Figure 24 for details). The pattern of piezoelement pairs depicted in Figure 59 was repeated on the remaining three sides of the beam.

The first step to prepare the composite beam for the attachment of the elements was to drill holes through the composite beam to accommodate the solder dots on the low voltage poled face of the prepared elements. Any frayed fibers due

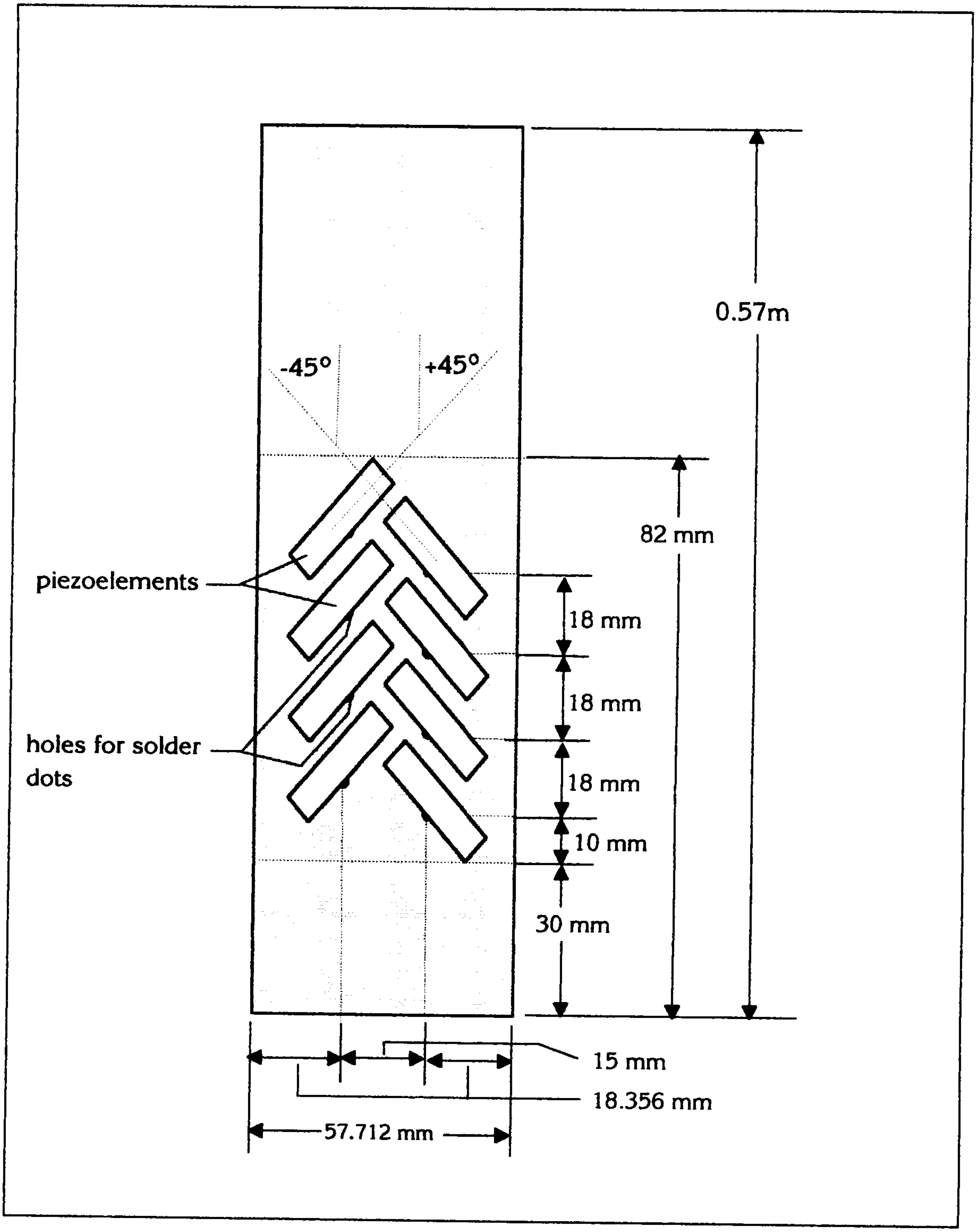

Figure 59 - Piezoelement layout on composite beam

to the drilling procedure were trimmed off. At this point, the composite beam was cleaned with the cleaner/degreaser.

The bonding of the piezoelements was done in eight steps. Four steps were required for the inside surface mounted elements, and four steps were required for the outside surface mounted elements. The details of the first step for mounting the piezoelements follows. All eight piezoelements that were to be surface mounted to an inside wall of the beam were bonded simultaneously. In order to accomplish the simultaneous bonding of the eight piezoelements a mounting guide was manufactured of plexiglass. The plexiglass had layout guide lines etched into its surface to aid in the proper alignment of the elements. Channels were routed into the mounting guide to accommodate the lead wires from the elements during the bonding of the elements to the beam. The top surface of the mounting guide was then covered with a layer of the 3M Scotch tape to prevent any bonding between the mounting guide and the composite beam due to excess epoxy. The piezoelements were secured lightly to the mounting guide with two small pieces of tape between the high voltage poled face of the element and the mounting guide. For this procedure, the tape was looped back onto itself to produce the effect of double sided tape. At this point, all of the elements on the plexiglass mounting guide were labeled for identification. The labeling of the piezoelements and their respective lead wires is shown in Figure 60. Thirty gage teflon coated thermocouple wire was used for the lead wire for the high voltage face of each element. The prepared elements secured on the mounting guide were then cleaned with the cleaner/degreaser to assure a good bonding surface. The prepared group of eight

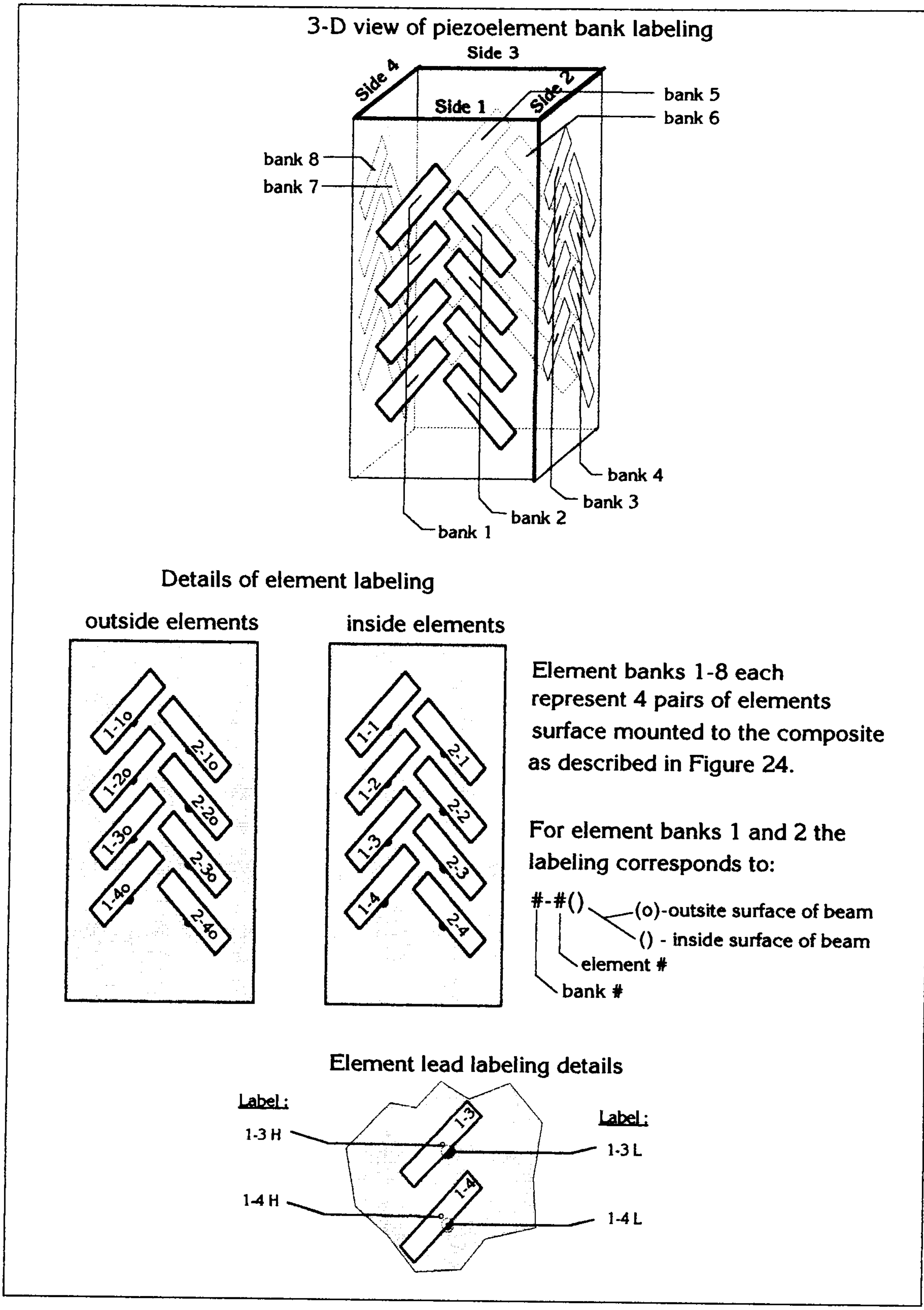

Figure 60 - Details of element and element lead wire labeling

piezoelements was then ready to be bonded to an inside wall of the composite beam.

The plexiglass mounting guide was then secured horizontally with the directionally prepared low voltage faces of the piezoelements facing up. Then, bonding epoxy was applied to each of the elements. The same mixture ratio of the Eccobond LV-45 epoxy resin/catalyst was used for bonding the prepared piezoelements to the composite beam as for the aluminum plate model. The application of the epoxy to the elements for bonding was also done in the same manner in the case of the aluminum plate model (please refer to section 6.1.3 for details). When all of the elements on the mounting guide had the epoxy applied to them, the composite beam was positioned on the mounting guide and held secure for the 24 hour room temperature cure. The details of the bonding configuration of the composite beam with respect to the mounting guide are shown in Figure 61.

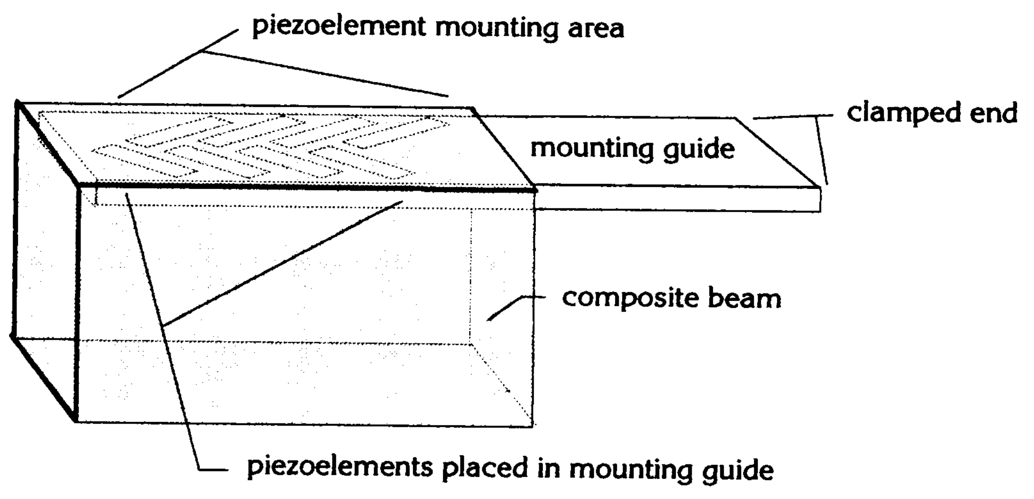

Figure 61 - Details of piezoelement bonding procedure

After the 24 hour cure, the plexiglass mounting guide was carefully detached from the bonded piezoelements. The finished product of the above procedure was a set of uniformly bonded elements mounted where a conventional element mounting technique would be very difficult, if not impossible.

The technique developed for mounting the piezoelements to the inside wall of the composite beam was repeated on the three remaining inside walls of the composite beam. At this point, the entire process was repeated for the four outside walls of the composite cylinder. This completed the fabrication of the composite beam with surface mounted piezoelements. Photographs of the completed composite beam with piezoelements are shown in Figures 62 to 64.

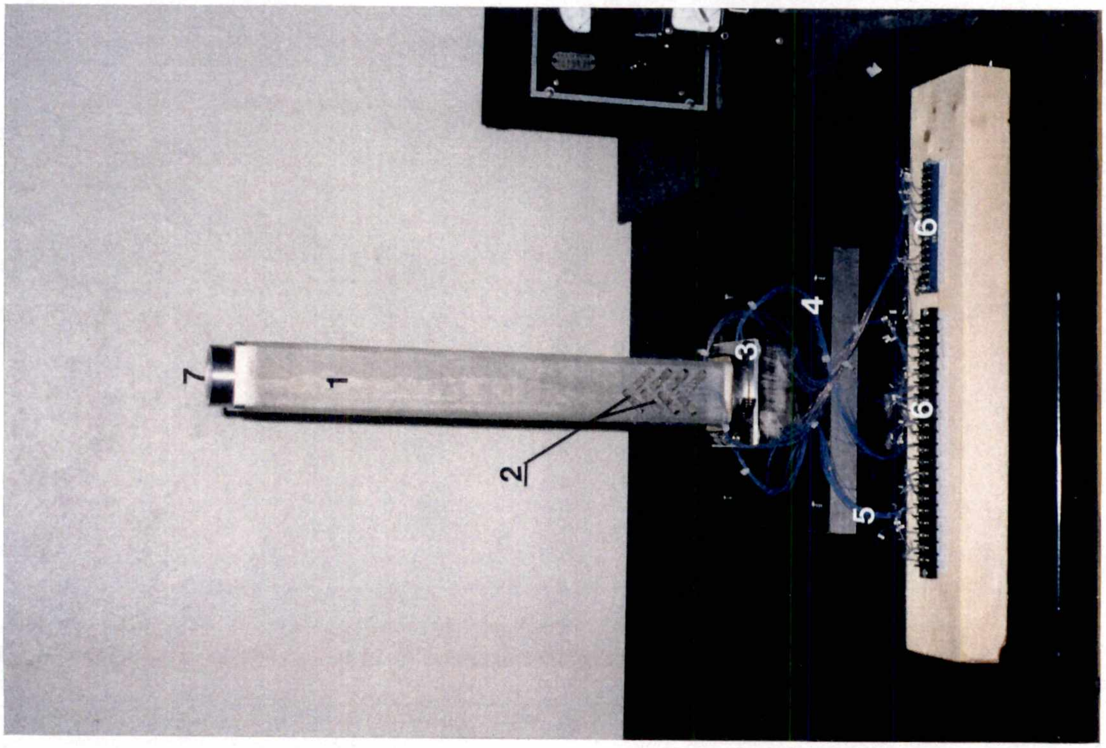

Figure 62 - Photograph of composite beam with piezoelements

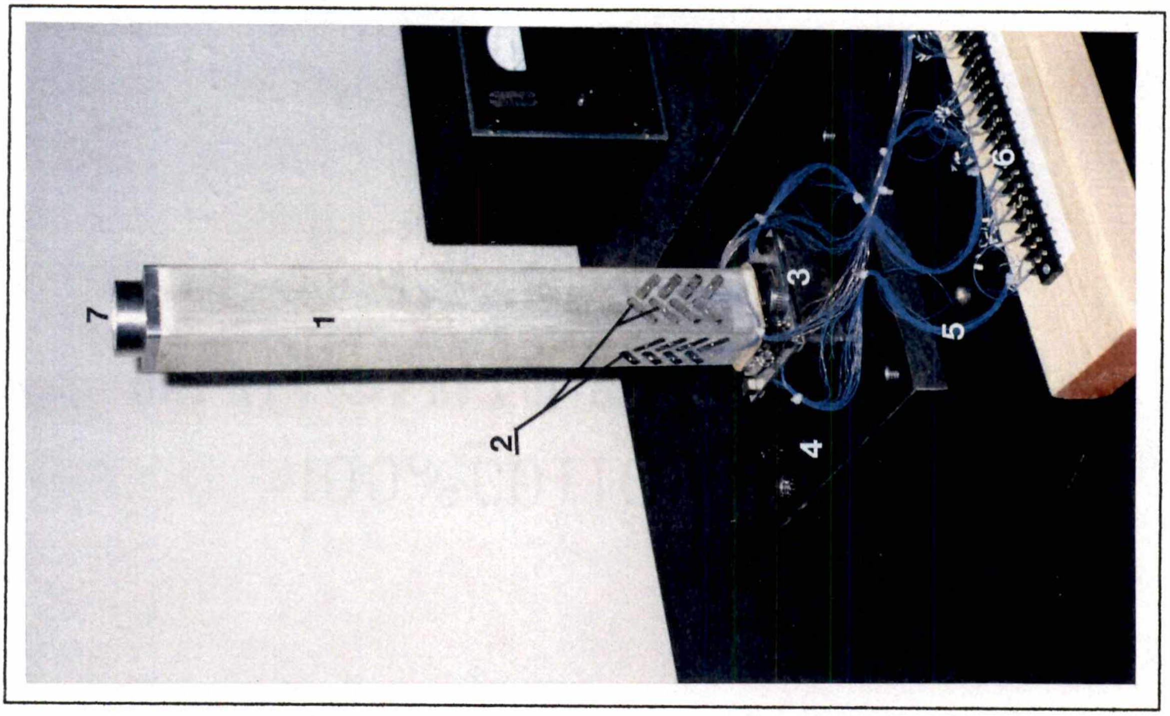

Figure 63 - Photograph of composite beam with piezoelements and aluminum chuck

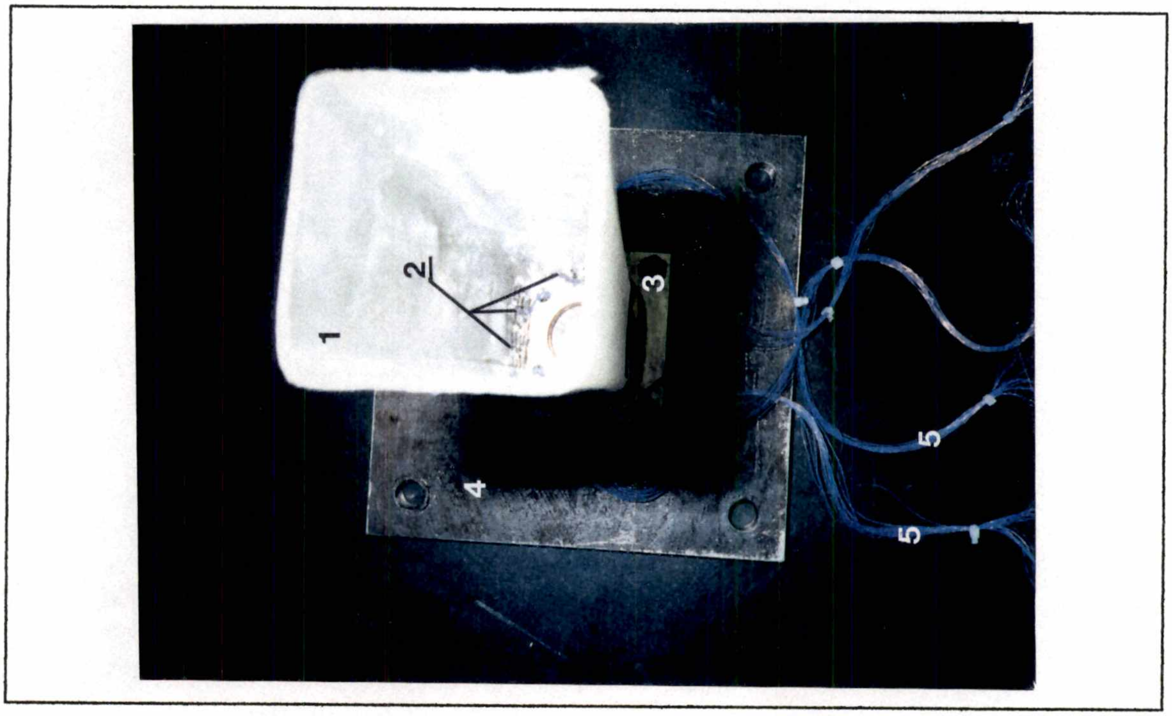

Figure 64 - Photograph of inside of composite beam with piezoelements

Referring to Figures 62 to 64, the labeling of the composite beam with piezoelements refers to:

1. Composite beam
2. Piezoelectric elements
3. Mounting base for composite beam
4. Torsional and bending testing rig (base only)
5. Piezoelement lead wires
6. Piezoelement lead bus
7. Aluminum chuck (used for experimental data collection)

An aluminum chuck was clamped into the free end of the composite beam. The purpose for the aluminum chuck was twofold: firstly, it provided a base for the mounting of a mirror used in the process of the optical measurements of bending and twisting displacements of the beam; secondly, it provided a base for the application of external forces used for the experimental evaluations of the flexural rigidity and the torsional rigidity of the beam. The chuck remained clamped to the free end of the beam during all experiments. The dimensions of the chuck are shown in Figure 65. Referring to Figure 65, the geometric details for two different mirror mounting setups are shown for optical measurement of bending and torsional displacements of the composite beam.

Please note: From this point on in the Thesis, the composite beam with the attached piezoelements will be referred to as the 'composite beam', whereas the composite beam (no elements attached) will be referred to as the 'beam specimen' or 'beam'.

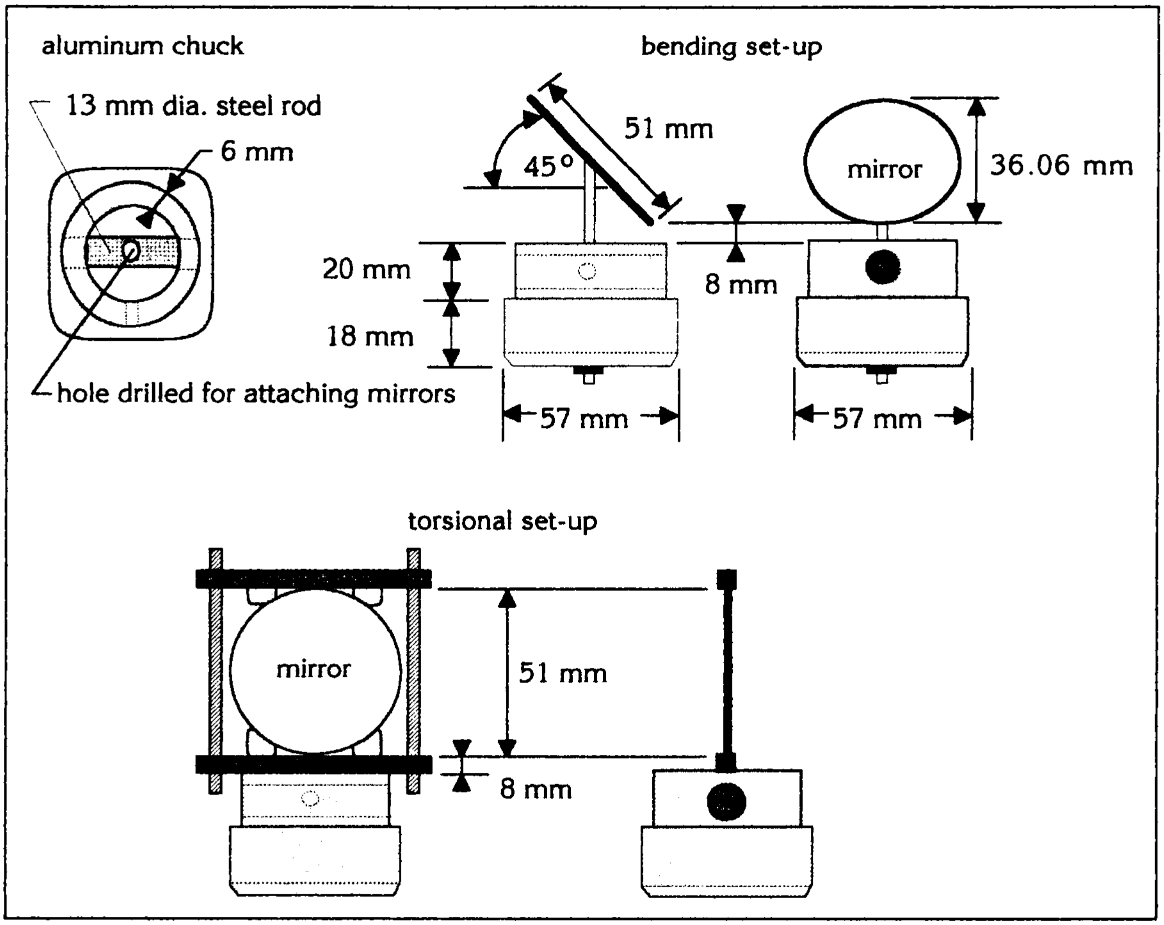

Figure 65 - Aluminum chuck dimensions

7.2 Investigation of flexural and torsional rigidity of the composite beam with piezoelements

Experiments were done to determine the flexural and torsional rigidity of the composite beam with piezoelements. For the case of flexural rigidity, a comparison between the experimental value and that of a theoretical value for the flexural rigidity was done to study the effects of surface mounting the piezoelements to the composite beam. However, no data correlation for the experimental torsional rigidity of the composite beam was done. Both of the bending and torsional rigidity experiments were the last set of experiments performed on the composite beam. This was to prevent any element damage prior the piezoelement induced static and dynamic displacement activation of the piezo-actuator experiments. However, no damage due to the deflections externally induced to the composite beam was noticed.

7.2.1 Experimental investigation of flexural rigidity of the composite beam with piezoelements

The set-up for the experimental investigation of flexural rigidity of the composite beam is shown schematically in Figure 66. For this experiment, the piezoelement end of the composite beam was clamped to the mounting base of the testing rig. A force was applied to the chuck so as to induce a bending deflection of the free end of the composite beam. The deflections of the free end of the composite beam were measured optically with a mirror and a laser (details of mirror geometry in Figure 65). The laser used for all composite beam experiments was a

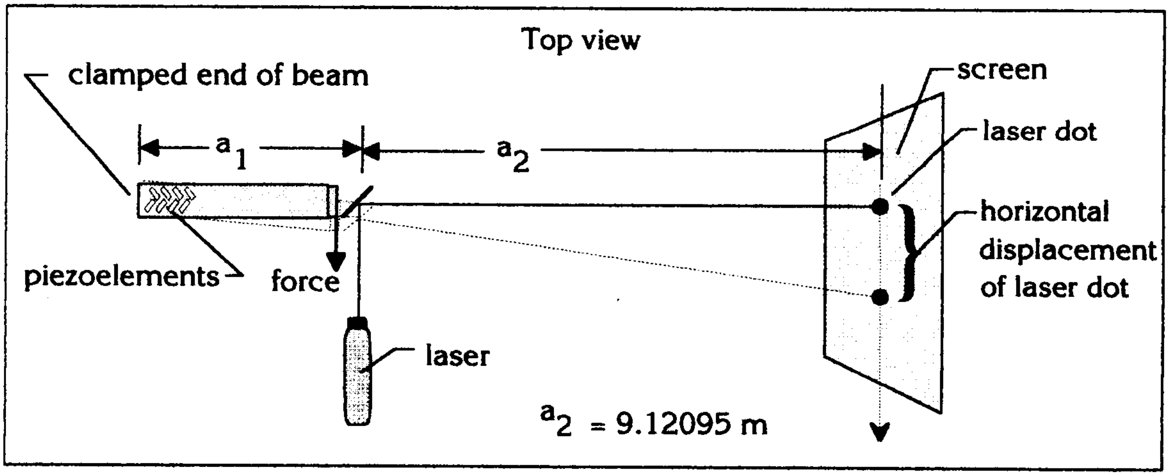

Figure 66 - Experiment set-up for flexural rigidity of composite beam

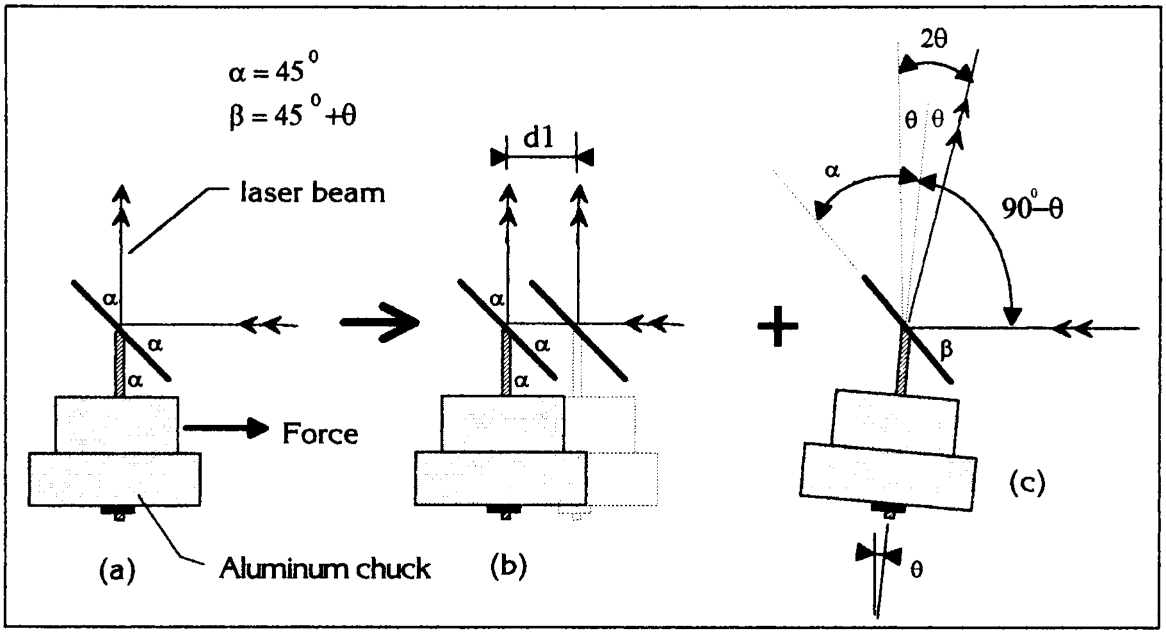

Figure 67 - Optical response of laser beam movement from induced bending composite beam: (a) force loading, prior to deflection, (b) translation of laser beam, (c) rotation of laser beam

Spectra Physics Stailite™ Model 120-Helium/Neon 15 mW laser. Figure 67 shows the combined translational and rotational effects of the composite beam free end with respect to the optical response of the laser. When the beam undergoes a bending displacement, the free end of the beam experiences a translational displacement and a rotation (Figure 67). The deflection of the composite beam free end due to the externally applied force was equal to the translational displacement (d1) of the beam shown in Figure 67. Optically, the rotational displacement of the free end of the beam adds a component to the laser dot displacement not representative of the true bending deflection. The laser dot refers to the resulting movement seen on a screen in Figure 66.

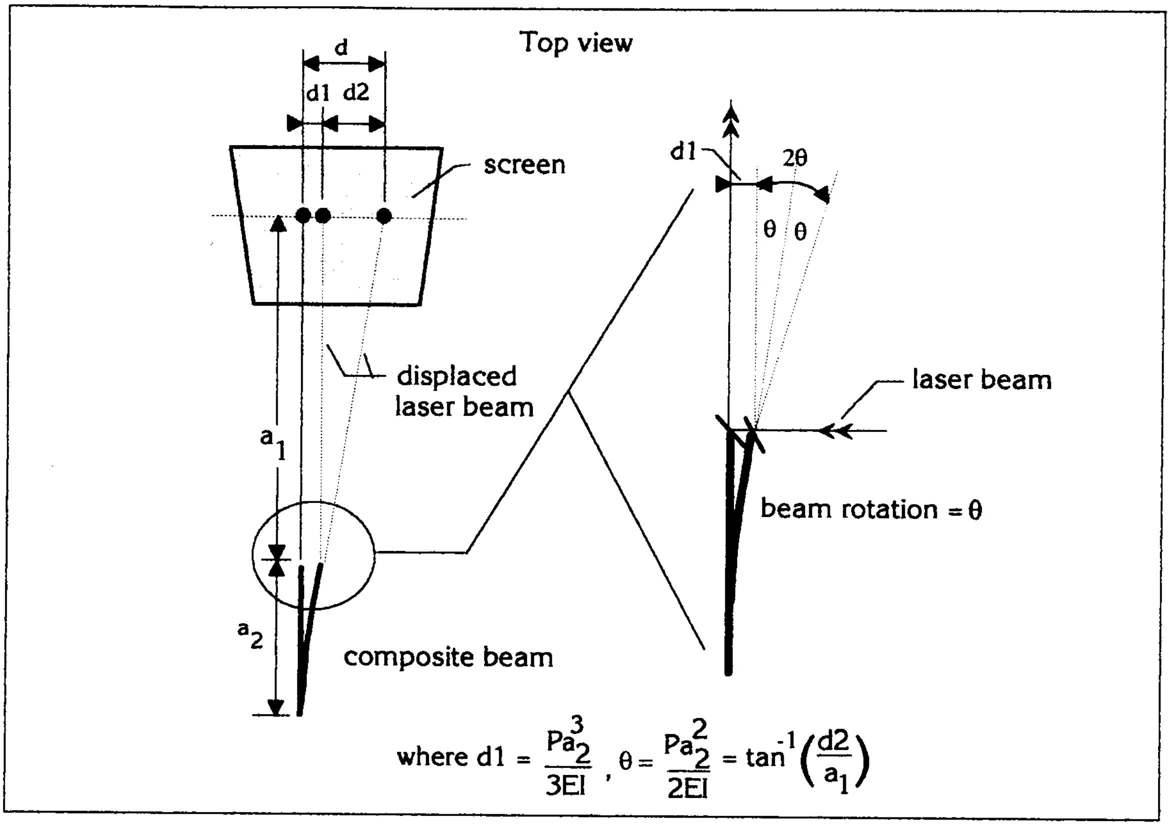

Figure 68 - Laser dot displacement components for bending of composite beam

The deflection of the free end of the composite beam due to the application of the force as depicted in Figure 66 is shown in Figure 68. With the relationships developed for the components of the laser dot displacement, the relation between the applied force (P) and the laser dot deflection (d) was found to be

$$d=\frac{Pa_2^3}{3EI}+a_1\tan\left(\frac{Pa_2^2}{2EI}\right) \qquad (24)$$

where the deflection of the composite beam (d1) is equal to the first term in equation (24) and the displacement of the laser dot due to the rotation of the free end of the composite beam (d2) is given by the second term of equation (24). All components for the composite beam experimental set-up in equation (24) are known except for the modulus of elasticity of the beam (E). Therefore, for a known externally applied bending force and the resulting measured laser dot displacement, the value for the modulus of elasticity for the composite beam was solved for iteratively.

The externally applied bending force (P) versus the displacement of the laser dot (d) is shown in Figure 69. The movement of the laser dot during the experiment followed a horizontal path on the screen. This horizontal laser dot movement rigidity indicated pure bending with no torsional displacements in the beam.

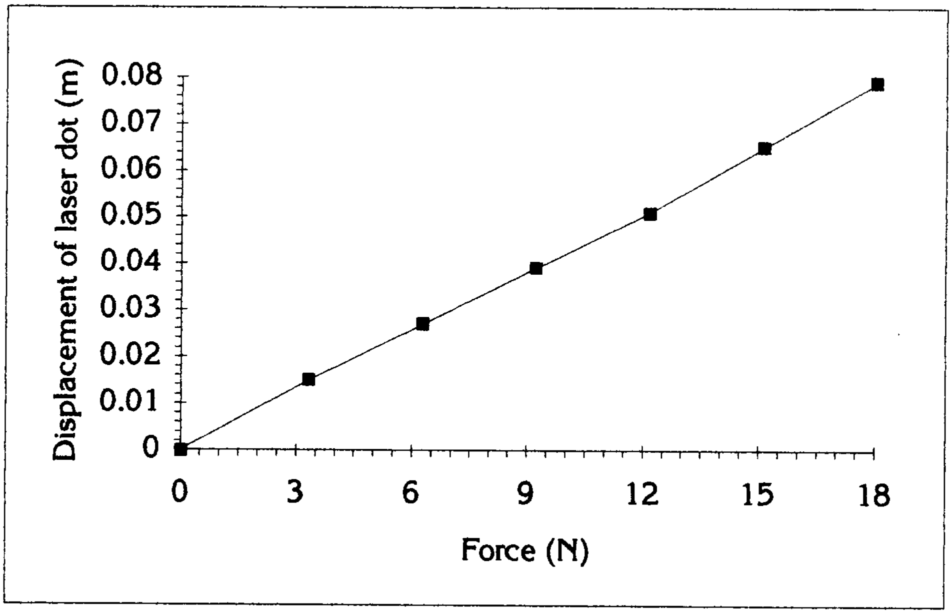

Figure 69 - Externally applied force versus laser dot displacement for bending rigidity of the composite beam

Since the data plotted in Figure 69 was nearly linear, an arbitrary force versus displacement was chosen for the calculation of E. The values used for the calculation were a laser dot displacement of d = 6.5E-2 m due to an applied bending force of 14.749 N was used. The experimental value for the modulus of elasticity of the composite beam was found to be 1.079E+10 Pa. The corresponding value for the flexural rigidity of the composite beam was 473.71 Nm^2. The ratio of the defection of the free end of the composite beam to the displacement of the laser dot (d1/d) was found to be 1.7012 E-2. This value (d1/d) was used for all remaining experiments to calculate composite beam bending deflection.

The theoretical value for the flexural rigidity of the composite beam was determined with Rayleigh's energy method applied to beams. The working equation for the natural frequency of a beam with a mass attached at the distance x from the base of the base is given by [26]

$$\varpi^2 = \frac{EI}{\rho A L^4}\left(\frac{\frac{\pi^4}{4}}{\left(12-\frac{32}{\pi}\right)+\frac{8M}{\rho AL}\left(1-\cos\frac{\pi x}{2l}\right)^2}\right) \qquad (25)$$

The natural frequencies for the composite beam were found experimentally. Equation (25) was used to calculate the modulus of elasticity by using the experimental value for the natural frequency for the composite beam. The first mode of bending for the composite beam corresponds to a natural frequency of 37.99 Hz. The method of obtaining this for the natural frequency for the composite beam is presented in detail in a later section. When this value for the natural frequency was used in equation (25), a theoretical value of 1.02369 E+10 Pa for the flexural modulus was calculated. This is equivalent to a value of 449.42 Nm^2 for the flexural rigidity of the composite beam. A difference of 5.126% between the experimental and theoretical values for the flexural rigidity of the composite beam exist, respectively. Also, the experimental value for the flexural modulus was used to solve for the theoretical value for the natural frequency of the composite beam. This calculation resulted in a theoretical value of 39.0 Hz for the natural frequency. A 2.65% difference between the two values exist. This discrepancy can be attributable to modeling the composite beam as a beam with constant physical properties, thus simplifying the complex nature of the bonded piezoelements. However, the results obtained are satisfactory considering the simplicity of the analytical model. All calculations for section 7.2.1 can be found in Appendix 5.

7.2.2 Experimental investigation of torsional rigidity of the composite beam with piezoelements

The experimental investigation of torsional rigidity of the composite beam was much less complex than for the flexural rigidity case. For the torsional rigidity case, the optical response of the laser beam used for measuring the externally induced twist of the composite beam due to an externally applied moment was straightforward. Figure 70 is a diagram of the experiment set-up for the torsional rigidity of the composite beam. Referring to Figure 70, the aluminum chuck was secured to an axle rod that was connected to the top and bottom of the test rig with sealed bearings. The axle rod was to ensure that a purely torsional displacement of

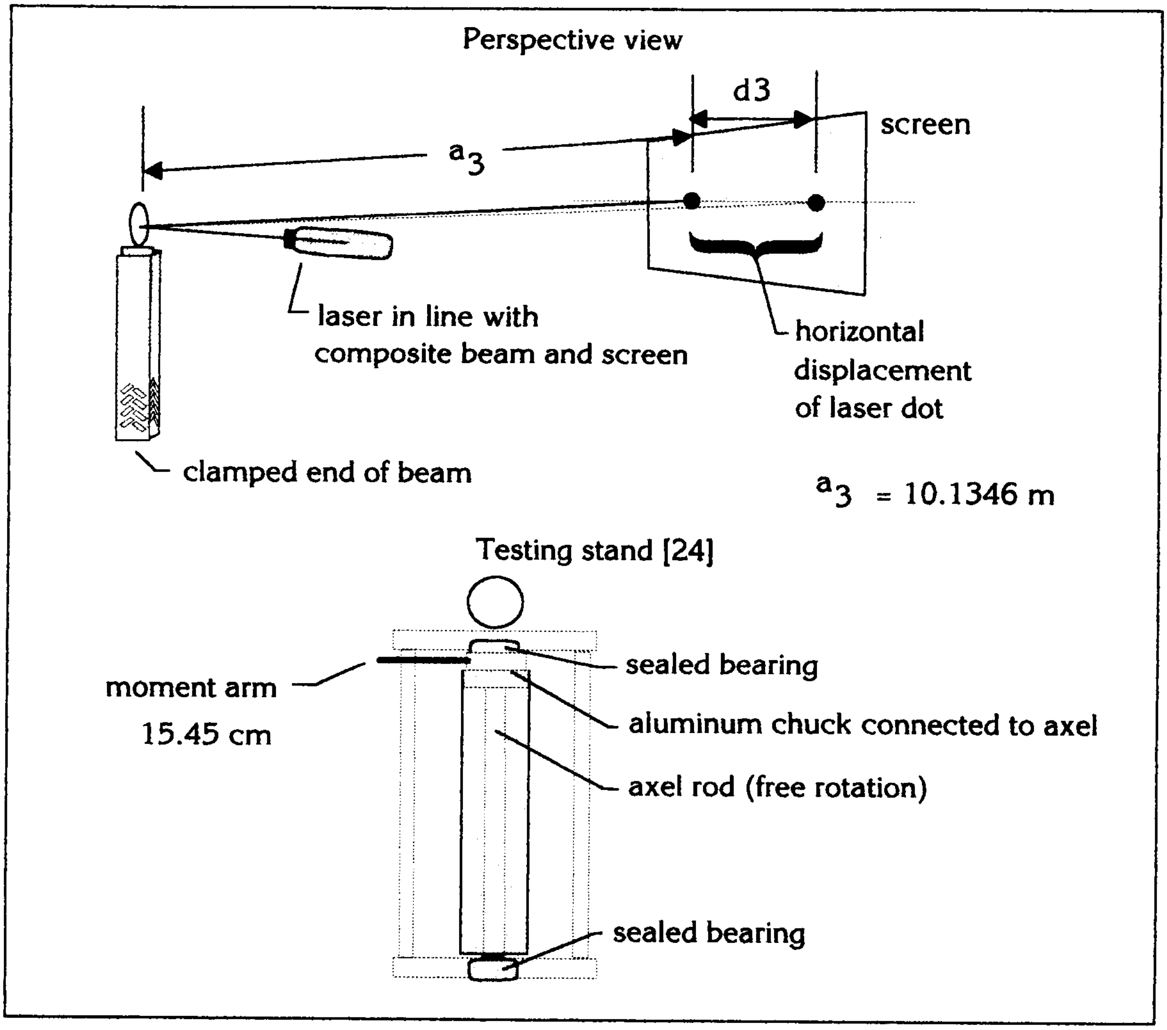

Figure 70 - Experiment set-up for torsional rigidity of composite beam

the beam would result from the externally applied moment. The length moment arm of the externally applied moment was 15.45 cm. Figure 71 shows the results of the externally induced twist of the composite beam (deg) versus the applied moment [Nm] obtained in the torsional rigidity experiment. The movement of the laser dot during the experiment followed a horizontal path on the screen. This horizontal laser dot movement indicated pure torsional displacement with no bending displacements in the beam.

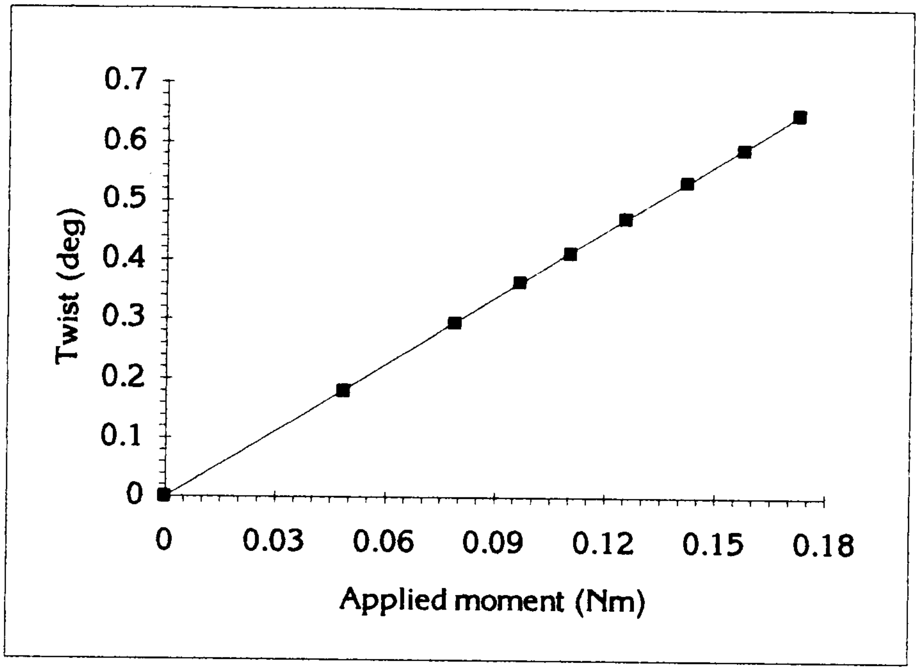

Figure 71 - Applied moment versus torsional displacement for torsional rigidity of composite beam

Since the measured twist of the beam versus the externally applied moment was very linear, an arbitrary data point was used for the calculation for the torsional rigidity. The experimental results for the torsional rigidity of the beam were obtained using the values of an applied moment of 0.1721 Nm and induced twist of 1.113 E-2 radians. Using these values, the shear modulus was found to be 1.0991 E+8 Pa. The torsional rigidity of the composite beam was found to be 7.2383 Nm^2. All calculations for section 7.2.2 can be found in Appendix 6.

7.3 Investigation of piezo-actuator static induced bending and torsional displacements

The experimental set-up for the piezo-actuator induced bending and torsional displacements were similar to the experimental set-up for the flexural and torsional rigidity investigations, respectively. All induced static bending and torsional displacements of the composite beam were due exclusively to the activation of the piezoelements.

7.3.1 Investigation of piezo-actuator induced bending displacements

The experimental setup for the piezoelement induced static bending deflections of the composite beam is shown schematically in Figure 72. The physical set-up of the experiment for the measurement of the bending deflection of

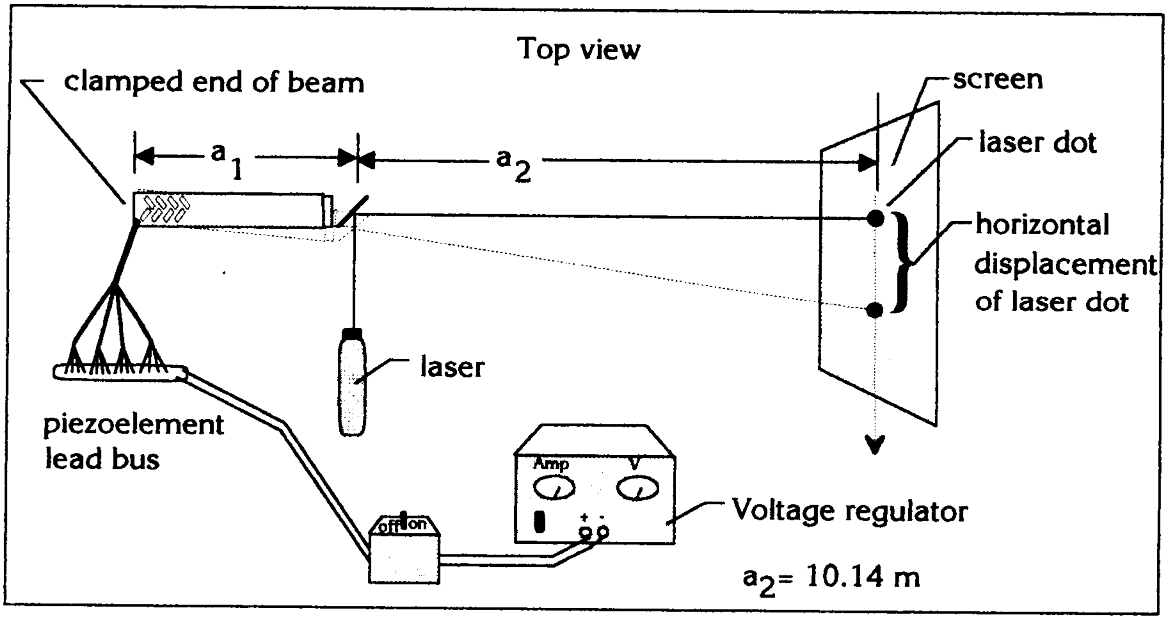

Figure 72 - Experiment set-up for composite beam static bending deflections

the composite beam was the same for that in Section 7.2.1.

7.3.2 Details of piezoelement activation potential sequence for bending displacement of the composite beam

In order to induce the desired bending displacement of the plate, the elements must be activated in the proper sequence. Figure 73 shows the composite beam loading configuration used to induce bending displacement.

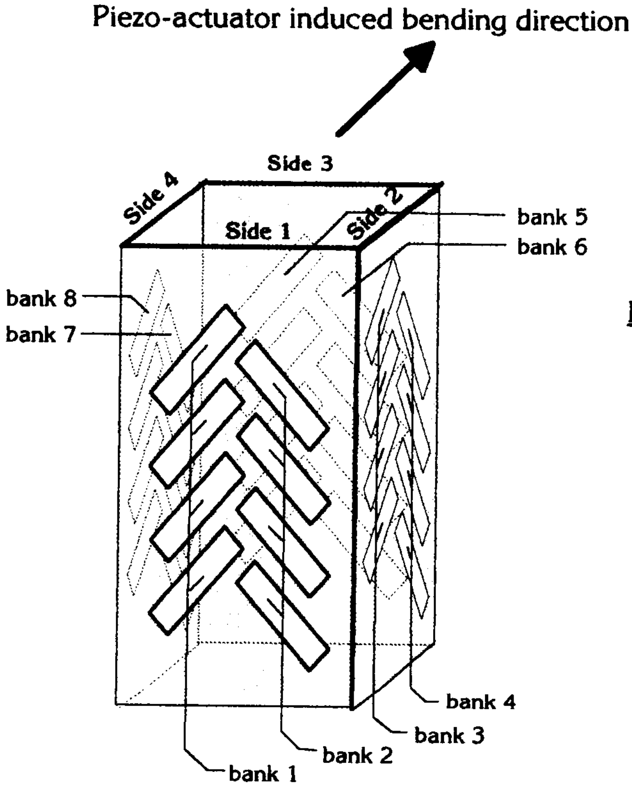

Element banks	Activation
1,2,3,8	elongation
4,5,6,7	contraction

Figure 73 - Composite beam loading for piezo-actuator induced bending

Referring to Figure 73, element banks 1 and 2 (both outer and inner elements) were activated to induce longitudinal elongation of side one of the composite beam. Element banks 5 and 6 (both outer and inner elements) were activated to induce longitudinal contraction of side three of the composite beam. Element banks 3 (side four) and 8 (side two) (both outer and inner elements) were activated to induce longitudinal elongation. Element banks 4 (side four) and 7 (side two) (both outer and inner elements) were activated to induce longitudinal contraction. To develop the described loading of the plate, the elements were given the activation voltages listed in Table 21 (please refer to Figure 60 for details of element labeling).

Table 21- Activation potential details for static bending displacement

Element no.	Direction of activation potential (Volts)	Element no.	Direction of activation potential (Volts)
1-1o to 1-4o	(-)	5-1o to 5-4o	(+)
1-1 to 1-4	(-)	5-1 to 5-4	(+)
2-1o to 2-4o	(-)	6-1o to 6-4o	(+)
2-1 to 2-4	(-)	6-1 to 6-4	(+)
3-1o to 3-4o	(-)	7-1o to 7-4o	(+)
3-1 to 3-4	(-)	7-1 to 7-4	(+)
4-1o to 4-4o	(+)	8-1o to 8-4o	(-)
4-1 to 4-4	(+)	8-1 to 8-4	(-)

7.3.3 Data correlation for the statically bending displacement of the composite beam

When the maximum activation potential was applied through the elements, no optically measurable displacements could be made. However, it was apparent that some deflection of the beam existed. This knowledge comes from observing the behavior of the laser dot on the screen. When the elements were activated, the laser dot appeared to have some change of position. However, no hard data for the induced deflection of the composite beam was collected.

7.3.4 Investigation of piezo-actuator induced torsional displacements

The experimental setup for the induced static torsional deflections of the composite beam is shown schematically in Figure 74. The physical set-up of the experiment for the measurement of the torsional deflection of the composite beam was similar for that in Section 7.2.2. The axle rod used for the torsional rigidity investigation was removed, as well as the moment arm assembly.

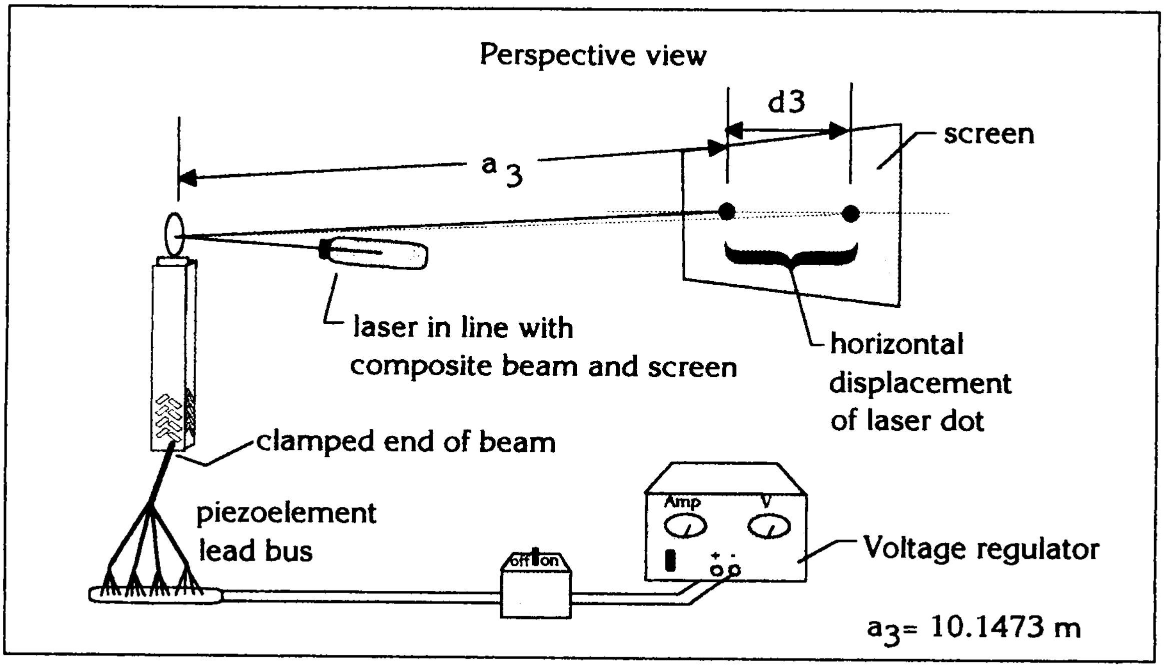

Figure 74 - Experiment set-up for composite beam static torsioanl displacements

7.3.5 Details of piezoelement activation potential sequence for torsional displacement of the composite beam

In order to induce the desired torsional displacement of the plate, the elements must be activated in the proper sequence. Figure 75 shows the composite beam loading configuration used to induce torsional displacements. The reasoning behind the activation sequence is that each side of the beam behaves like the aluminum plate model (layout two) in shear. Therefore, when the elements are activated, twisting of the composite beam will result with no axial elongation or bending in the composite beam. In order to induce the twisting of the beam, the

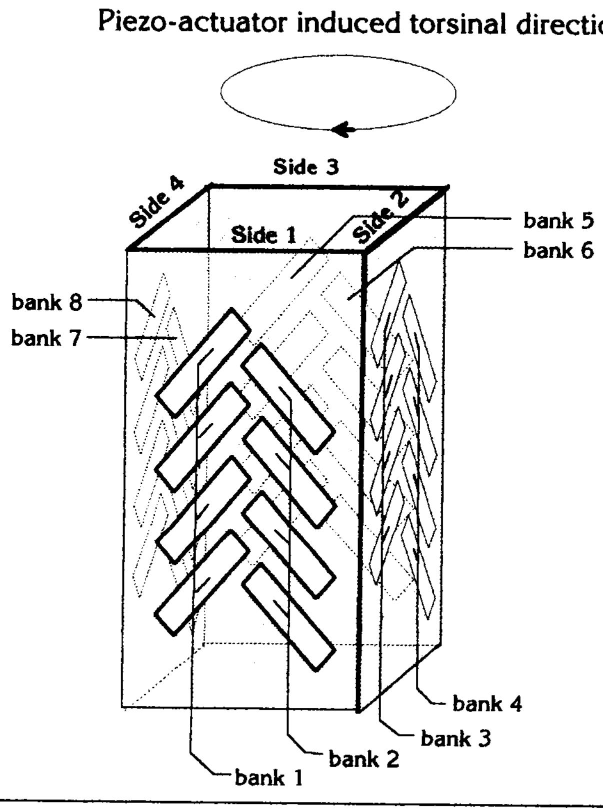

Element banks	Activation
2,4,6,8	elongation
1,3,5,7	contraction

Figure 75 - Composite beam loading for piezo-actuator induced torsional displacment

elements were given the activation voltages listed in Table 22 (please refer to Figure 60 for details of element labeling).

Table 22- Activation potential details for static torsional displacement

Element no.	Direction of activation potential (Volts)	Element no.	Direction of activation potential (Volts)
1-1o to 1-4o	(-)	5-1o to 5-4o	(-)
1-1 to 1-4	(-)	5-1 to 5-4	(-)
2-1o to 2-4o	(+)	6-1o to 6-4o	(+)
2-1 to 2-4	(+)	6-1 to 6-4	(+)
3-1o to 3-4o	(-)	7-1o to 7-4o	(-)
3-1 to 3-4	(-)	7-1 to 7-4	(-)
4-1o to 4-4o	(+)	8-1o to 8-4o	(+)
4-1 to 4-4	(+)	8-1 to 8-4	(+)

7.3.6 Data correlation for the torsional displacement of the composite beam

To generate torsional displacements, values for the activation potential of 30, 60, 90, 120, and 150 volts were applied through the elements on the composite beam. The results for the torsional displacement of the composite beam versus the activation potential for the piezoelements are shown in Figure 76.

The results plotted in Figure 76 show that the composite beam had consistently greater magnitudes of twist to the left (counterclockwise) than to the right (clockwise). This phenomenon was probably the result of the non-uniform material properties due to the overlap of the composite fibers during the fabrication of the beam. Had the overlap of the fibers been positioned perfectly along the corner of beam, the non-symmetric twisting characteristics of the composite beam would have been reduced. Figure 77 shows the magnitude of the discrepancy between the clockwise and counter clockwise twisting of the composite beam versus the activation potential through the elements.

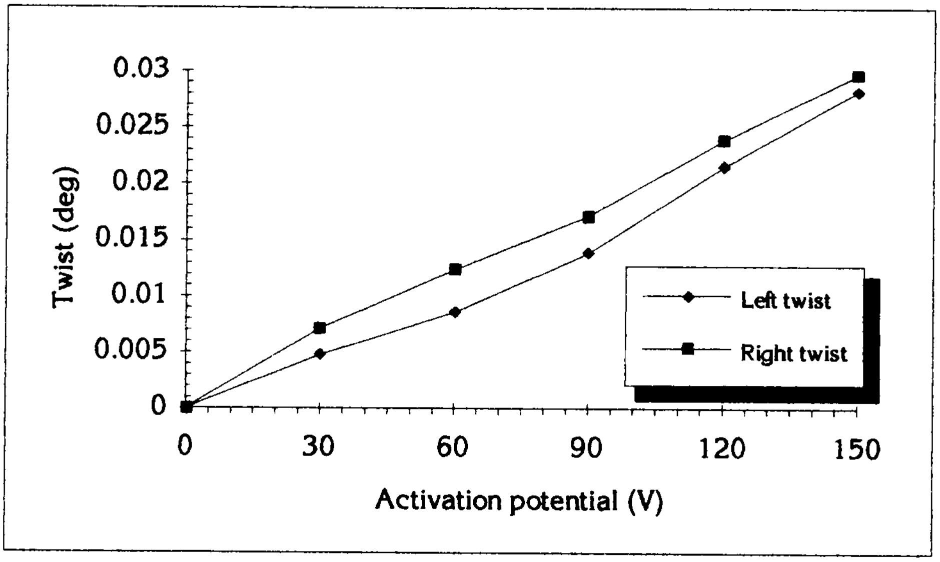

Figure 76 - Static induced torsional displacement versus activation potential

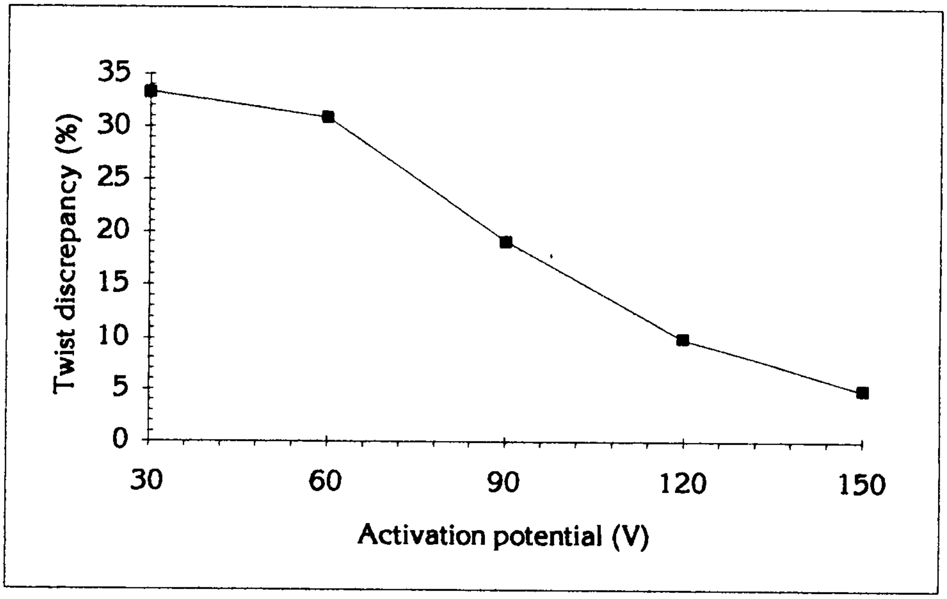

Figure 77 - Magnitude of twist discrepancy between counterclockwise and clockwise static torsional displacements

Referring to Figure 77, It was apparent that as the activation potential increased, the non-symmetric characteristics of the composite beam decreased. At low activation levels, the increased stiffness due to the overlapping composite overrides the symmetrically induced torsional moment of the activated piezoelements. At higher activation levels, the effects of the overlapping composite were overcome by the presence of a much larger symmetrically induced moment from the activated piezoelements.

Although the displacements of the laser dot during the experiment were small, it remained horizontal throughout the full range of the applied activation voltages. A state of pure bending would have resulted in a vertical laser dot displacement of the composite beam. Any coupling of bending and torsional displacement would have resulted in a laser dot displacement inclined at an angle with respect to the horizontal plane of the screen. Figure 78 shows the details for laser dot responses due to coupled bending and torsional displacements for both experimental set-ups. Therefore, the horizontal displacement of the laser dot indicated that a minimum of bending displacements occurred. Therefore, the composite beam was capable of generating almost pure torsional displacements with no discernible bending deformations. All pertinent data for section 7.3.6 can be found in Appendix 7.

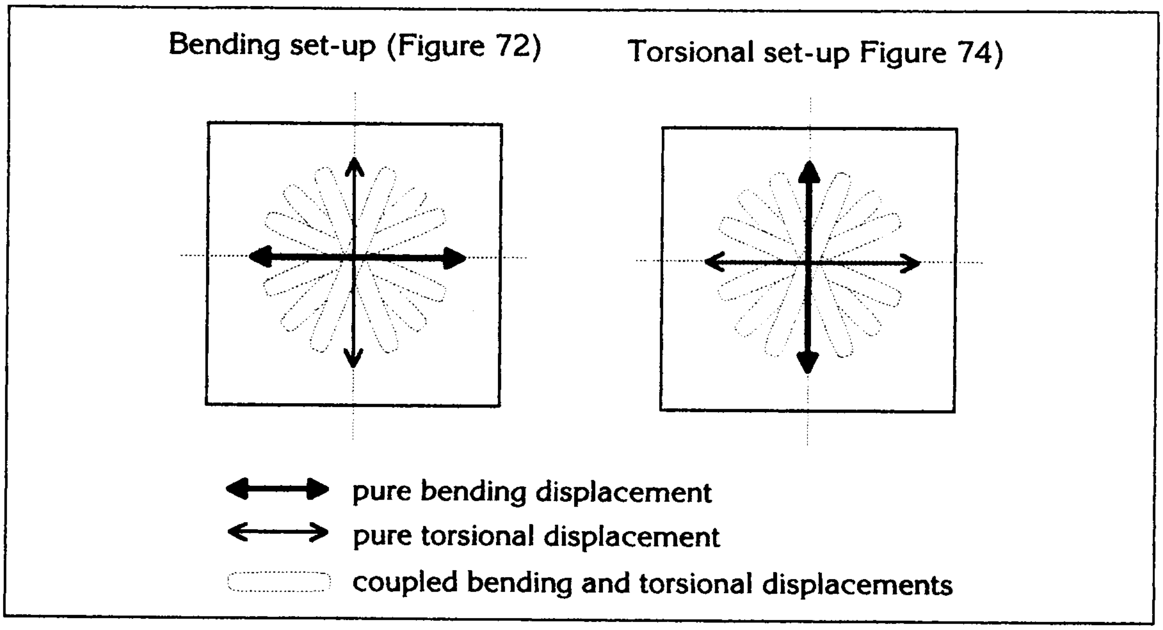

Figure 78 - Laser dot responses for coupled composite beam displacements

7.4 Investigation of piezo-actuator induced bending and torsional resonance

In order to obtain the maximum displacements of the composite beam, the piezoelectric actuators were activated at the resonant frequencies of the composite beam. The experimental set-up for the piezo-actuator resonance induced bending and torsional displacements was the exact same as the experimental set-up for the static displacement tests. The only addition to the experimental set-ups for the static displacement tests were the addition of strain gages mounted to the beam and a controllable voltage source.

7.4.1 Investigation of piezo-actuator induced bending resonance

The experimental setup for the resonance induced bending deflection and modal analysis of the composite beam is shown schematically in Figure 79. The physical set-up of the experiment for the measurement of the bending defection of the composite beam was the same for that in Section 7.2.1. Three strain gages were attached to the diagonally opposing overlap corner of the composite beam. The piezoelements were driven by a Piezo Amplifier Model 60-102 purchased from Piezo Systems Inc.. The amplifier was capable of delivering a positive sine wave output of 0 to +/-200 V DC or +/- 100 V DC true sine wave output. The amplifier had a gain

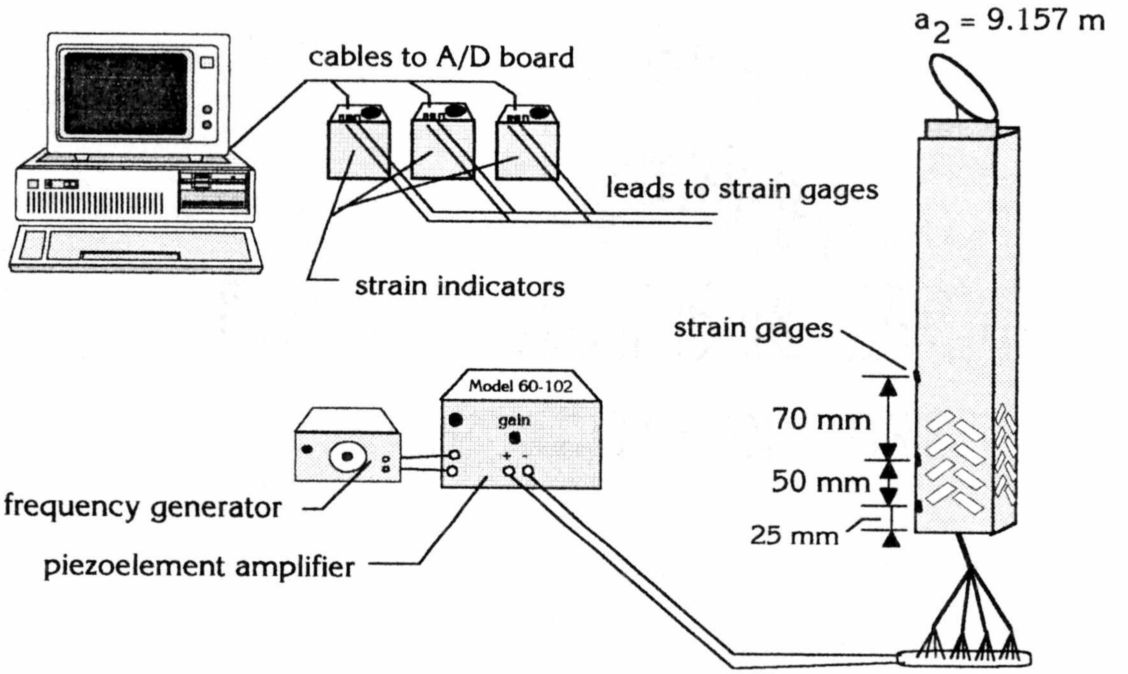

Note: the beam was excited with an impulse, or by the activated piezoelements with this set-up. The optics for measurement were the same as Figure 72.

Figure 79 - Experiment set-up for composite beam bending resonance and modal analysis

control for increasing an input voltage from 0 to 20 times. The input signal to the amplifier was provided by a Model 110 Wavetek Function Generator. The frequency generator was capable of producing a positive sine wave output of 0 to 10 V or +/- 5 V true sine wave output.

7.4.2 Investigation of composite beam bending modal frequencies

The natural frequencies of the composite beam were obtained experimentally. An impulse was delivered to the free end of the composite beam (please refer to Figure 79). It was important to induce the bending vibrations with an impulse parallel to the bending direction to reduce any effects of torsional displacement. The strain gage/indicator sent the composite beam response due the externally applied impulse to the A/D board. The composite beam response to the impulse is shown graphically in Figure 80.

An FFT [27] analysis of the frequency response shown in Figure 81 showed that the composite beam has two distinct bending modal natural frequencies. The modal frequencies for the beam were 37.99 Hz and 158.74 Hz. By analyzing the three strain gage responses, it was determined the first mode of bending corresponds to a natural frequency of 37.99 Hz. The three strain gages showed that the strain states at the three different locations on the composite beam were the in phase with one another. That is, all three locations of the beam were experiencing simultaneous extension or compression. Figure 82 shows the strain states (mV indicator output) of the three locations on the composite beam. The three locations

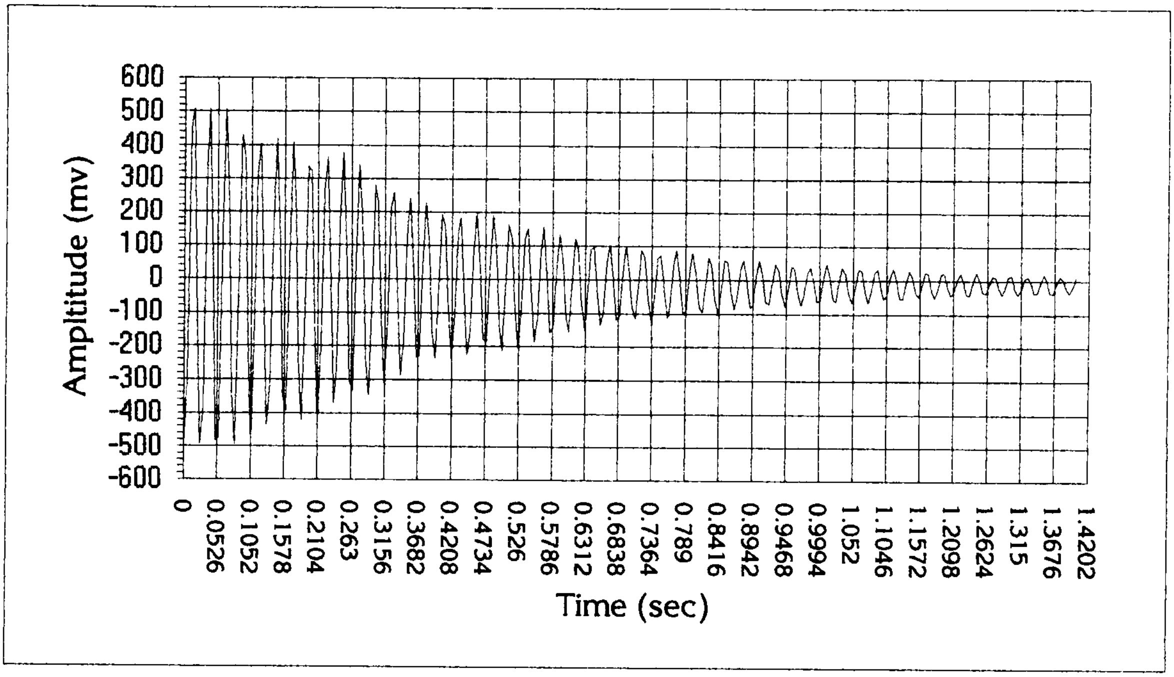

Figure 80 - Composite beam response to a bending impulse

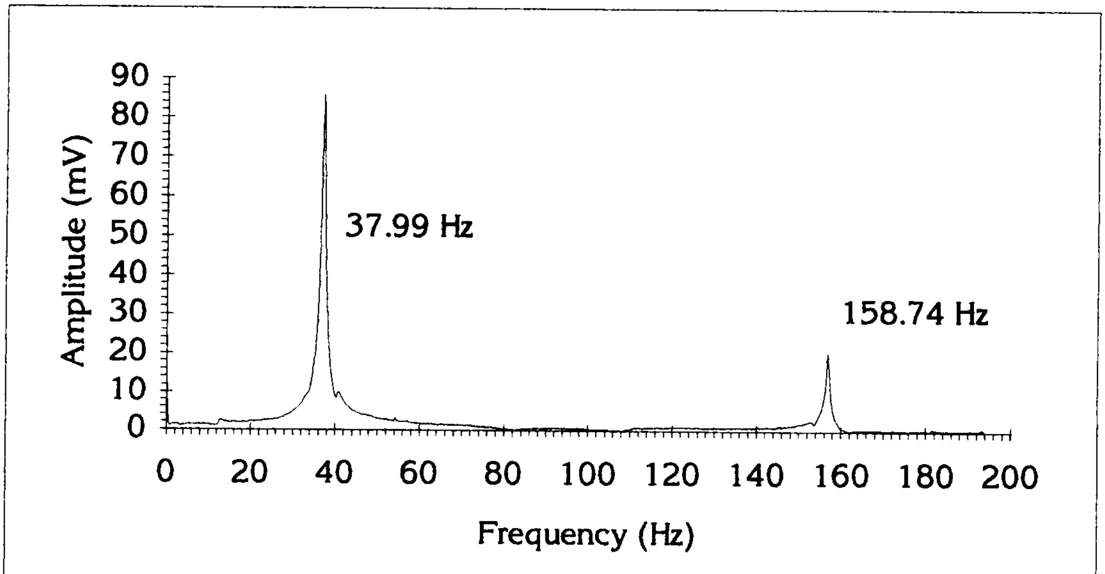

Figure 81 - FFT analysis results of composite beam bending modal frequencies

(please refer to Figure 79) on the composite beam experiencing the same strain state leads to the conclusion that the beam was experiencing first mode bending.

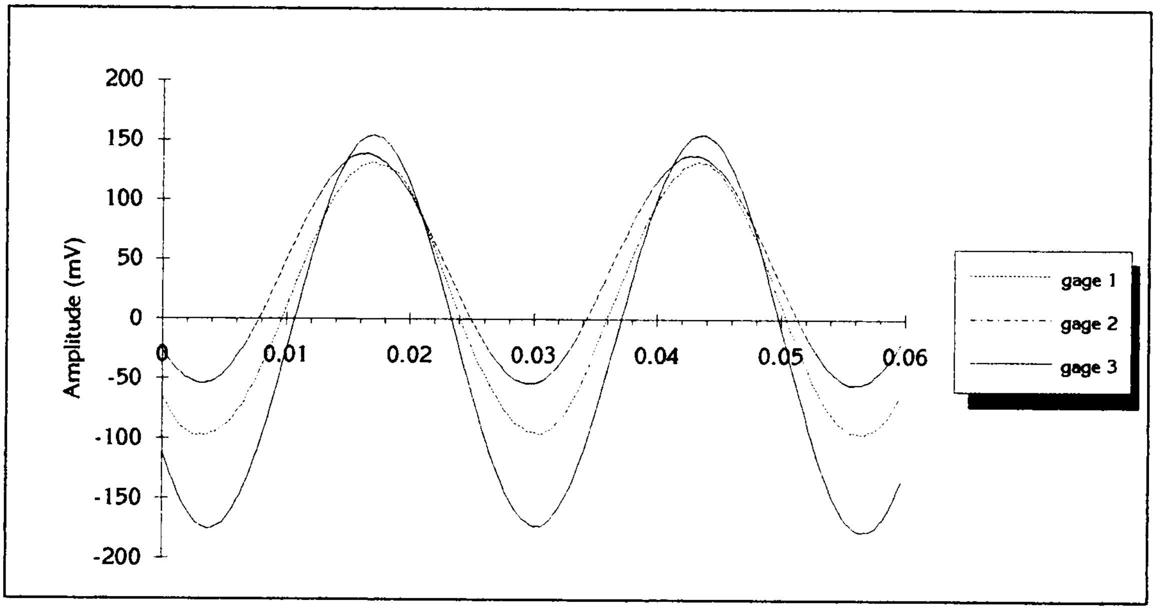

Figure 82 - Strain states (gage responses) for first mode bending for the composite beam

7.4.3 Data correlation of piezo-actuator induced bending resonance

The experiments for the displacements due to the resonance induced bending for the composite beam were done with the amplifier set-up to deliver an activation voltage of +/- 100 V DC true sine wave. This was done by setting the output voltage on the frequency generator to its maximum output. Since the +/- 100 V corresponds to only 66% of the maximum activation voltage, the maximum displacements of the beam were not found. However, since the dynamic activation of the piezoelements was more demanding on the elements than statically induced potentials, this safety margin was looked upon favorably.

When the piezo-actuators were dynamically activated with the sine wave activation potential, the maximum displacements of the laser dot were found to be at the following frequencies: 38 +/- 1 Hz, and 162 +/- 1 Hz. The data for these results is shown in Table 23. For the tabulated results in Table 23, the laser dot displacement represents the full motion of the laser dot from left to right.

Table 23 - Maximum bending displacements of composite beam.

Freq.(hz)	Displacement of laser dot (m)				Deflection of Beam (m)
	Trial 1	Trial 2	Trial 3	Avg.	
38	0.026	0.025	0.026	0.025666667	0.000444033
162	0.038	0.04	0.037	0.038333333	?

From Table 23 it was shown that the maximum induced bending resonance occurred at the activation frequency of 38 Hz. The difference between the externally induced modal frequency of 37.99 Hz and the modal frequency value found by the piezo-actuator induced resonance was negligible. The difference between the externally induced modal frequency of 158.74 Hz and the modal frequency value found by the piezo-actuator induced resonance of 162 Hz was 2.05%. Apparently, the FFT analysis was a very accurate method to predict the modal frequencies for the composite beam. Referring to Table 23, even though the laser dot displacement was greater for the activation frequency of 162 Hz, the bending displacement for this case was not calculated. This was due to the fact that the true shape of the beam was not known at this modal frequency. However, these results do confirm that the 38 Hz modal frequency was the first bending mode frequency for the composite beam.

Inspection of the laser dot during the piezo-actuator induced bending resonance for the case of 38 Hz showed an axial path along the horizontal axis of the screen. This showed that the beam experienced a state of pure bending. The path of the laser dot for the first mode resonance of the composite beam was at an angle of 6.2° with respect to the horizontal. This result can be explained as follows: either that the first mode of bending was affected by the non-uniform material properties of the composite due to the overlap of composite fibers; or, that coupled bending and torsional displacements occurred. Due the optical geometry for the experiment, pure torsional rotation of the beam would result in the laser dot following a vertical path (please refer to Figure 78). The result of a coupled displacement of the composite beam would be a laser dot path at an angle to the horizontal axis. Therefore, as the torsional component of the coupling increased, the angle with respect to the horizontal axis would also increase. For the experimental results obtained at the activation frequency of 158.74 Hz, this analogy provides a bending displacement of 4.44 E-4 m coupled with a torsional rotation of 2.4 E-2 degrees. The other explanation for the 6.2° angle of the laser dot was that the non-symmetrical physical properties overrides the pure bending capabilities at this frequency. This is analogous to the case for the static torsional induced case. The analogy is that where the static torsional case over came the adverse effects of the of the non symmetrical properties of the beam as the activation potential increased, the induced bending at resonance over comes the adverse effects at the higher modal frequency.

7.4.4 Investigation of piezo-actuator induced torsional resonance

The experimental setup for the resonance induced torsional rotation and modal analysis of the composite beam is shown schematically in Figure 83. The physical set-up of the experiment for the measurement of the torsional rotation of the composite beam was the similar for that in Section 7.2.2. The only differences were those listed in section 7.4.1.

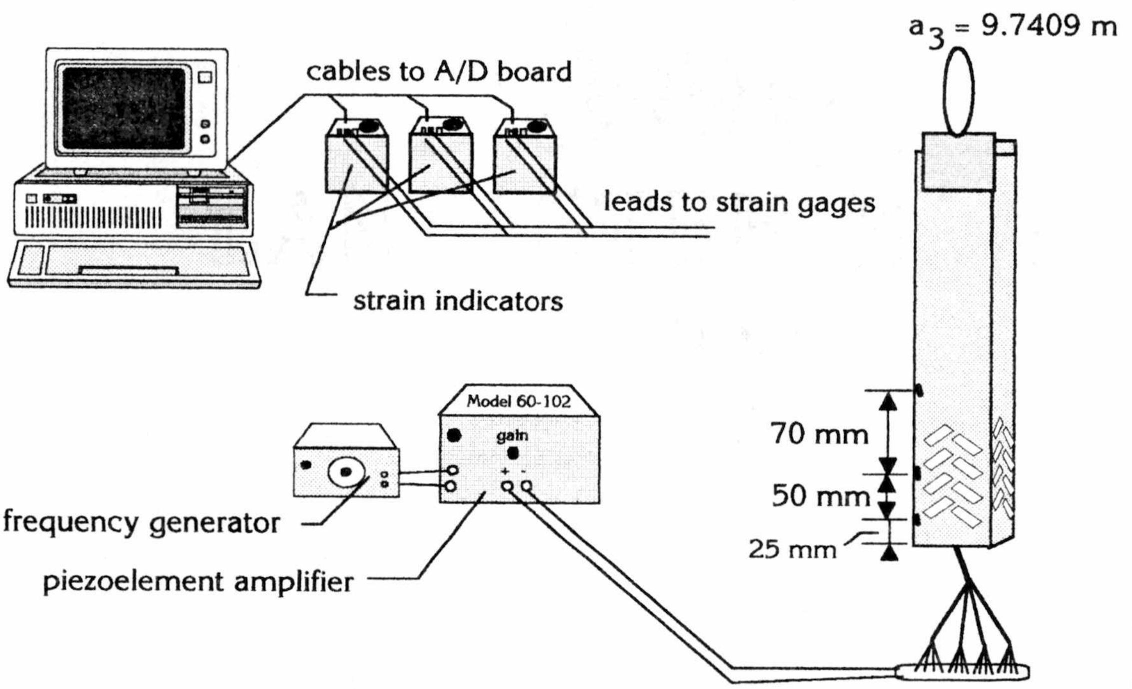

Note: the beam was excited with an impulse, or by the activated piezoelements with this set-up. The optics for measurement were the same as Figure 74.

Figure 83 - Experiment set-up for composite beam torsional resonance and modal analysis

7.4.5 Investigation of composite beam torsional modal frequencies

An impulse was delivered to the free end of the composite beam (please refer to Figure 83). It was important to induce the torsional vibrations with an impulse parallel to the torsional displacement plane to reduce any effects of bending displacements. The composite beam response to the impulse is shown graphically in Figure 84.

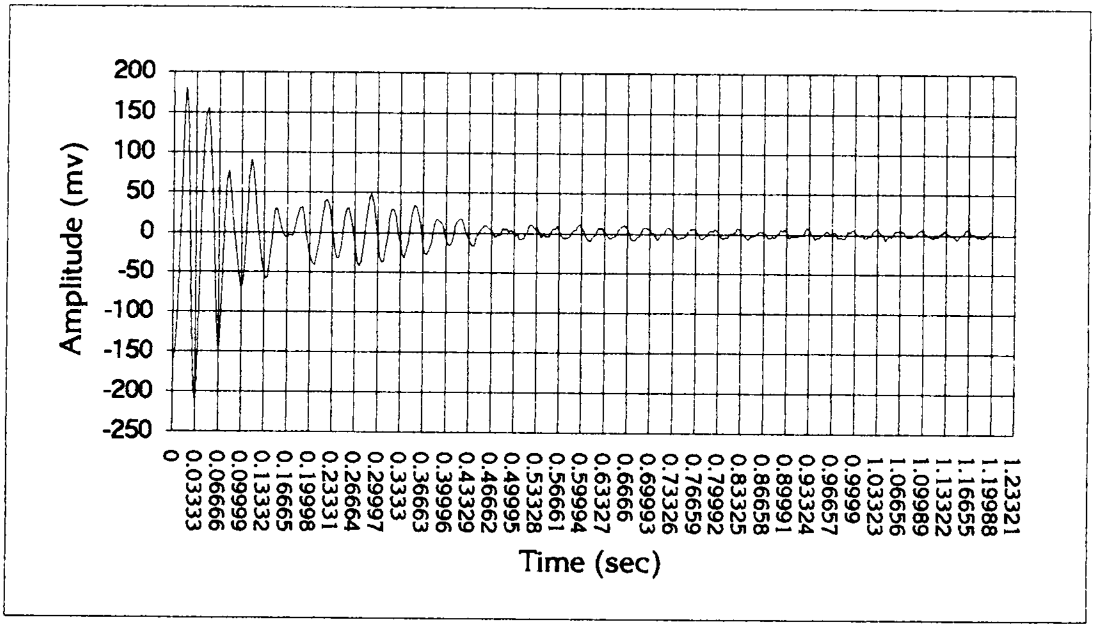

Figure 84 - Composite beam response to a torsional impulse

The FFT analysis of the frequency response shown in Figure 85 showed that the composite beam had two distinct modal natural frequencies due to the applied impulse. The modal frequencies for the beam were found to be 32.904 Hz and 196.0 Hz. It will be shown that the 32.904 Hz modal frequency was due to coupling of torsional and bending displacements of the beam, and that the 196.0 Hz modal frequency was the first torsional natural frequency.

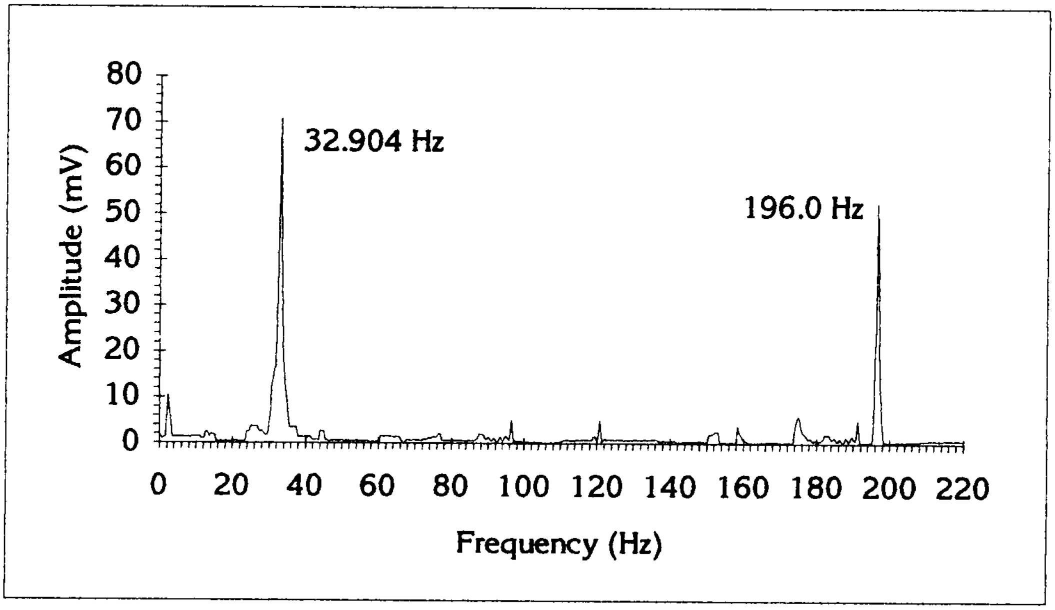

Figure 85 - FFT analysis results of composite beam torsional modal frequencies

7.4.6 Data correlation of piezo-actuator induced torsional resonance

The experiments for the displacements due to the resonance induced torsional displacement for the composite beam were done with the same amplifier set-up as for the bending case. The same activation of +/- 100 V for the experiments. When the piezo-actuators were dynamically activated with the sine wave activation potential, the maximum displacements of the laser dot were found to be at the following frequencies: 30 +/- 1 Hz, and 200 +/- 1 Hz. The data for these results is shown in Table 24. For the tabulated results in Table 24, the laser dot displacement represents the full motion of the laser dot from left to right for 30 Hz, and from top to bottom for 200 Hz.

Table 24 - Maximum torsional displacements of composite beam.

Freq.(hz)	Displacement of laser dot (m)				Twist of Beam (deg)
	Trial 1	Trial 2	Trial 3	Avg.	
30	0.025	0.027	0.027	0.026333333	pure bending
200	0.027	0.028	0.027	0.027333333	0.16077

From Table 24 it was shown that the maximum induced bending resonance occurred at the activation frequency of 200 Hz. The difference between the externally induced modal frequency of 196.0 Hz and the modal frequency value found by the piezo-actuator induced resonance was 9.68.04%. The difference between the externally induced modal frequency of 32.904 Hz and the modal frequency value found by the piezo-actuator induced resonance of 30 Hz was 7.27%. The FFT analysis results were relatively accurate for the torsional case as well.

Referring to Table 24, the laser dot displacement for the activation frequency of 200 Hz gave a value of 0.16077 degrees. The displacement for the laser dot was 0.026333 m. Inspection of the laser dot during the piezo-actuator induced torsional resonance for the case of 200 Hz showed an axial path along the horizontal axis of the screen. This showed that the beam experienced a state of pure torsional displacement. The path of the laser dot for the activation frequency of 30 Hz was nearly vertical with respect to the screen. The result of the laser dot displacement observation was that the beam was experiencing coupling between bending and torsional displacements (please refer to section 7.3.6 and Figure 78 for details). These results showed that the composite beam's response to the input actuation frequency of 30 Hz is from the was coupled, whereas the composite beam response the actuation frequency of 200 Hz was pure torsional displacement. Therefore, the first torsional modal frequency was 196 Hz.

CHAPTER 8

CONCLUSIONS

This research has attempted to evaluate the feasibility of generating non-coupled bending and torsional displacements in thin-walled composite and metallic structural members using piezoelectric elements as presented by [20]. The numerical analysis and experimental models used to validate the concepts of non-coupled piezoelement induced displacements are concluded upon here.

The analytical analysis of an aluminum plate with piezoelements surface mounted in two configurations predicted non-coupled shearing and bending displacements of the free edge of the plate. Although not reported, an analysis of the elongation of the plate due to the activated piezoelements resulted in non-coupled axial displacements of the plate. Therefore, non-coupled displacements for the three possible displacement types of a structure were predicted.

The numerical analysis of the aluminum plate model also predicted non-coupled shearing and bending displacements. Although the numerical analysis results for the displacements for the plate model were on the order of 75% smaller than those predicted by the analytical analysis, they did provide insight into the details of the deformations induced by the activated piezoelements. It was seen that restraining the free end of the plate model with a rigid steel bar reduced any micro edge deformations and ensured even bending displacements of the free edge of the plate.

The experimental results of the aluminum plate model with piezoelements showed that the activated piezoelements were capable of generating the displacements predicted by the analytical analysis, both in shear and bending. It was also shown that the addition of the piezoelements increased the shear modulus of the aluminum plate by 45.25%, and an increase of the bending rigidity of the aluminum by 114.75%. These increases provide insight to the changes of the mechanical properties of a substrate due to the addition of discretely attached piezoelements in a pattern to induce non-coupled displacements.

The experimental results obtained using the composite beam with piezoelements showed that generating non-coupled bending and torsional displacements are feasible. Statically induced non-coupled torsional displacements of the composite beam on the order of 0.03° were feasible. Piezoelement induced first mode composite beam resonance resulted in a maximum bending deflection of 4.44033 E-4 m at 38 Hz and maximum torsional rotation of 0.16077° at 200 Hz. The bending resonance at 38 Hz was slightly coupled, whereas the higher modal bending resonance at 162 Hz resulted in a pure torsional displacement of the beam. Therefore, the activation of the piezoelements at the higher bending modal frequency resulted in non-coupled bending of the composite beam. The torsional resonance at 200 Hz was non-coupled rotation whereas the lower modal torsional resonance at 30 Hz resulted in pure bending. Therefore, the 200 Hz modal frequency was the first torsional modal frequency of the composite beam.

The testing of the aluminum plate model and the composite beam model proved that non-coupled displacements in structural members using piezoelectric elements is possible.

REFERENCES

REFERENCES

1 Crawley, E. F. and de Luis, J., 1987, "Use of Piezoelectric Actuators as Elements of Intelligent Structures", *AIAA* Journal, Vol. 25, No. 10.

2 Bailey, T. and Hubbard, J. E., 1985, "Distributed piezoelectric polymer active vibration control of a cantilever beam", *Journal of Guidance and Control*, Vol. 8, No. 1, pp. 605-611.

3 Baz, A. and Poh, S., 1988, "Performance of an Active Control System with Piezoelectric Actuators", *Journal of Sound and Vibration*, Vol. 126, No. 2, pp. 327-343.

4 Tzou, H. S. and Garde, M., 1989, "Theoretical Analysis of a Multilayered Thin Shell Coupled with Piezoelectric Shell Actuators for Distributed Vibration Controls", *Journal of Sound and Vibration*, Vol. 126, No. 2, pp. 327-343.

5 Chan, W.P., Samak, D.K., and Chopra, I., 1991, "Development of Scaled Rotor Using Smart Structures Technology", *Proceedings of the Fourth Workshop on Dynamics and Aeroelastic Stability Modeling of Rotorcraft Systems*, University of Maryland, College Park, Maryland.

6 Barrett, R.M., "Intelligent Rotor Blade and Structures Development Using Directionally Attached Piezoelectric Crystals", Master's Thesis, University of Maryland, College Park, May 1990.

7 Barrett, R.M., "Active Plate and Missile Wing Development Using EDAP Elements", Paper presented at the Third International Conference on Adaptive Structures, November 9-11, San Diego, Ca.

8 Wood, E. R. et al., 1985, "On Developing and Flight Testing a Higher Harmonic Control System" , *Journal of the American Helicopter Society*, Vol. 30, No.1.

9 Hammond, C. E., 1983, "Wind Tunnel Results Showing Rotor Vibratory Loads Reduction Using Higher Harmonic Blade Pitch", *Journal of the American Helicopter Society*, Vol. 28, No.1.

10 Cudney, H.H., Alberts, T.E. and Colvin, J. A., "A Classical Approach to Structural Control with Piezoelectrics", AIAA-92-2462-CP, The 33rd AIAA/ASME/ASCE/AHS/ASC SDM Conference Proceedings, pp. 2118-2126, Dallas, TX, April 13-15, 1992.

11 Allik ,H., Hughes, T.J.R., "Finite Element Method for Piezoelectric Vibration", *International Journal for Numerical Methods in Engineering*, Vol. 2, 151-157 (1970).

12 Lee, C.K., Moon, F.C., "Modal Sensors/Actuators", *Journal of Applied Mechanics*, Vol. 57, June 1990.

13 Lin, M. W. and Rogers, C.A., "Formulation of a Beam Structure with Induced Strain Actuators Based on an Approximated Linear Shear Stress Field", AIAA-92-2524-CP, The 33rd AIAA/ASME/ASCE/AHS/ASC SDM Conference Proceedings, pp. 896-904, Dallas, TX, April 13-15, 1992.

14 Wang, B.T., and Rogers, C.A., "Modeling of Finite - Length Spatially - Distributed Induced Strain Actuators for Laminate Beams and Plates", Journal of Intelligent Material Systems and Structures, Vol.2, No.1, 1991, pp.38-58. Paper No. AIAA-91-1258.

15 Chaudry, Z., and Rogers, C. A., "Enhanced Structural Control with Discretely Attached Induced Strain Actuators", AIAA-92-2404-CP, The 33rd AIAA/ASME/ASCE/AHS/ASC SDM Conference Proceedings, pp. 548-565, Dallas, TX, April 13-15, 1992.

16 Wang, B., and Rogers, C.A., "Laminate Plate Theory for Spatially Distributed Induced Strain Actuators" , *Journal of Composite Materials*, Vol. 25 , April 1991.

17 Lee, C.K., Moon, F.C., "Laminated piezopolymer plates for torsion and bending sensors and actuators", *Journal Acoust. Soc. Am.*, Vol. 85, No. 6, June 1989.

18 Crawley, E.F., and Lazarus, K.B., "Induced Strain Actuation of Isotropic and Ansiotropic Plates", *AIAA* Journal, Vol. 29, No.6, January, 1990.

19 Ha, S., Keilers, C. and Chang, F, "Finite Element Analysis of Composite Structures Containing Distributed Piezoceramic Sensors and Actuators", *AIAA* Journal, Vol. 30, No.3, March 1990.

20 Grzegorz, Kawiecki, Assistant Professor, Department of Mechanical and Aerospace Engineering, University of Tennessee, Knoxville, Tn., Personal communication.

21 Jones, R. M., Mechanics of Composite Materials, "Macromechanical Behavior of a Laminate", Scripta Book Co., 1975, pp. 147 to 171.

22 Lin, M.W., Graduate Project Associate, Virginia Polytechnic Institute and State University, Blacksburg, Va., Personal communication.

23 Kensley, R.S., Piezo Systems Inc., Advanced Technology Group, Cheif Engineer., Personal communication.

24 Hu, Chenyi, Graduate student, Mechanical Engineering, University of Tennessee.

25 Smith, Winthrop P., Graduate teaching assistant, Aerospace Engineering, University of Tennessee.

26 Shames, I.H., Dym, C.L., Energy and Finite Element Methods in Structural Mechanics, Hemisphere Pub. Corp.; McGraw Hill, c1985.

27. Higdon, Dennis, Electronics Specialist, Department of Mechanical and Aerospace Engineering, University of Tennessee

APPENDICES

APPENDIX 1

DATA FILES FOR MODIFIED CLPT ANALYSIS

The data files used to solve the analytical model using the modified CLPT follow. The data files listed within this appendix are duplicates of the actual files submitted to MACSYMA. However, the actual files that were submitted did not have comments. Any comments contained within parenthesis within the input files were added at a later date. However, the output files for the expressions for the laminate shear strains and curvature strains were pasted into the appendix as is.

Four data files were run to obtain the final form magnitude of the shear and curvature strains. These cases are listed below:

<u>Shear strains</u>

Case 1. Laminate plate with piezo-actuators at -45°, activated in compression

Case 2. Laminate plate with piezo-actuators at +45°, activated in compression

<u>Curvature strains</u>

Case 3. Laminate plate with piezo-actuators at -45°, top layer of piezo-actuators activated in tension, bottom layer of piezo-actuators activated in compression.

Case 4. Laminate plate with piezo-actuators at +45°, top layer of piezo-actuators activated in tension, bottom layer of piezo-actuators activated in compression.

The data files for cases (1) and (3) are listed in their entirety. Cases (2) and (4) are not listed, but the differences them was minor. The only difference between case (1) and (2) was the value for the bonding angle and the sign of the actuation strain. The only differences between cases (3) and (4) was the sign for the bonding angle. The input data files and the expressions for the shear and curvature strains follow.

Symbols used for Modified CLPT

amij	Components of actuator extensional stiffness matrix
aaijj	Components of substrate (aluminum) extensional stiffness matrix
bmij	Components of actuation bending matrix
dmij	Components of actuator bending stiffness matrix
daij	Components of substrate (aluminum) bending stiffness matrix
	where m= l (lower) and u (upper), i=1 to 6, j=1 to 6
d31	Piezoelectric charge coefficient
e11,e22	Axial strains induced in laminate
e11	Shear strain induced in laminate
k11,k22	Planar curvatures induced in laminate
k12	coupled curvature induced in laminate

es	Modulus of elasticity of substrate (aluminum)
e1effo	Longitudinal effective modulus of elasticity (piezoelements)
e2teffo	Transverse effective modulus of elasticity
lambda	Free induced strain from piezo-actuators
gs	Shear modulus of substrate (aluminum)
t	Transpose matrix
tact	Thickness of piezo-actuator
tal	Thickness of substrate (aluminum)
v	Poisson's ratio
x	Longitudinal bonding angle of piezoelements with respect to laminate x-axis
zN	Distance measured from neutral axis of laminate, N=1 to 3

DATA FILE FOR CASE 1

(This data file attempts to calculate the shear strains in the laminate plate generated by the piezoelectric elements bonded at -45 degrees and activated in compression.)

(Laminate geometry)

```
z3:tal/2+tact;
z2:tal/2;
z1:-tal/2;
z0:-tal/2-tact;
```

(Physical properties of actuator)

```
v12:v;
```

```
v21:v;
g12a:ga;
g21a:ga;
```

(Physical properties of substrate (aluminum))

```
v12a:v;
v21a:v;
g12s:es/2/(1+v);
g21s:es/2/(1+v);
e1s:es;
e2s:es;
```

(Components of piezo-actuator extensional stiffness matrix)

(lower laminae)

```
al11:(eleffo*(z3-z2))/(1-v12*v21);
al12:v12*(eteffo*(z3-z2))/(1-v12*v21);
al22:(eteffo*(z3-z2))/(1-v12*v21);
al16:0;
al26:0;
al66:g12a*(z3-z2);
```

(upper laminae)

```
au11:(eleffo*(z1-z0))/(1-v12*v21);
au12:v12*(eteffo*(z1-z0))/(1-v12*v21);
au22:(eteffo*(z1-z0))/(1-v12*v21);
au16:0;
au26:0;
au66:g12a*(z1-z0);
```

(Components of aluminum substrate extensional matrix)

```
aa11:(e1s*(z2-z1))/(1-v12a*v21a);
aa12:v12*(e2s*(z2-z1))/(1-v12a*v21a);
aa22:(e2s*(z2-z1))/(1-v12a*v21a);
aa16:0;
aa26:0;
aa66:g12s*(z2-z1);
```

(Angle of longitudinal rotation of elements with respect to laminate axis)

```
x:-%pi/4;
```

(Transpose matrix)

t:matrix([cos(x)^2,sin(x)^2,2*cos(x)*sin(x)],[sin(x)^2,cos(x)^2,-2*cos(x)*sin(x)],[
-cos(x)*sin(x),cos(x)*sin(x),cos(x)^2-sin(x)^2]);

(Upper and lower piezoelement laminae extensional stiffness)

apql:matrix([al11,al12,al16],[al12,al22,al26],[al16,al26,al66]);
apqu:matrix([au11,au12,au16],[au12,al22,au26],[au16,au26,au66]);

r:matrix([1,0,0],[0,1,0],[0,0,2]);

ti:t^^-1;
ri:r^^-1;

(Transposed extensional stiffness matrix, lower and upper piezoelement laminae)

adpl:ti.apql.r.t.ri;

adpu:ti.apqu.r.t.ri;

(Addition of both piezoelement extensional stiffness matrices)

am:adpl+adpu;
am:ratsimp(am);

(Aluminum substrate extensional stiffness matrix)

alam:matrix([aa11,aa12,aa16],[aa12,aa22,aa26],[aa16,aa26,aa66]);

(Laminate stiffness matrix comprised of extensional stifnesses of both piezoelement laminae and the aluminum laminae)

als:alam+am;

(actuation strain vector)

sap:matrix([lambda],[lambda],[0]); (assume the piezoelements produce no shear)

(solving equation 12)

aaa:am.sap;

ali:als^^-1;
su:ali.aaa;

ee11:row(su,1);

```
ee22:row(su,2);
ee12:row(su,3);

e11:ratsimp(ee11);
e22:ratsimp(ee22);
e12:ratsimp(ee12);
```

(Opening an output file for the strain solutions)

```
writefile("e12nc.out");

e11:factor(e11);
e22:factor(e22);
e12:factor(e12);
```

(Physical and geometrical properties of aluminum and piezoelements)

```
tact:.191*10^-3;
tal:.292*10^-3;
v : .33;
es : 63*10^9;
eleffo : 56.2*10^9;
eteffo : 11.5*10^9;
d31:190*10^-12;
volt:150;
lambda:volt*d31/tact;
```

(Solving for maximum activation potential (150 volts))

```
ev(e11);
ev(e22);
ev(e12);

closefile();
quit();
```

OUTPUT FILE FOR CASE 1

```
(D57)                SYS$USER2:[WIN]E12NC.OUT;1


(C58) e11:factor(e11);

                                             2              2        2
(D58) MATRIX([- TACT (2 ES ETEFFO TAL V  + 4 ETEFFO  TACT V  - ES ETEFFO TAL V
```

```
+ ELEFFO ES TAL V - ES ETEFFO TAL - ELEFFO ES TAL - 4 ELEFFO ETEFFO TACT)

                                             2                       2
LAMBDA/((ES TAL + 2 ETEFFO TACT) (ES TAL V  + 2 ETEFFO TACT V  - ES TAL

- 2 ELEFFO TACT))])

(C59) e22:factor(e22);

                                        2              2          2
(D59) MATRIX([- TACT (2 ES ETEFFO TAL V  + 4 ETEFFO  TACT V  - ES ETEFFO TAL V

+ ELEFFO ES TAL V - ES ETEFFO TAL - ELEFFO ES TAL - 4 ELEFFO ETEFFO TACT)

                                             2                       2
LAMBDA/((ES TAL + 2 ETEFFO TACT) (ES TAL V  + 2 ETEFFO TACT V  - ES TAL

- 2 ELEFFO TACT))])

(C60) e12:factor(e12);

(D60) MATRIX([2 ES (ETEFFO - ELEFFO) TACT TAL (V + 1) LAMBDA

                                      2                       2
/((ES TAL + 2 ETEFFO TACT) (ES TAL V  + 2 ETEFFO TACT V  - ES TAL

- 2 ELEFFO TACT))])


(C61) tact:.191*10^-3;

(D61)                    1.91e-4

(C62) tal:.292*10^-3;

(D62)                    2.92e-4

(C63) v : .33;

(D63)                    0.33

(C64) es : 63*10^9;
```

```
(D64)                    63000000000

(C65) eleffo : 56.2*10^9;

(D65)                    5.62e10

(C66) eteffo : 11.5*10^9;

(D66)                    1.15e10

(C67) d31:190*10^-12;

                        19
(D67)               ------------
                    100000000000

(C68) volt:150;

(D68)                    150

(C69) lambda:volt*d31/tact;

(D69)                 1.492147e-4

(C70) ev(e11);

(D70)               [ 4.719518e-5 ]

(C71) ev(e22);

(D71)               [ 4.719518e-5 ]

(C72) ev(e12);

(D72)               [ 7.317492e-5 ]

(C73) closefile();
```

REDUCED OUTPUT FILE FOR CASE 2

```
(D57)            SYS$USER2:[WIN]E12PE.OUT;1

(C61) tact:.191*10^-3;

(D61)                  1.91e-4

(C62) tal:.292*10^-3;

(D62)                  2.92e-4

(C63) v : .33;

(D63)                   0.33

(C64) es : 63*10^9;

(D64)                63000000000

(C65) eleffo : 56.2*10^9;

(D65)                  5.62e10

(C66) eteffo : 11.5*10^9;

(D66)                  1.15e10

(C67) d31:190*10^-12;

                      19
(D67)            ------------
                 100000000000

(C68) volt:150;

(D68)                   150
```

(C69) lambda:volt*d31/tact;

(D69) 1.492147e-4

(C70) ev(e11);

(D70) [- 4.719518e-5]

(C71) ev(e22);

(D71) [- 4.719518e-5]

(C72) ev(e12);

(D72) [7.317492e-5]

(C73) closefile();

DATA FILE FOR CASE 3

(This data file attempts to calculate the curvature strains in the laminate plate generated by the piezoelectric elements bonded at -45 degrees with top actuator lamine activated in extension and the bottom layer laminae actvated in compression)

(Laminate geometry)

z3:tal/2+tact;
z2:tal/2;
z1:-tal/2;
z0:-tal/2-tact;

(Physical properties of actuator)

v12:v;
v21:v;
g12a:ga;
g21a:ga;

(Physical properties of substrate (aluminum))

```
v12a:v;
v21a:v;
g12s:es/2/(1+v);
g21s:es/2/(1+v);
e1s:es;
e2s:es;

(Components of Piezo-actuator bending matrix)

        (lower laminae)

dl11:(1/3)*(eleffo*(z3^3-z2^3))/(1-v12*v21);
dl12:(1/3)*v12*(eteffo*(z3^3-z2^3))/(1-v12*v21);
dl22:(1/3)*(eteffo*(z3^3-z2^3))/(1-v12*v21);
dl16:0;
dl26:0;
dl66:(1/3)*g12a*(z3^3-z2^3);

        (upper laminae)

du11:(1/3)*(eleffo*(z1^3-z0^3))/(1-v12*v21);
du12:(1/3)*v12*(eteffo*(z1^3-z0^3))/(1-v12*v21);
du22:(1/3)*(eteffo*(z1^3-z0^3))/(1-v12*v21);
du16:0;
du26:0;
du66:(1/3)*g12a*(z1^3-z0^3);

(Components of actuation bending matrix)

        (upper laminae)

bl11:(1/2)*(eleffo*(z3^2-z2^2))/(1-v12*v21);
bl12:(1/2)*v12*(eteffo*(z3^2-z2^2))/(1-v12*v21);
bl22:(1/2)*(eteffo*(z3^2-z2^2))/(1-v12*v21);
bl16:0;
bl26:0;
bl66:(1/2)*g12a*(z3^2-z2^2);

        (lower laminae)

bu11:(1/2)*(eleffo*(z1^2-z0^2))/(1-v12*v21);
bu12:(1/2)*v12*(eteffo*(z1^2-z0^2))/(1-v12*v21);
bu22:(1/2)*(eteffo*(z1^2-z0^2))/(1-v12*v21);
bu16:0;
bu26:0;
bu66:(1/2)*g12a*(z1^2-z0^2);
```

(Components of aluminum substrate bending stiffness matrix)

```
da11:(1/3)*(e1s*(z2^3-z1^3))/(1-v12a*v21a);
da12:(1/3)*v12*(e2s*(z2^3-z1^3))/(1-v12a*v21a);
da22:(1/3)*(e2s*(z2^3-z1^3))/(1-v12a*v21a);
da16:0;
da26:0;
da66:(1/3)*g12s*(z2^3-z1^3);
```

(Angle of longitudinal rotation of elements with respect to laminate axis)

```
x:-%pi/4;
```

(Transpose matrix)

```
t:matrix([cos(x)^2,sin(x)^2,2*cos(x)*sin(x)],[sin(x)^2,cos(x)^2,-2*cos(x)*sin(x)],[
-cos(x)*sin(x),cos(x)*sin(x),cos(x)^2-sin(x)^2]);


dpql:matrix([dl11,dl12,dl16],[dl12,dl22,dl26],[dl16,dl26,dl66]);
dpqu:matrix([du11,du12,du16],[du12,du22,du26],[du16,du26,du66]);

bpql:matrix([bl11,bl12,bl16],[bl12,bl22,bl26],[bl16,bl26,bl66]);
bpqu:matrix([bu11,bu12,bu16],[bu12,bu22,bu26],[bu16,bu26,bu66]);

r:matrix([1,0,0],[0,1,0],[0,0,2]);

ti:t^^-1;
ri:r^^-1;
```

(Transposed piezo-actuator bending stiffness matrices (upper and lower laminae))

```
ddpl:ti.dpql.r.t.ri;
ddpu:ti.dpqu.r.t.ri;
```

(Transposed piezo-actuation bending stiffness matrices (upper and lower laminae))

```
bdpl:ti.bpql.r.t.ri;
bdpu:ti.bpqu.r.t.ri;

am:ddpl+ddpu;
bm:bdpl-bdpu; (To generate bending)

alam:matrix([da11,da12,da16],[da12,da22,da26],[da16,da26,da66]);
```

(Laminate stiffness matrix composed of bending stiffnesses of both piezoelement laminae and the aluminum laminate)

```
als:alam+am;
```

(Actuation strain vector)

```
sap:matrix([lambda],[lambda],[0]); (assume the piezoelements produce no shear)
```

(Solving equation 13)

```
aaa:bm.sap;

ali:als^^-1;
su:ali.aaa;
kk11:row(su,1);
kk22:row(su,2);
kk12:row(su,3);

k11:ratsimp(kk11);
k22:ratsimp(kk22);
k12:ratsimp(kk12);
```

Opening an output file for the curvature strains)

```
writefile("k12nc.out");

k11:factor(k11);
k22:factor(k22);
k12:factor(k12);
```

(Physical and geometrical properties of aluminum and piezoelements)

```
tact:.191*10^-3;
tal:.292*10^-3;
v : .33;
es : 63*10^9;
eleffo : 56.2*10^9;
eteffo : 11.5*10^9;
d31:190*10^-12;

volt:150;
lambda:volt*d31/tact;

ev(k11);
ev(k22);
```

```
ev(k12);

volt:125;
lambda:volt*d31/tact;

ev(k11);
ev(k22);
ev(k12);

volt:100;
lambda:volt*d31/tact;

ev(k11);
ev(k22);
ev(k12);

volt:75;
lambda:volt*d31/tact;

ev(k11);
ev(k22);
ev(k12);

closefile();
quit();
```

OUTPUT FILE FOR CASE 3

```
(D73)                SYS$USER2:[WIN]K12NC.OUT;1


(C74) k11:factor(k11);

                                                       3 2              2              2 2
(D74) MATRIX([6 TACT (TAL + TACT) (2 ES ETEFFO TAL  V  + 12 ETEFFO  TACT TAL  V

                  2      2      2                   2      3  2                   3
+ 24 ETEFFO  TACT  TAL V  + 16 ETEFFO  TACT  V  - ES ETEFFO TAL  V

                     3                   3                   3
+ ELEFFO ES TAL  V - ES ETEFFO TAL  - ELEFFO ES TAL

                                        2                          2
```

```
- 12 ELEFFO ETEFFO TACT TAL  - 24 ELEFFO ETEFFO TACT  TAL

                              3                   3                      2
- 16 ELEFFO ETEFFO TACT ) LAMBDA/((ES TAL  + 6 ETEFFO TACT TAL

                         2                    3
+ 12 ETEFFO TACT  TAL + 8 ETEFFO TACT )

        3  2                         2  2                        2      2
(ES TAL  V  + 6 ETEFFO TACT TAL  V  + 12 ETEFFO TACT  TAL V

                        3  2        3                        2                  2
+ 8 ETEFFO TACT  V  - ES TAL  - 6 ELEFFO TACT TAL  - 12 ELEFFO TACT  TAL

                        3
- 8 ELEFFO TACT ))])

(C75) k22:factor(k22);


                                                                       3 2              2            2 2
(D75) MATRIX([6 TACT (TAL + TACT) (2 ES ETEFFO TAL  V  + 12 ETEFFO  TACT TAL  V

                  2       2        2                2      3  2                 3
+ 24 ETEFFO  TACT  TAL V  + 16 ETEFFO  TACT  V  - ES ETEFFO TAL  V

                      3                    3                  3
+ ELEFFO ES TAL  V - ES ETEFFO TAL  - ELEFFO ES TAL

                                   2                        2
- 12 ELEFFO ETEFFO TACT TAL  - 24 ELEFFO ETEFFO TACT  TAL

                              3                   3                      2
- 16 ELEFFO ETEFFO TACT ) LAMBDA/((ES TAL  + 6 ETEFFO TACT TAL

                         2                    3
+ 12 ETEFFO TACT  TAL + 8 ETEFFO TACT )

        3  2                         2  2                        2      2
(ES TAL  V  + 6 ETEFFO TACT TAL  V  + 12 ETEFFO TACT  TAL V

                        3  2        3                        2                  2
+ 8 ETEFFO TACT  V  - ES TAL  - 6 ELEFFO TACT TAL  - 12 ELEFFO TACT  TAL

                        3
- 8 ELEFFO TACT ))])

(C76) k12:factor(k12);
```

(D76) $\mathrm{MATRIX}([- 12\ \mathrm{ES}\ (\mathrm{ETEFFO} - \mathrm{ELEFFO})\ \mathrm{TACT}\ \mathrm{TAL}^3\ (\mathrm{TAL} + \mathrm{TACT})\ (V + 1)\ \mathrm{LAMBDA}$

$/((\mathrm{ES}\ \mathrm{TAL}^3 + 6\ \mathrm{ETEFFO}\ \mathrm{TACT}\ \mathrm{TAL}^2 + 12\ \mathrm{ETEFFO}\ \mathrm{TACT}^2\ \mathrm{TAL} + 8\ \mathrm{ETEFFO}\ \mathrm{TACT}^3)$

$(\mathrm{ES}\ \mathrm{TAL}^3\ V^2 + 6\ \mathrm{ETEFFO}\ \mathrm{TACT}\ \mathrm{TAL}^2\ V^2 + 12\ \mathrm{ETEFFO}\ \mathrm{TACT}^2\ \mathrm{TAL}\ V^2$

$+ 8\ \mathrm{ETEFFO}\ \mathrm{TACT}^3\ V^2 - \mathrm{ES}\ \mathrm{TAL}^3 - 6\ \mathrm{ELEFFO}\ \mathrm{TACT}\ \mathrm{TAL}^2 - 12\ \mathrm{ELEFFO}\ \mathrm{TACT}^2\ \mathrm{TAL}$

$- 8\ \mathrm{ELEFFO}\ \mathrm{TACT}^3))])$

```
(C77) tact:.191*10^-3;

(D77)                1.91e-4

(C78) tal:.292*10^-3;

(D78)                2.92e-4

(C79) v : .33;

(D79)                0.33

(C80) es : 63*10^9;

(D80)                63000000000

(C81) eleffo : 56.2*10^9;

(D81)                5.62e10

(C82) eteffo : 11.5*10^9;

(D82)                1.15e10

(C83) d31:190*10^-12;
```

(D83) $\dfrac{19}{100000000000}$

(C84) volt:150;

(D84) 150

(C85) lambda:volt*d31/tact;

(D85) 1.492147e-4

(C86) ev(k11);

(D86) [0.443414]

(C87) ev(k22);

(D87) [0.443414]

(C88) ev(k12);

(D88) [- 0.190278]

(C89) volt:125;

(D89) 125

(C90) lambda:volt*d31/tact;

(D90) 1.243456e-4

(C91) ev(k11);

(D91) [0.369512]

(C92) ev(k22);

```
(D92)                   [ 0.369512 ]

(C93) ev(k12);

(D93)                   [ - 0.158565 ]


(C94) volt:100;

(D94)                     100

(C95) lambda:volt*d31/tact;

(D95)                   9.947645e-5


(C96) ev(k11);

(D96)                   [ 0.295609 ]

(C97) ev(k22);

(D97)                   [ 0.295609 ]

(C98) ev(k12);

(D98)                   [ - 0.126852 ]


(C99) volt:75;

(D99)                     75

(C100) lambda:volt*d31/tact;

(D100)                  7.460733e-5


(C101) ev(k11);
```

```
(D101)                    [ 0.221707 ]

(C102) ev(k22);

(D102)                    [ 0.221707 ]

(C103) ev(k12);

(D103)                    [ - 0.095139 ]

(C104) closefile();
```

REDUCED OUTPUT FILE FOR CASE 4

```
(D73)                SYS$USER2:[WIN]K12PE.OUT;1

(C77) tact:.191*10^-3;

(D77)                     1.91e-4

(C78) tal:.292*10^-3;

(D78)                     2.92e-4

(C79) v : .33;

(D79)                      0.33

(C80) es : 63*10^9;

(D80)                   63000000000

(C81) eleffo : 56.2*10^9;

(D81)                    5.62e10

(C82) eteffo : 11.5*10^9;

(D82)                    1.15e10
```

```
(C83) d31:190*10^-12;

                          19
(D83)                ------------
                     100000000000


(C84) volt:150;

(D84)                     150

(C85) lambda:volt*d31/tact;

(D85)                1.492147e-4


(C86) ev(k11);

(D86)                [ 0.443414 ]

(C87) ev(k22);

(D87)                [ 0.443414 ]

(C88) ev(k12);

(D88)                [ 0.190278 ]


(C89) volt:125;

(D89)                     125

(C90) lambda:volt*d31/tact;

(D90)                1.243456e-4


(C91) ev(k11);
```

```
(D91)                    [ 0.369512 ]

(C92) ev(k22);

(D92)                    [ 0.369512 ]

(C93) ev(k12);

(D93)                    [ 0.158565 ]


(C94) volt:100;

(D94)                       100

(C95) lambda:volt*d31/tact;

(D95)                    9.947645e-5


(C96) ev(k11);

(D96)                    [ 0.295609 ]

(C97) ev(k22);

(D97)                    [ 0.295609 ]

(C98) ev(k12);

(D98)                    [ 0.126852 ]


(C99) volt:75;

(D99)                       75

(C100) lambda:volt*d31/tact;

(D100)                   7.460733e-5
```

```
(C101) ev(k11);

(D101)                [ 0.221707 ]

(C102) ev(k22);

(D102)                [ 0.221707 ]

(C103) ev(k12);

(D103)                [ 0.095139 ]

(C104) closefile();
```

APPENDIX 2

COMPARISON BETWEEN PIN-FORCE, STRAIN-ENERGY AND LSSVM EQUIVALENT FORCE MODELS

The expressions for the pin-force and the strain-energy equivalent forces for pure bending and extension are very straightforward. However, the expressions for the LSSVM model were much more involved. The equivalent force and moment for the three models for the cases of pure extension and bending were solved for using Quick Basic. The results of these calculations for varying values of voltage potential are shown in Table 25. Note that the tabulated values are for the equivalent force applied to single nodes in the finite element models. Although the LSSVM equivalent force did decrease slightly in magnitude near the edge of the piezoelement, the maximum value obtained was used in the Table 25.

Table 25 - Comparison between equivalent force models for pure extension and bending

	Pure extension		
Activation potential (V)	Strain-energy (N)	Pin-force (N)	LSSVM (V)
0	0	0	0
75	1.12983	2.34673	1.88670
100	1.50644	3.12897	2.51599
125	1.88304	3.91122	3.14499
150	2.25965	4.69346	3.77399
	Pure bending		
0	0	0	not applicable
75	1.12983	1.12983	
100	1.50644	1.50644	
125	1.18830	1.18830	
150	2.25965	2.25965	

The Quick Basic computer codes for the calculations are listed below.

Computer code for the strain-energy and pin-force equivalent force models

```
CLS
' Strain-energy and pin-force models for axial force and bending moment

ta = .191 * 10 ^ -3             'Thickness of actuator
tb = .292 * 10 ^ -3             'Thickness of substrate (aluminum)
eb = 63 * 10 ^ 9                'Elastic modulus of substrate
ea = 56.2 * 10 ^ 9              'Elastic modulus of actuator
d31 = 190 * 10 ^ -12            'charge coefficient
b = 6.35 * 10 ^ -3              'width of actuator
phi = (tb * eb) / (ta * ea)     'Effective stiffness ratio

PRINT "This for strain-energy axial force"
volt = 75
FOR n = 1 TO 4

lambda = volt * d31 / ta
Feq = (tb * eb * b * lambda) / (6 + phi)
PRINT volt, "v", Feq, "Newtons per node"
volt = volt + 25
NEXT n

PRINT
PRINT "This is for moment (both strain energy and pin-force)"
n = 1
volt = 75
FOR n = 1 TO 4

lambda = volt * d31 / ta
Meq = (tb ^ 2 * eb * b * lambda) / (6 + phi)
Feq = Meq / tb
PRINT volt; " v  "; Meq; " Meq  "; Feq; " Newtons per node  "
volt = volt + 25
NEXT n

PRINT
PRINT "This for pin-force axial force"
volt = 75
FOR n = 1 TO 4
```

```
lambda = volt * d31 / ta
Feq = (tb * eb * b * lambda) / (2 + phi)
PRINT volt, "v", Feq, "Newtons per node"
volt = volt + 25
NEXT n
```

Computer code for the LSSVM equivalent force model

```
' LSSVM model for axial force and bending moment

CLS
l = (1 * .0254) / 2           'Half length of actuator
a = .191 * 10 ^ -3            'Thickness of actuator
b = (.292 * 10 ^ -3) / 2      'Half thickness of substrate (aluminum)
h = .25 * .0254               'Width of actuator
es = 63 * 10 ^ 9              'Axial modulus of substrate
ea = 56.2 * 10 ^ 9            'Effective axial modulus of actuator
gs = es / (2 * (1 + .33))     'Shear modulus of substrate
ga = ea / (2 * (1 + .33))     'Shear modulus of actuator
d31 = 190 * 10 ^ -12          'Piezoelectric charge coefficient


'Expressions for eta values (constant)

  eta1a = (3 * ga * gs) * (a * ea + b * es)
  eta1b = (a * b * ea * es) * (a * gs + b * ga)
eta1 = (eta1a / eta1b) ^ .5

  eta2a = 2 * (b ^ 2) * es - (a * ea) * (a + b)
  eta2b = (b ^ 3) * es + (a * ea) * (3 * (b ^ 2) + 3 * a * b + (a ^ 2))
  eta2c = -ga * gs * 24
  eta2d = (a ^ 2) * (b ^ 2) * ea * es
  eta2e = gs * (4 * (b ^ 3) * es + (a * ea) * (4 * (b ^ 2) * -a * b - (a ^ 2)))
  eta2f = 4 * (a + b) * ga
  eta2g = 2 * (b ^ 2) * es + (a * ea) * (a + 3 * b)
 eta2h = eta2a * eta2b * eta2c
 eta2i = (eta2e + eta2f * eta2g) * eta2d
eta2j = eta2h / eta2i

eta2 = (eta2j) ^ .5

' Expressions for k values (constant)

k0a = 6 * gs
```

```
kOb = 2 * (b ^ 2) * es - (a * ea) * (a + b)
kOc = (b ^ 3) * es + (a * ea) * (3 * (b ^ 2) + 3 * a * b + (a ^ 2))
kOd = 4 * (b ^ 3) * es + (a * ea) * (4 * (b ^ 2) - a * b - (a ^ 2))
kO = kOa * kOb * kOc * kOd

k1a = (b * es + a * ea)
k1b = ((a * gs) * (3 * b * es + a * ea) + 2 * (b ^ 2) * es * ga)
k1 = k1a * k1b

k8a = (2 * (b ^ 5) * es ^ 2) * (20 * b + 11 * a)
  k8b = (a * (b ^ 2) * ea * es)
  k8c = 4 * (b ^ 3) - 49 * a * (b ^ 2) - 43 * (a ^ 2) * b - 8 * (a ^ 3)
k8d = k8b * k8c
  k8e = (a ^ 2) * (ea ^ 2)
  k8f = 12 * (b ^ 4) + 3 * a * (b ^ 3) - 25 * (a ^ 2) * (b ^ 2)
  k8g = -20 * (a ^ 3) * b - 4 * (a ^ 4)
  k8fg = k8f + k8g
k8h = k8e * k8fg
k8 = (-3 * gs) * (k8a + k8d - k8h)

k9a = 2 * (b ^ 3) * es - ((a ^ 2) * ea) * (3 * b + a)
 k9b = (3 * (8 * b + 5 * a)) * gs
 k9c = (2 * (b ^ 2) * es - (a * ea) * (b + a))
  k9d = -ea * es * (eta2 ^ 2) * (a ^ 2) * b
  k9e = 2 * (b ^ 2) + 3 * a * b + a
 k9f = k9b * k9c
 k9g = k9d * k9e
k9 = k9a * (k9f + k9g)

k10 = -(a * gs) * (5 * b * es + a * ea) - 4 * (b ^ 2) * es * ga

k11 = (4 * b * es) * (a * gs + b * ga)

OPEN "ext.out" FOR OUTPUT AS #1

FOR n = 0 TO 100
   x = n * .000127
v = 150                     'Applied voltage
delta = 0

lambdat = (v * d31) / a      'Free induced strain of top actuator
lambdab = (v * d31) / a      'Free induced strain of bottom actuator

' Expressions for force and moment values

fs1 = -a * b * ea * es * h * (lambdat + lambdab - 2 * delta)
```

```
fs2 = (EXP(eta1 * x) + EXP(-(eta1 * x))) / (EXP(eta1 * l) + EXP(-(eta1 * l)))
fs3 = k10 + k11 * fs2
fs = (fs1 * fs3) / (2 * k1)
f = fs / 2
PRINT x, f
WRITE #1, x, f
NEXT n

n = 0
PRINT
STOP
OPEN "bnd.out" FOR OUTPUT AS #2

FOR n = 0 TO 100
   x = n * .000127
v = 150                    'Applied voltage

lambdat = -(v * d31) / a      'Free induced strain of top actuator
lambdab = (v * d31) / a       'Free induced strain of bottom actuator

ms1 = -2 * a * (b ^ 3) * ea * es * h * (lambdat - lambdab)
ms2 = (EXP(eta2 * x) + EXP(-(eta2 * x))) / (EXP(eta2 * l) + EXP(-(eta2 * l)))
ms3 = k8 + k9 * ms2
ms = (ms1 * ms3) / (3 * k0)
eqf = ms / (b * 2)

PRINT x, eqf
NEXT n
```

APPENDIX 3

DATA AND CALCULATIONS FOR THE SHEAR MODULUS OF PLATE WITH PIEZOELEMENTS

For the shear modulus calculation of the aluminum plate, the dimensions for layout two were used. They are shown schematically in Figure 86.

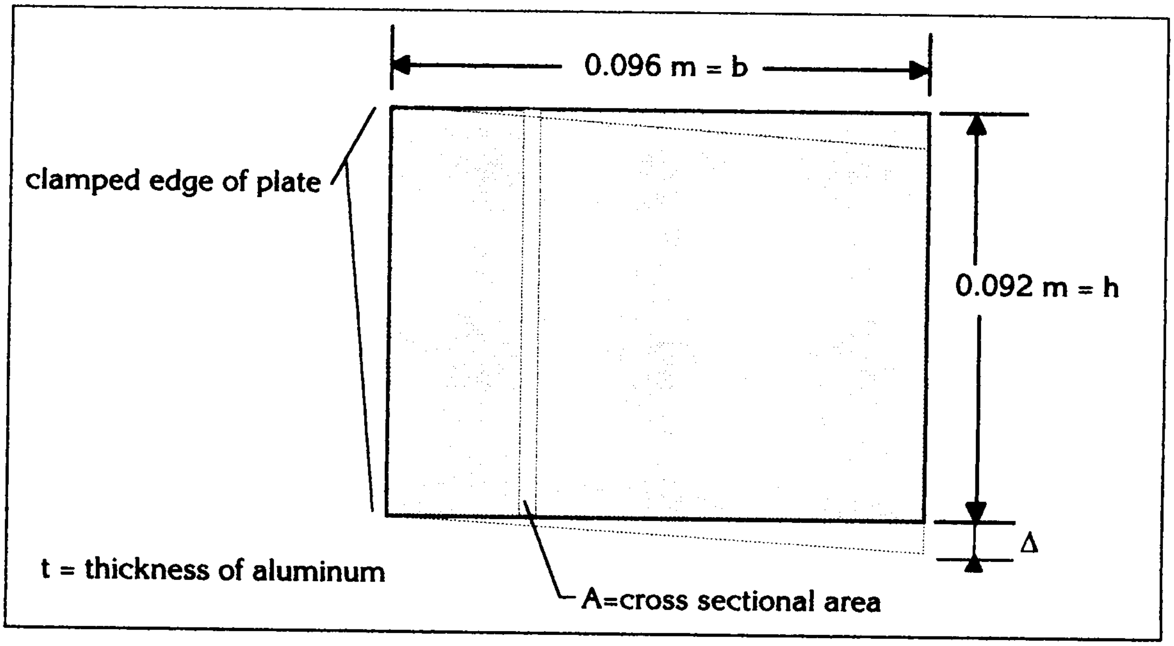

Figure 86 - Plate geometry for shear modulus calculation

The working equations for the shear modulus for the plate model, found in any mechanics of materials reference are as follows

Shear stress $$\tau = G\gamma = \frac{P}{A} = \frac{P}{ht} \quad (26)$$

Shear strain $$\gamma = \frac{\Delta}{b} \quad (27)$$

Shear modulus $$G = \frac{\tau}{\gamma} = \frac{P}{ht}\left(\frac{b}{\Delta}\right) \quad (28)$$

The assumptions for the plate are that there are no elements bonded to the surface and that the influence due to the rigid bar is neglected. The data for the externally induced force versus the plate displacement is in Table 26.

Table 26 - Applied force (N) and resulting induced shear displacement

Force (N)	Actual displ. (m)	Regression displ. (m)
0	0	0
51.16057	0.000004953	5.54977E-06
95.64278	9.8298E-06	1.03751E-05
140.125	1.49758E-05	1.52004E-05
184.6072	2.06248E-05	2.00257E-05
229.0894	2.48666E-05	2.48511E-05

The data used for the calculation of the experimental shear modulus of the plate was 200 N corresponding to a displacement of 2.17E-5. This data point is located on the linear regression line. The data for the plate was placed into a spreadsheet and the value for the shear modulus was obtained. The data is listed below.

tplate	b (m)	h(m)
2.79E-04	0.096	0.092
Δ	P (N)	
2.17E-05	200	
G(exp)	G(plate)	% difference
3.440E+10	2.37E+10	45.25

The theoretical value for the shear modulus was obtained from mechanics of materials. The difference between the experimental value and the theoretical value was 45.25%. Therefore, the addition of piezoelements bonded to the aluminum plate in layout two resulted in an increase of the shear modulus on the order of 1.07 E+10 Pa.

APPENDIX 4

DATA AND CALCULATIONS FOR THE BENDING RIGIDITY OF THE PLATE WITH PIEZOELEMENTS

For the bending rigidity calculation of the aluminum plate, the dimensions for layout two were used (please refer to figure 68).

The working equations for the bending rigidity for the plate model, found in any mechanics of materials reference are as follows

Bending rigidity $$EI=-\frac{Pb^3}{3\upsilon} \qquad (29)$$

Moment of inertia $$I=\frac{ht^3}{12} \qquad (30)$$

The experimental results in Table 27 were used for the calculation. The assumptions for the plate are that there are no elements bonded to the surface and that the influence due to the rigid bar is neglected. The data point used for the calculation was the force of 0.06257 N corresponding to 8.155982 E-3 m shear displacement (from linear regression).

Table 27 - Applied force (N) and resulting induced bending displacement

Force (N)	Actual displ. (m)	Regression displ. (m)
0	0	0
0.1353	0.0016	0.001764146
0.2334	0.0030	0.003042514
0.3315	0.0040	0.004320881
0.6257	0.0080	0.008155982
0.8218	0.0110	0.010712716

The value for the bending rigidity was solved for using a spreadsheet. The results for the experimental and theoretical bending rigidities are shown below.

tplate	I	h(m)	L
0.0002794	1.6722E-13	0.092	0.096
v	P (N)	b (m)	
8.16E-03	0.625667	2.79E-04	
E(exp)	E(theo)	% difference	
1.353E+11	6.300E+10	114.7495	
BR(Exp)	BR(plate)	% diference	
0.0226	0.0105	114.7495	

As can be seen, the addition of the piezoelements to the plate increases the bending rigidity of the plate by 114.749%. Therefore, the addition of piezoelements bonded to the aluminum plate in layout two resulted in an increase of the bending rigidity on the order of 0.0121 Nm.

APPENDIX 5

DATA AND CALCULATIONS FOR THE FLEXURAL RIGIDITY OF THE COMPOSITE BEAM WITH PIEZOELEMENTS

In order to determine the experimental value for the flexural rigidity of the composite beam with piezoelements, it was necessary to develop an understanding of the optics of the beam experiment set-up (as described in section 7.2.1). Equation (24) shows the relationship between the laser dot displacement (d), the externally applied force (P), and the modulus of elasticity (E) of the composite beam. The data for the laser dot displacement (please refer to Figure 66) resulting from an the externally applied force is shown in Table 28. Although the beam deflections are listed in Table 28, they have not been determined at this point.

Table 28 - Laser dot displacement resulting from externally applied force

Force (N)	Laser dot displ. (m)	Beam deflection (m)
0	0	0
3.339181	0.015	0.0002595
6.281191	0.027	0.0004671
9.223201	0.039	0.0006747
12.16521	0.051	0.0008823
15.10722	0.065	0.0011245
18.04923	0.079	0.0013667

Referring to Figure 69, the laser dot displacement versus an externally applied force is nearly linear. With this information, an arbitrary data point on the plot was chosen to iteratively solve for the modulus of elasticity of the composite beam using Equation (24). The known values in equation (24) are as follow:

$P = 15.10772$ N	externally applied force
$d = 0.065$ m	laser dot displacement
$t = 3.556$ E-4 m	thickness of composite
$w = 0.057$ m	effective width of composite beam
$I = \frac{2(w^3 t)}{12} + 2\left(\frac{w}{2}\right)^2 tw = 4.3903$ E-8 m^4	moment of inertia
$a_1 = 0.473$ m	effective length of beam
$a_2 = 9.21095$	distance between a_1 and screen (Figure 72)
d1	deflection of beam tip

Using these numbers to iteratively solve for (E), the values for d1/d = 1.7012 E-2 and E=1.079 E+10 N/m^2 were obtained. This ratio of d1/d resulted in the values for the composite beam deflection due to the externally applied force. These values are shown in Table 28. The flexural rigidity of the beam was equal to the product of (E) and the moment of inertia. The experimental flexural rigidity of the composite beam was found to be 473.1 Nm^2.

The theoretical value for the flexural rigidity of the composite beam was found with equation (25). For equation (25), the following values are known: These values were developed by [20] for the composite beam.

$I = 4.410\ E\text{-}8\ m^4$	moment of inertia for beam and piezoelements
$\rho AL = 0.07$ Kg	mass of beam and elements
$M = 0.234$ Kg	mass of aluminum chuck and mirror assembly
$L = 0.455$ m	effective length of beam
$\omega = f_1 2\pi$ rad/s	first bending mode frequency

With the first bending mode frequency of 37.99 Hz (section 7.4.2) and the values in equation (20), a value of 449.42 Nm^2 was obtained for the theoretical flexural rigidity. A difference of 5.126% between the experimental and the theoretical value for the flexural rigidity of the composite beam was noticed. Also, equation (25) was used to predict the first mode of bending for the composite beam by solving for w using the experimental value for the modulus of elasticity. This resulted in a predicted first mode bending frequency of 39.0 Hz. The difference between the actual and predicted values for the first bending mode of the composite beam was on the order of 2.65%.

Two Quick basic codes were written to solve for the experimental and theoretical flexural rigidities of the composite beam, respectively. They are listed on the following pages:

```
'   Program for iteratively solving for the value of the flexural rigidity
CLS
PRINT "input the value for e"

INPUT f

e = f * 10 ^ 10

d = .065
p = 1.5405 * 9.8067
a1 = .473
a2 = 9.12095
wb = .057
tb = .0003556
i = 2 * (wb ^ 3 * tb) / 12 + 2 * (wb / 2) ^ 2 * tb * wb

dd = (a2 * TAN((p * a2 ^ 2) / (e * i)) + (p * a1 ^ 3) / (3 * e * i))
d1 = (p * a1 ^ 3) / (3 * e * i)
d2 = a1 * TAN((p * a1 ^ 2) / (e * i))
r = d1 / d

PRINT "The value for the modulus of elasticity calculated is", e, "N/m^2"
PRINT "The value for the bending displacement is ", d1, "m"
PRINT "The ratio of d1/d= "; r
PRINT dd, d
STOP


' Program for finding theoretical flexural rigidity

w = .239 / 9.8067
M = .239                        'mass of aluminum chuck
g = 9.8067
l = .455                        'effective lenght of beam
pi = 3.1415927#
i = 4.39E-08                    'moment of inertia
f = 37.99                       'FFT results of first modal frequency of
                                'composite beam

omega = f * 2 * pi
Et = 1.079E+10

E1 = (omega ^ 2 * .07 * l ^ 3) / i
E2 = (pi ^ 4 / 4) / ((12 - 32 / pi) + (8 * M / .07))
E = E1 / E2
```

```
omega1 = (((Et * i) / (.07 * l ^ 3)) * E2) ^ .5
gnn = omega1 / (2 * pi)

PRINT E, gnn
STOP
```

APPENDIX 6

DATA AND CALCULATIONS FOR THE TORSIONAL RIGIDITY OF THE COMPOSITE BEAM WITH PIEZOELEMENTS

The working equations for the torsional rigidity of the composite beam, found in any mechanics of materials reference are as follow

Shear modulus $$G=\frac{ML}{J_s\theta_{rad}} \qquad (31)$$

Polar moment of area $$J_s = 4A^2\frac{t}{4w} \qquad (32)$$

The data obtained for the torsional displacement due to an externally induced moment to the composite beam is shown below in Table 29.

Table 29 - Laser dot displacement resulting from externally applied moment

Laser dot displ, (m)	Twist (rad)	Twist (deg)	mass (Kg)	Force (N)	Moment arm	moment
0	0	0	0	0	15.45 cm	0
0.032	0.0031652	0.1813517	0.3405	0.313814	0.1545 m	0.0483
0.052	0.0051434	0.2946949	0.4405	0.509948		0.0785
0.064	0.0063303	0.3626998	0.5405	0.627629		0.0967
0.073	0.0072204	0.4137028	0.6405	0.715889		0.1102
0.083	0.0082095	0.470372	0.7405	0.813956		0.1253
0.094	0.0092975	0.5327071	0.8405	0.92183		0.142
0.104	0.0102865	0.5893743	0.9405	1.019897		0.1571
0.114	0.0112755	0.6460403	1.0405	1.117964		0.1722

Referring to Figure 71, the laser dot displacement versus an externally applied moment is nearly linear. With this information, an arbitrary data point From Table 29 was chosen to evaluate the experimental shear modulus of the composite beam using Equations (30) and (31). The values used for the calculation were as follow:

$M = 0.1722$ Nm	externally applied moment
$\theta_{rad} = 0.0112866$	torsional rotation of beam
$t = 3.556$ E-4 m	thickness of composite
$w = 0.057$ m	effective width of composite beam
$A = w^2$	effective cross section area of beam

Using these values, the experimental value for the shear modulus was 1.0991 E+8 Pa and the torsional rigidity of the composite beam was 7..2383 Nm^2. A Quick basic program was used to evaluate equations (30) and (31). A listing of the program used is below.

```
' Program for torsional rigidity of composite beam

w = .057                              'Width of composite beam       (m)
t = .014 * .0254                      'Thickness of composite beam   (m)
Ms = .1722                            'Moment applied                (Nm)
theat = .0112866                      'Angle twist                   (rad)
Js = (4 * w ^ 4 * t) / (w * 4)        'Polar moment of area          (m^4)
l = .473                              'Effective lenght of beam      (m)

G = (Ms * l) / (Js * theat)           'Shear modulus                 (N/m^2)
```

```
tr = Js * G                    'Torsional rigidity          (Nm^2)

PRINT Js, G, tr
STOP
```

APPENDIX 7

DATA FOR THE STATIC TORSIONAL DISPLACEMENTS OF THE COMPOSITE BEAM WITH PIEZOELEMENTS

The results of the torsional displacements due the statically induced potential through the piezoelements are shown in Table 30. The plots of the data in Table 30 can be found in Figures 76 and 77.

Table 30 - Static torsional displacement results of the composite beam

Actvation V	L#1 (mm)	L#2 (mm)	L#3 (mm)	L av. (mm)	L av. (m)	Twist (rad)	Twist (deg)
0	0	0	0	0.0000	0	0	0
30	1	0.8	0.8	0.8667	0.00087	8.27E-05	0.004738
60	1.8	1.5	1.4	1.5667	0.00157	0.000149	0.008565
90	2.9	2.3	2.4	2.5333	0.00253	0.000242	0.01385
120	4.2	3.8	3.8	3.9333	0.00393	0.000375	0.021504
150	5.7	5	4.8	5.1667	0.00517	0.000493	0.028247
	R#1 (mm)	R#2 (mm)	R#3 (mm)	R av. (mm)	R av. (m)		
0	0	0	0	0.0000	0	0	0
30	1.2	1.7	1	1.3000	0.0013	0.000124	0.007107
60	2.2	2.6	2	2.2667	0.00227	0.000216	0.012392
90	3.2	3.2	3	3.1333	0.00313	0.000299	0.01713
120	4.9	4.1	4.1	4.3667	0.00437	0.000417	0.023873
150	5.9	5.1	5.3	5.4333	0.00543	0.000518	0.029705

VITA

Winthrop P. Smith was born on February 19, 1968 in Knoxville, Tn. He graduated from Dobyns Bennet High School, Kingsport, Tn, Student Body President, in 1986. He received the degree of Bachelor of Science in Aerospace Engineering from North Carolina State University in August 1991. In August of 1991 he entered the University of Tennessee Graduate School, where he will receive his Master of Science degree in Aerospace Engineering in December 1993. He is a member of AIAA and ASC.

He is the co-autor with Kawiecki, G., of "Twist and Torque Generating in Thin-Walled Composite Members Using Piezoelectric Elements", Proceedings of 7th Technical Conference of the American Society of Composites, University Park. Pa., October 13-15, 1992.